Acknowledgements

I acknowledge Professor *L. Håkan Gustavsson*, my thesis-adviser, for his enthusiasm in my research-work and also for trusting me that I could do it. His contribution to this thesis is many-folded and, thus, inseparable. He has been a constructive critic of the details of my research-work and also of the manuscript. And, I thank him for providing me with that luxury.

I gratefully acknowledge the University of Peradeniya, Sri Lanka, for providing me all the necessary support that I required to pursue this study.

I thank *Lena Larsson*, *Gunnel Henriksson* and *Rose-Marie Lövenstig* for their invaluable assistance during these years. Particular thanks are due to Rose-Marie for her enduring patience with the commas which kept changing their places between two versions of the manuscripts of two of the papers.

Contributions of *Torbjörn Löfqvist* towards this thesis are indirect, but important. I thank him specially for the conversations that we have had when I was in despair about my research-work and also when I was terribly angry with someone, which indeed happened, and happens, very often.

I thank *Allan Holmgren* warmly for his enthusiasm in explaining to me the complicated equipments in the laboratory and their complex functions. I also thank him with due respects for making me feel at home in situations that were strange for me.

My thanks are due to *Per Gren* for helping me in my attempts to grasp the experimental side of fluid mechanics, for keeping pace with me on the skiing track in Abisko (despite the fact he is a very good skier) and for the interesting conversations that we have had about our cats.

I am greatly indebted to *Hernán Tinoco* and to *John Wyller* for their generosity in promptly sharing their knowledge, in the atmosphere where everyone is so very occupied with their own achievements.

Yang Qi Xing and *Siv Leth* are thanked many times for providing the intellectual and friendly atmosphere that I am used to in the universities of my home country, Sri Lanka.

I thank *David J. Benney*, professor at Massachusetts Institute of Technology, for providing me the valuable assistance that I badly needed in grasping the nonlinear aspects of shear-flow instability. Special thanks are due to *Dennis L. Porch III*, to *M. T. Kouo*, and to *Martha Adams*, of MIT, for making my three-months stay there as comfortable as possible.

This work has in part been financially supported by the National Swedish Board for Technical Development through its program for basic research (STUF).

Completion of this thesis would not have been possible without the unfailing hospitality shown to me by *Renu Sinha* and her family. In devoid of that and the countably *few friends* that I have here, I would have felt that my husband, our cats and I have been living on an iceberg with occasional glimpse of humanity.

This list of acknowledgements would be far from complete without I acknowledging *my parents*, *my brothers*, *my teachers* and *all the others* who enthusiastically and unselfishly assisted me in my gain. At times, assisting me meant sacrifices on their behalves, yet they went ahead and saw to it that I gained. Today, I wonder what made them to be like that, and pray for the courage when it is my turn to assist in others gain.

Bibliography

ALAVYOON, F., HENNINGSON, D. S. & ALFREDSSON, P. H. 1986 Turbulent spot in plane Poiseuille flow - flow visualization. *Phys. Fluids* **29**, 1328-1331.

BAYLY, B. J. 1986 Three-dimensional instability of elliptical flow. *Phys. Rev. Lett.* **57**, 2160-2163.

BAYLY, B. J., ORSZAG, S. A. & HERBERT, T. 1988 Instability mechanisms in shear-flow transition. *Ann. Rev. Fluid Mech.* **20**, 359-391.

BENNEY, D. J. & GUSTAVSSON, L. H. 1981 A new mechanism for linear and nonlinear hydrodynamic instability. *Stud. Appl. Math.* **64**, 185-209.

BETCHOV, R. & CRIMINALE, W. O. 1966 Spatial instability of the inviscid jet and wake. *Phys. Fluids* **9**, 359-362.

BREUER, K. S. 1988 The development of a localized disturbance in a boundary layer. PhD thesis, Massachusetts Institute of Technology, USA.

CARLSON, D. R., WIDNALL, S. E. & PEETERS, M. F. 1982 A flow-visualization study of transition in plane Poiseuille flow. *J. Fluid Mech.* **121**, 487-505.

CRAIK, A. D. D. 1985 *Wave interactions and fluid flows.* Cambridge University press.

DAVEY, A. 1973 A simple numerical method for solving Orr-Sommerfeld problems. *Quart. J. Mech. Appl. Math.* **26**, 401-411.

DAVIES, S. J. & WHITE, C. M. 1928 An experimental study of the flow of water in pipes of rectangular section. *Proc. Roy. Soc. London* **A119**, 92-107.

DIPRIMA, R. C. & HABETLER, G. J. 1969 A completeness theorem for non-selfadjoint eigenvalue problems in hydrodynamic stability. *Arch. Rat. Mech. Anal.* **34**, 218-227.

DIPRIMA, R. C. & STUART, J. T. 1983 Hydrodynamic stability. *J. Appl. Mech.* **50**, 983-991.

DRAZIN, P. G. & REID, W. H. 1981 *Hydrodynamic stability.* Cambridge University press.

ELLINGSEN, T. & PALM, E. 1975 Stability of linear flow. *Phys. Fluids* **18**, 487-488.

EMMONS, H. W. 1951 The laminar-turbulent transition in a boundary layer: Part 1. *J. Aero. Sci.* **18**, 490-498.

GASTER, M. 1968 Growth of disturbances in both space and time. *Phys. Fluids* **11**, 723-727.

GRAEF, M. 1961 Zur Instabilität ebener Riselfilme bei Berücksichtung der Oberflächenspannung. Max-Plank Institut für Strömungsforschung, Bericht 1.

GREN, P. 1987 Laser Doppler Measurement of turbulent spots on a water table. In *Structured surfaces and turbulence*. Licentiate thesis 1987:04L, Luleå University of Technology, Sweden.

GROSCH, C. E. & SALWEN, H. 1968 The stability of steady and time-dependent plane Poiseuille flow. *J. Fluid Mech.* **34**, 177-205.

GUSTAVSSON, L. H. 1978 On the evolution of disturbances in boundary layer flows. PhD thesis TRITA-MEK-78-02, Royal Institute of Technology, Sweden.

GUSTAVSSON, L. H. 1981 Resonant growth of three-dimensional disturbances in plane Poiseuille flow. *J. Fluid Mech.* **112**, 253-264.

GUSTAVSSON, L. H. 1986 Excitation of direct resonances in plane Poiseuille flow. *Stud. Appl. Math.* **75**, 227-248.

GUSTAVSSON, L. H. 1989 Direct resonance of nonaxisymmetric disturbances in pipe flow. *Stud. Appl. Math.* **80**, 95-108.

GUSTAVSSON, L. H. 1990 Energy growth of three-dimensional disturbances in plane Poiseuille flow. Submitted to *J. Fluid Mech.*

GUSTAVSSON, L. H. & HULTGREN, L. S. 1980 A resonance mechanism in plane Couette flow. *J. Fluid Mech.* **98**, 149-159.

GUSTAVSSON, L. H. & ÖGREN, J.-E. 1983 Observations of turbulent spots on a water table. In *Noise radiation from drill steels* (by J.-E. Ögren). Doctoral Thesis 1983:23D, Luleå University of Technology, Sweden.

HENNINGSON, D. S. 1988 The inviscid initial value problem for a piecewise linear mean flow. *Stud. Appl. Math.* **78**, 31-56.

HENNINGSON, D. S. & ALFREDSSON, P. H. 1987 The wave structure of turbulent spots in plane Poiseuille flow. *J. Fluid Mech.* **178**, 405-421.

HERBERT, T 1976 Periodic secondary motions in a plane channel. In *Proc. Int. Conf. Numer. Methods Fluid Dyn.* (ed. A. I. van de Vooren and P. J. Zandbergen), p. 235. Springer-Verlag.

HERBERT, T 1983 Stability of plane Poiseuille flow - theory and experiment. *Fluid Dyn. Trans.* **11**, 77-126.

HUERRE, P. & MONKEWITZ, P. A. 1985 Absolute and convective instabilities in free shear layers. *J. Fluid Mech.* **159** 151-168.

ITOH, N 1974 Spatial growth of finite wave disturbances in parallel and nearly parallel flows: Part 1. *Trans Japan Soc. Aero. Space Sci.* **17**, 160-174.

JONES. C. A. 1988 Multiple eigenvalues and mode classification in plane Poiseuille flow. *Q. J. Mech. Appl. Math.* **41**, 363-382.

KAO, T. W. & PARK, C. 1970 Experimental investigations of the stability of channel flows. Part I. *J. Fluid Mech.* **43**, 145-164.

KARNITZ, M. A., POTTER, M. C. & SMITH, M. C. 1974 An experimental investigation of transition of a plane Poiseuille flow. *J. Fluids Eng.* **96**, 384-388.

KIM, J. & MOSER, R. D. 1989 On the secondary instability in plane Poiseuille flow. *Phys. Fluids* A1, 775-777.

KOCH, W. 1986 Direct resonances in Orr-Sommerfeld problems. *Acta Mech.* **58**, 11-29.

LANDAHL, M. T. 1975 Wave breakdown and turbulence. *SIAM J. Appl. Math.* **28**, 735-756.

LANDAHL, M. T. 1980 A note on an algebraic instability of inviscid parallel shear flows. *J. Fluid Mech.* **98**, 243-251.

LIN, C. C. 1955 *The theory of hydrodynamic stability.* Cambridge University press.

LIN, C. C. 1961 Some mathematical problems in the theory of the stability of parallel flows. *J. Fluid Mech.* **10**, 430-438.

LINDBERG, P.-A., FAHLGREN, E. M., ALFREDSSON, P. H. & JOHANSSON, A. V. 1985 An experimental study of the structure and spreading of turbulent spots. In *laminar-turbulent transition* (ed. Kozlov), Springer, 617-624.

MACK, L. M. 1976 A numerical study of the temporal eigenvalue spectrum of the Blasius boundary layer. *J. Fluid Mech.* **73**, 497-520.

MASLOWE, S. A. 1981 Shear flow instabilities and transition. In *Hydrodynamic instabilities and the transition to turbulence* (ed. H. L. Swinney and J. P. Gollub), p. 181-228. Springer-Verlag.

MEKSYN, D. 1964 Stability of laminar flow between parallel planes for two- and three-dimensional finite disturbances. *Zeitschrift für Physik* **178**, 159-172.

MEKSYN, D. & STUART, J. T. 1951 Stability of viscous motion between parallel planes for finite disturbances. *Proc. Roy. Soc. London* A**208**, 517-526.

MITCHENER, M. 1954 Propagation of turbulence from an instantaneous point disturbance. *J. Aero. Sci.* **21**, 350-351.

NARASIMHA, R. 1985 The laminar-turbulent transition zone in the boundary layer. *Prog. Aerospace Sci.* **21** 29-80.

NARAYANAN, M. A. B. & NARAYANA, T. 1967 Some studies on transition from laminar to turbulent flow in a two-dimensional channel. *Z. Angew. Math. Phys.* **18**, 642-650.

NISHIOKA, M., IIDA, S. & ICHIKAWA, Y. 1975 An experimental investigation of the stability of plane Poiseuille flow. *J. Fluid Mech.* **72**, 731-751.

NOETHER, F. 1921 Das Turbulenzproblem. *Z. Angew. Math. Mech.* **1**, 125-138 and 218-219.

ORR, W. M'F. 1907 The stability or instability of the steady motions of a perfect liquid and a viscous liquid. *Proc. Roy. Irish Acad.* A**27**, 9-27 and 69-138.

ORSZAG, S. A. 1971 Accurate solution of the Orr-Sommerfeld stability equation. *J. Fluid Mech.* **50**, 689-703.

ORSZAG, S. A. & PATERA, A. T. 1981 Subcritical transition to turbulence in planar shear flows. In *Transition and turbulence* (ed. R. E. Meyer) p. 127-146. Academic Press.

ORSZAG, S. A. & PATERA, A. T. 1983 Secondary instability of wall-bounded shear flows. *J. Fluid Mech.* **128**, 347-385.

PATEL, V. C. & HEAD, M. R. 1969 Some observations on skin friction and velocity profiles in fully developed pipe and channel flows. *J. Fluid Mech.* **38**, 181-201.

PEKERIS, C. L. & SHKOLLER, B. 1967 Stability of plane Poiseuille flow to periodic disturbances of finite amplitude in the vicinity of the neutral curve. *J. Fluid Mech.* **29**, 31-38.

REYNOLDS, O. 1883 An experimental investigation of the circumstances which determine whether the motion of water shall be direct or sinuous, and of the law of resistance in parallel channels. *Phil. Trans. Roy. Soc. London* **174**, 935-982.

REYNOLDS, W. C. & POTTER, M. C. 1967 Finite-amplitude instability of parallel shear flows. *J. Fluid Mech.* **27**, 465-492.

SCHENSTED, I. V. 1961 Contributions to the theory of hydrodynamic stability. PhD thesis, University of Michigan, USA.

SOMMERFELD, A. 1908 Ein Beitrag zur hydrodynamischen Erklärung der turbulenten Flüssigkeitsbewegung. *Proceedings 4th International Congress of Mathematicians*, Rome, III p. 116-124.

SQUIRE, H. B. 1933 On the stability for three-dimensional disturbances of viscous fluid flow between parallel walls. *Proc. Roy. Soc. London* **A142**, 621-628.

STUART, J. T. 1958 On the nonlinear mechanics of hydrodynamic stability. *J. Fluid Mech.* **4**, 1-21.

STUART, J. T. 1960 On the nonlinear mechanics of wave disturbances in stable and unstable parallel flows: Part 1. *J. Fluid Mech.* **9**, 353-370.

STUART, J. T. 1965 The production of intense shear layers by vortex stretching and convection. *AGARD* Report **514**.

THOMAS, L. H. 1953 The stability of plane Poiseuille flow. *Phys. Rev.* **91**, 780-783.

WATSON, J. 1960 On the nonlinear mechanics of wave disturbances in stable and unstable parallel flows: Part 2. *J. Fluid Mech.* **9**, 371-389.

Zahn, J.-P., Toomre, J., Spiegel, E. A. & Gough, D. O. 1974 Nonlinear cellular motions in Poiseuille channel flow. *J. Fluid Mech.* **64**, 319-345.

Appendices

"... Some things you *can't* find out; but you will never know you can't by guessing and supposing: no, you have to be patient and go on experimenting until you find out that you can't find out...... By experiment I know that wood swims, and dry leaves, and feathers, and plenty of other things; therefore by all that cumulative evidence you know that a rock will swim; but you have to put up with simply knowing it, for there isn't any way to prove it - up to now. But I shall find a way..."

- MARK TWAIN, 1905 (*Eve's Diary*)

Paper I

J. Fluid Mech. (1989), *vol.* 201, *pp.* 13–34
Printed in Great Britain

Degeneracies of the temporal Orr–Sommerfeld eigenmodes in plane Poiseuille flow

By RAJARATNAM SHANTHINI
Division of Fluid Mechanics, Luleå University of Technology, S-951 87 Luleå, Sweden

(Received 21 April 1988)

Degenerating stable temporal Orr–Sommerfeld eigenmodes are studied for plane Poiseuille flow. The discrete spectrum of the eigenmodes is shown to possess infinitely many degeneracies, each appearing at a certain combination of k (the modulus of resultant wavenumber) and αR (the streamwise wavenumber time the Reynolds number). The eigenmodes are found to degenerate in a specific manner which confines the streamwise phase velocities of the degeneracies to be around $\frac{2}{3}$ of the centreline velocity. The responses of the degeneracies are investigated through the initial-value problem. The responses of the first four symmetric and the first two antisymmetric degeneracies are evaluated numerically for arbitrary initial disturbances expanded in terms of Chebyshev polynomials. The first symmetric and the first antisymmetric degeneracies exhibit temporal growth of the amplitudes in the wavenumber space. The maximum amplitudes are at most 7 times larger than the corresponding initial amplitudes. The amplitudes of the responses of the other four degeneracies decay rapidly owing to their higher damping rates. The time for which the degeneracy-response is in the growing phase is shown to be stretched with increasing Reynolds number. The degeneracies can therefore be active for longer periods of time at larger Reynolds numbers.

1. Introduction

The simplest approach to the question of laminar to turbulence transition in parallel shear flows is that by Orr & Sommerfeld (see e.g. Drazin & Reid 1981). For plane Poiseuille flow, the traditional two-dimensional investigations on the linear stability of the temporal Orr–Sommerfeld (OS) eigenmodes predict the critical Reynolds number R to be 5772.22 (Orszag 1971), where R is based on the centreline velocity and the channel half-height. Recent experiments on plane Poiseuille flow (Carlson, Widnall & Peters 1982; Alavyoon, Henningson & Alfredsson 1986) have shown that the initial stages of transition are accompanied by localized regions of turbulence known as turbulent spots. According to the latter, these spots cannot be generated for $R < 1100$, whichever the disturbance is, whereas for $R > 2200$, which is obviously an apparatus-dependent value, the turbulent spots appear randomly without the use of external excitation. The experimental transition R is hence much lower than the theoretical prediction for instability. Nevertheless, according to the above experiments, the turbulent spots are accompanied by strong oblique linear waves, suggesting the validity of the linear stability approach at least in some parts of the spot environment.

Extensive numerical computations of the Orr–Sommerfeld (OS) equation (Orszag 1971; Mack 1976) have shown that the major part of the temporal eigenmodes is stable, leading to exponential decay in time, and therefore, in general, considered unimportant from the transition point of view. Detailed mappings of these stable eigenmodes, as carried out in this study, have revealed the interesting feature of degeneracy, i.e. two simple OS modes coalesce to form a single OS mode of order 2. Degeneracy can possibly lead to algebraic growth for a short initial period followed by eventual decay. This and other related features of importance, discussed in §2.2, are the main focuses of this study.

The earliest reference to degenerating eigenmodes seems to have appeared in the PhD thesis of Schensted (1961). Even though she did not consider this phenomenon to be probable in systems such as plane Poiseuille flow, she studied some of the mathematical consequences of degeneracy. Later, Betchov & Criminale (1966) came across a few pairs of coalescing eigenmodes, unexpectedly as claimed, in their calculations concerning combined stability problems, in space and time, of the inviscid laminar jet and wake. Gaster (1968) showed, by considering the analyticity of the characteristic function determining the eigenvalues, why eigenmodes of order 2 (i.e. degeneracies) *must* occur. He also analysed the influence of such modes on the perturbation generated by a pulse input. In the inviscid laminar jet and wake cases, the results seemed not in favour of the time-growing instability. Degeneracies among stable spatial OS eigenmodes in plane Poiseuille flow as well as in boundary-layer type mean flows were recently analysed by Koch (1986). He assessed the physical relevance of a degenerated mode pair by the inverse of the corresponding spatial damping rate. According to Koch, the spatial degeneracy mechanism plays a passive role in the laminar-to-turbulence transition in plane Poiseuille flow and an active role in boundary-layer type flows.

Degeneracies among stable temporal OS eigenmodes in plane Poiseuille flow are of concern in the present paper. A methodical search for these degenerating eigenmodes (§3) and their responses (§4) are the objectives of the study. The excitation of the degeneracies is studied through the initial-value problem, which seems well suited for the purpose, and the formulation of the problem follows somewhat that of Gustavsson (1986). The analyses are carried out in three-dimensional space, and thereby the obliquity of the linear waves is accounted for.

2. Analysis

2.1. *Problem formulation*

For plane Poiseuille flow, the evolution of the non-dimensionalized vertical component, $v(x, y, z, t)$, of a small three-dimensional perturbation velocity field is governed by the linearized equation

$$\left(\frac{\partial}{\partial t}+U\frac{\partial}{\partial x}\right)\nabla^2 v-U''\frac{\partial v}{\partial x}=\frac{1}{R}\nabla^4 v. \tag{1}$$

This equation has been rendered non-dimensional with channel half-height h and centreline velocity U_0 as the characteristic length and velocity scales. The Reynolds number is defined as $R = U_0 h/\nu$, where ν is the kinematic viscosity. x, y and z are the non-dimensional streamwise, vertical and spanwise directions, respectively. The dimensionless steady basic velocity profile is parabolic and is given by $U = 1-y^2$, and therefore $U'' = -2$, where the prime denotes the y-derivative. ∇^2 denotes the Laplacian. Solid walls, extending to infinity in the x- and z-directions, bound the flow at $y = \pm 1$. Thus the impermeable and no-slip conditions at the wall boundaries yield

$$v=\frac{\partial v}{\partial y}=0 \quad \text{at} \quad y=\pm 1. \tag{2}$$

Double Fourier transformation of $v(x, y, z, t)$ on the homogeneous spatial coordinates x and z, with real positive wavenumbers α and β, respectively, and Laplace transformation on the time coordinate t, with complex s, transform (1) to

$$(\mathrm{D}^2-k^2)^2\phi - \mathrm{i}\alpha R\left(U+\frac{s}{\mathrm{i}\alpha}\right)(\mathrm{D}^2-k^2)\,\phi + \mathrm{i}\alpha R U''\phi = -R\Delta. \tag{3}$$

Here $\mathrm{D} = \mathrm{d}/\mathrm{d}y$, $k^2 = \alpha^2+\beta^2$, and the forcing function Δ is given by

$$\Delta = \left(\frac{\partial^2}{\partial y^2}-k^2\right)\hat{v} \quad \text{at} \quad t = 0, \tag{4}$$

where $\hat{v} = \hat{v}(\alpha, y, \beta, t)$ and $\phi = \phi(\alpha, y, \beta, s)$. By the transformation

$$s = -\mathrm{i}\alpha c, \tag{5a}$$

the homogeneous operator of (3) is identified with the traditional OS operator. Yet another transformation

$$c' = c+\mathrm{i}\frac{k^2}{\alpha R} \tag{5b}$$

is carried out in order to avoid the computational difficulties due to the presence of k^4 term in (3), at large values of k. Consequently (3) can be rewritten as

$$(\mathrm{D}^2-k^2)\,\mathrm{D}^2\phi - \mathrm{i}\alpha R(U-c')(\mathrm{D}^2-k^2)\,\phi + \mathrm{i}\alpha R U''\phi = -R\Delta, \tag{6a}$$

and the boundary condition (2) as

$$\phi = \mathrm{D}\phi = 0 \quad \text{at} \quad y = \pm 1, \tag{6b}$$

where $\phi = \phi(\alpha, y, \beta, c')$.

The formal solution to (6a, b) obtained by the method of variation of parameters is given as (compare with Gustavsson 1986)

$$\phi = -R\left\{F_r+\frac{F_{13}}{E_{13}}+\frac{F_{24}}{E_{24}}\right\}, \tag{7a}$$

where

$$\begin{aligned} F_r(y) = {} & \phi_1(y)\left\{\int_0^y K_1(\eta)\,\Delta(\eta)\,\mathrm{d}\eta-\int_0^1 K_1(\eta)\,\Delta_s(\eta)\,\mathrm{d}\eta\right\}, \\ & +\phi_3(y)\left\{\int_0^y K_3(\eta)\,\Delta(\eta)\,\mathrm{d}\eta-\int_0^1 K_3(\eta)\,\Delta_s(\eta)\,\mathrm{d}\eta\right\} \\ & +\phi_2(y)\left\{\int_0^y K_2(\eta)\,\Delta(\eta)\,\mathrm{d}\eta-\int_0^1 K_2(\eta)\,\Delta_a(\eta)\,\mathrm{d}\eta\right\} \\ & +\phi_4(y)\left\{\int_0^y K_4(\eta)\,\Delta(\eta)\,\mathrm{d}\eta-\int_0^1 K_4(\eta)\,\Delta_a(\eta)\,\mathrm{d}\eta\right\}, \end{aligned} \tag{7b}$$

$$\begin{aligned} F_{13}(y) = {} & -\phi_1(y)\int_0^1 \{E_{23}K_2(\eta)+E_{43}K_4(\eta)\}\,\Delta_s(\eta)\,\mathrm{d}\eta \\ & -\phi_3(y)\int_0^1 \{E_{12}K_2(\eta)+E_{14}K_4(\eta)\}\,\Delta_s(\eta)\,\mathrm{d}\eta \end{aligned} \tag{7c}$$

and

$$\begin{aligned} F_{24}(y) = {} & -\phi_2(y)\int_0^1 \{E_{14}K_1(\eta)+E_{34}K_3(\eta)\}\,\Delta_a(\eta)\,\mathrm{d}\eta \\ & -\phi_4(y)\int_0^1 \{E_{21}K_1(\eta)+E_{23}K_3(\eta)\}\,\Delta_a(\eta)\,\mathrm{d}\eta. \end{aligned} \tag{7d}$$

$\{\phi_\nu\}_{\nu=1}^4$ are the linearly independent solutions to the fourth-order linear homogeneous operator of (6a). (This operator will be referred to as the (reduced) OS operator.) $\{K_\nu\}_{\nu=1}^4$ are the cofactors of $\{\phi_\nu'''\}_{\nu=1}^4$, respectively, in the matrix

$$\bar{\boldsymbol{W}}(y) = \begin{bmatrix} \phi_1 & \phi_2 & \phi_3 & \phi_4 \\ \phi_1' & \phi_2' & \phi_3' & \phi_4' \\ \phi_1'' & \phi_2'' & \phi_3'' & \phi_4'' \\ \phi_1''' & \phi_2''' & \phi_3''' & \phi_4''' \end{bmatrix}. \tag{8}$$

By successive differentiations of K_ν with respect to y, it can be shown that $\{K_\nu\}_{\nu=1}^4$ are the linearly independent solutions to the adjoint of the (reduced) OS operator and thus satisfy

$$(\mathrm{D}^2-k^2)\,\mathrm{D}^2K_\nu - \mathrm{i}\alpha R(U-c')(\mathrm{D}^2-k^2)K_\nu - 2\mathrm{i}\alpha RU'\mathrm{D}K_\nu = 0. \tag{9}$$

Since the (reduced) OS operator is symmetric in y, two of the four ϕ_ν, ϕ_1 and ϕ_3, are chosen to be symmetric and the other two, ϕ_2 and ϕ_4, antisymmetric with respect to $y=0$. Therefore the functions ϕ_ν and their y-derivatives, at $y=0$, are chosen such that

$$\bar{\boldsymbol{W}}(y=0) = \text{Identity matrix}. \tag{10a}$$

The values of K_ν and their y-derivatives, at $y=0$, are then calculated to be

$$\left.\begin{array}{cccccc} \nu & = & 1 & 2 & 3 & 4 \\ K_\nu & & 0 & 0 & 0 & 1 \\ K_\nu' & & 0 & 0 & -1 & 0 \\ K_\nu'' & & 0 & 1 & 0 & k^2+\mathrm{i}\alpha R(1-c') \\ K_\nu''' & & -1 & 0 & -k^2-\mathrm{i}\alpha R(1-c') & 0 \end{array}\right\} \tag{10b}$$

The forcing function Δ can conveniently be split into symmetric and antisymmetric parts, Δ_s and Δ_a, as $\Delta = \Delta_s + \Delta_a$. Finally,

$$E_{mn} = \phi_m\phi_n' - \phi_m'\phi_n \quad \text{at} \quad y=1 \quad (m,n=1,2,3,4). \tag{11}$$

At a prescribed $k-\alpha R$ combination, the poles of ϕ in the c'-plane, see (7a), are the zeros of the characteristic function $E(c',k,\alpha R)=0$, where

$$E = E_{13} = (\phi_1\phi_3' - \phi_1'\phi_3) = 0 \quad \text{at} \quad y=\pm 1 \tag{12a}$$

in the symmetric case, and

$$E = E_{24} = (\phi_2\phi_4' - \phi_2'\phi_4) = 0 \quad \text{at} \quad y=\pm 1 \tag{12b}$$

in the antisymmetric case.

Equations (12a,b) are the relations that determine the temporal (reduced) OS eigenvalues in the theory of normal modes. Thus a pole in the solution of the initial-value problem and an eigenvalue in the theory of normal modes refer to the same entity. The temporal eigenvalues (or the poles) c' of plane Poiseuille flow are purely discrete and infinite in number (Schensted 1961). With one exception, these eigenvalues lie in the fourth quadrant of the c'-plane up to about $\alpha R = 10000$, according to the numerical calculations of Orszag (1971) and Mack (1976). At some $k-\alpha R$ combinations, two of the simple eigenvalues degenerate into one, thus leading to an eigenvalue of order 2 (or a double pole). At these critical points, not only $E=$

0 but also $\partial E/\partial c' = 0$. Double poles occur in a systematic manner which is described in detail in §3. The consequences of the occurrences of the double poles are considered next.

2.2. *Response of a double pole*

For a prescribed $k-\alpha R$ combination and a specified forcing function Δ, the evaluation of the components of ϕ of $(7a)$ is a matter of straightforward numerical computations. However ϕ, being in the Fourier–Laplace space, is not informative enough. Since the explicit time dependence is of major interest, $\hat{v}$ is recovered upon Laplace inversion of ϕ according to

$$\hat{v}(\alpha, y, \beta, t) = \frac{1}{2\pi i}\int_{\gamma-i\infty}^{\gamma+i\infty} \phi(\alpha, y, \beta, s)\, e^{st}\, ds. \tag{13}$$

From the relations $(5a, b)$,

$$s = -\alpha\left[ic' + \frac{k^2}{\alpha R}\right].$$

Thus the integration in (13) is transformed to

$$\hat{v}(\alpha, y, \beta, t) = \frac{-i\alpha}{2\pi i}\int_{\infty+il}^{-\infty+il} \phi(\alpha, y, \beta, c')\exp\left[-\left(ic' + \frac{k^2}{\alpha R}\right)\alpha t\right]dc', \tag{14}$$

where $l = (\gamma/\alpha) + (k^2/\alpha R)$, and γ is so chosen that $c' = il$ lies above all the poles of ϕ.

The line integral of (14) can be transformed to a closed contour integral along contour Γ, which encloses all the poles of ϕ, provided the integrand in (14) integrated along Γ_r vanishes. Here Γ_r is a contour with infinite extensions, used for completing the contour Γ. Following the arguments of Schensted (1961), ϕ can be shown to be analytic everywhere except at its poles. Consequently, using the Residue theorem, the integration to be performed, after substituting ϕ of $(7a)$, is the following:

$$\hat{v}(\alpha, y, \beta, t) = \frac{i\alpha R}{2\pi i}\sum_{j=1}^{\infty}\left\{\int_{\Gamma_j}\left[\frac{F_{13}}{E_{13}} + \frac{F_{24}}{E_{24}}\right]\exp\left[-\left(ic' + \frac{k^2}{\alpha R}\right)\alpha t\right]dc'\right\}, \tag{15}$$

where the contour Γ_j, with infinitesimally small radius, encircles the isolated pole c'_j in the same sense as the contour Γ.

The contribution to $\hat{v}$ by an isolated pole $c'_0 (= c'_j)$ is then

$$\hat{v}\,|_{c'_0} = \frac{i\alpha R}{2\pi i}\int_{\Gamma_0}\frac{F}{E}\exp\left[-\left(ic' + \frac{k^2}{\alpha R}\right)\alpha t\right]dc', \tag{16}$$

where F and E represent F_{13} and E_{13} in the symmetric case, and F_{24} and E_{24} in the antisymmetric case.

If c'_0 is a *simple pole*, by use of the Cauchy Integral formula, we obtain

$$\hat{v}\,|_{c'_0} = i\alpha R\left[\frac{F}{\partial E/\partial c'}\right]_{c'_0}\exp\left[-\left(ic'_0 + \frac{k^2}{\alpha R}\right)\alpha t\right]. \tag{17}$$

when $c'_{i0} - (k^2/\alpha R) < 0$, $\hat{v}\,|_{c'_0}$ decays exponentially with time. Since all the poles considered in this study are of this type, the simple pole cases are of no interest.

If c'_0 is a *double pole*, the Cauchy Integral formula yields

$$\hat{v}\,|_{c'_0} = i\alpha R\frac{\partial}{\partial c'}\left\{\frac{F}{E}(c' - c'_0)^2\exp\left[-\left(ic' + \frac{k^2}{\alpha R}\right)\alpha t\right]\right\}_{c'_0}. \tag{18}$$

Considering the fact that both E and $\partial E/\partial c'$ vanish at the double pole and using Taylor series expansions of E and $\partial E/\partial c'$ about the double pole, (18) can be rewritten as

$$\hat{v}|_{c_0'} = \mathrm{i}\alpha R[r\,\mathrm{e}^{\mathrm{i}\theta}(\alpha t)+\rho\,\mathrm{e}^{\mathrm{i}\zeta}]\exp\left[-\left(\mathrm{i}c_0'+\frac{k^2}{\alpha R}\right)\alpha t\right], \tag{19a}$$

where

$$r\,\mathrm{e}^{\mathrm{i}\theta} = -\mathrm{i}\left[\frac{F}{G}\right]_{c_0'}, \qquad \rho\,\mathrm{e}^{\mathrm{i}\zeta} = \left[\frac{\partial F/\partial c'}{G}-\frac{FG_c}{G^2}\right]_{c_0'}, \tag{19b, c}$$

$$G = \frac{1}{2}\frac{\partial^2 E}{\partial c'^2}, \qquad G_c = \frac{1}{6}\frac{\partial^3 E}{\partial c'^3}. \tag{19d}$$

$\hat{v}|_{c_0'}$ is a function of y and αt. The time development of the amplitude R_r of $\hat{v}|_{c_0'}$ becomes

$$R_r = \alpha R[r^2(\alpha t)^2+2r\rho\cos(\theta-\zeta)(\alpha t)+\rho^2]^{\frac{1}{2}}\exp[c_{10}(\alpha t)], \tag{20}$$

where $c_{10} = c_{10}'-(k^2/\alpha R)$ from (5b), and $c_{10} < 0$ at the double poles investigated in this study.

It is seen from (20) that $R_r = \alpha R\rho$ at $\alpha t = 0$ and that R_r decays exponentially to zero as $\alpha t\rightarrow\infty$. The behaviour of R_r in the interval $\alpha t = 0$ to ∞ is crucially determined by the initial slope

$$\left.\frac{\partial R_r}{\partial(\alpha t)}\right|_{\alpha t=0} = \alpha R\rho\left[\frac{r}{\rho}\cos(\theta-\zeta)+c_{10}\right]. \tag{21}$$

Three cases are of particular interest.

Case (a). When $(r/\rho)\cos(\theta-\zeta) > -c_{10}$, the amplitude R_r grows with time for a short initial period and then decays to zero as shown in figure 1(a). The coordinate $(\alpha t, R_r)$ corresponding to the maximum point is given by

$$(\alpha t)_{\mathrm{m}} = \frac{-1}{c_{10}}\left[\frac{1+\Omega}{2}\right]-\frac{\rho}{r}\cos(\theta-\zeta) \tag{22a}$$

and

$$(R_r)_{\mathrm{m}} = -\alpha R\frac{r}{c_{10}}\left[\frac{1+\Omega}{2}\right]^{\frac{1}{2}}\exp[c_{10}(\alpha t)_{\mathrm{m}}], \tag{22b}$$

where

$$\Omega = \left[1-4c_{10}^2\frac{\rho^2}{r^2}\sin^2(\theta-\zeta)\right]^{\frac{1}{2}}. \tag{22c}$$

If $(R_r)_{\mathrm{m}}$ is large enough, the assumptions of the linear theory are violated and nonlinear effects may be initiated. The implications of such a state can only be analysed by nonlinear theories. On the other hand if $(R_r)_{\mathrm{m}}$ still lies within the range of the linear theory, the time taken for the maximum to be reached,

$$t_{\mathrm{m}} = \frac{(\alpha t)_{\mathrm{m}}}{\alpha R}R, \tag{23a}$$

plays an important role. Since αR is a given number for each double pole, increasing the Reynolds number stretches t_{m} so as to prolong the response of the double pole. Thus, the double pole acts almost as a neutrally stable mode, until $t = t_{\mathrm{m}}$, among the other exponentially decaying simple poles.

Case (b). When $(r/\rho)\cos(\theta-\zeta) \leqslant -c_{10}$ and $\Omega^2 \leqslant 0$, R_r monotonically decays in time

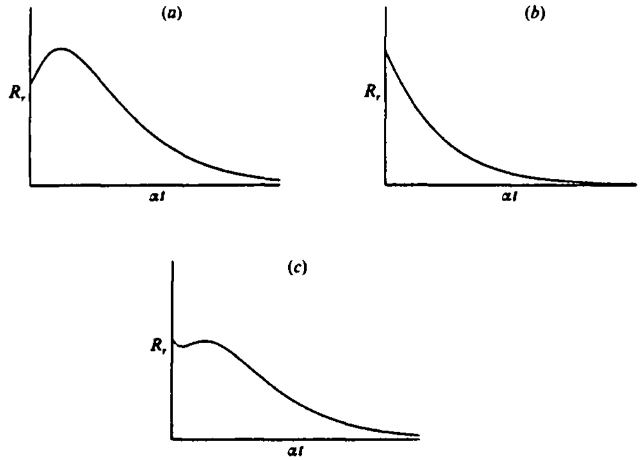

FIGURE 1. Temporal development of the amplitude R_r of the response $\hat{v}|_{c_0'}$ at a double pole. (*a*) Case (*a*); (*b*) case (*b*); (*c*) case (*c*).

as shown in figure 1(*b*). Since the decay is not purely exponential, the rate at which R_r decays is characterized by the time taken for, say, 25% decay of the initial amplitude $\alpha R\rho$,

$$t_d = \frac{(\alpha t)_d}{\alpha R} R, \tag{23b}$$

where $(\alpha t)_d$ is the positive solution to the nonlinear equation

$$(0.75\rho)^2 = \{r^2(\alpha t)_d^2 + 2r\rho\cos(\theta-\zeta)(\alpha t)_d + \rho^2\}\exp\{2c_{i0}(\alpha t)_d\}. \tag{24}$$

The Reynolds number, in this case, stretches t_d so as to slow down the decay rate of R_r. This time-stretching effect, even though also present in the simple-pole cases, can be more pronounced in the double-pole cases since the decay of the double-pole response is not purely exponential at finite αt-values.

Case (*c*). When $(r/\rho)\cos(\theta-\zeta) \leqslant -c_{i0}$ and $\Omega^2 > 0$, an interesting possibility occurs. Under these conditions, the αt-values at which $\partial R_r/\partial(\alpha t) = 0$, are either both negative or both positive. Of these two cases, the former is equivalent to case (*b*) in the positive-αt range. In the latter, as αt increases from zero, R_r experiences two extrema, a minimum followed by a maximum, and then eventually decays to zero, as shown in figure 1(*c*). The maximum point is expressed by $(\alpha t)_m$ and $(R_r)_m$ of (22*a*, *b*). Unlike in case (*a*), $(R_r)_m$ may or may not be larger than the initial amplitude $\alpha R\rho$. Consequently the time, which characterizes the temporal behaviour of R_r, is taken to be t_m of (23*a*) if $(R_r)_m \geqslant 0.75\alpha R\rho$ and to be t_d of (23*b*) if otherwise.

Apart from stretching the characteristic time, increasing R also increases β until $\beta = k$, as k and αR are constants at a double pole. In addition, since $\alpha \to 0$ as $R \to \infty$, structures elongated in the streamwise direction will be excited.

Which of the cases (*a*–*c*) will actually occur is discussed in §4.

3. The OS eigenmode structure and the degenerating pattern

3.1. *Numerical method*

Poles or (reduced) eigenvalues c' were evaluated, at prescribed k and αR, by numerically solving the (reduced) OS equation

$$(\mathrm{D}^2-k^2)\,\mathrm{D}^2\phi_\nu-\mathrm{i}\alpha R(U-c')(\mathrm{D}^2-k^2)\,\phi_\nu+\mathrm{i}\alpha R U''\phi_\nu=0, \tag{25}$$

with the condition that $\{\phi_\nu\}_{\nu=1}^{4}$ should satisfy the eigenvalue relation $E_{13}=0$ or $E_{24}=0$ at the wall $y=1$ (see (12*a*, *b*)). Adams interpolation formula with four steps was used for numerical integration of (25). Integration was started at the centreline $y=0$, with the values of ϕ_ν and their y-derivative specified by (10*a*), and proceeded towards the wall. Taylor expansion was used to evaluate the starting solutions at two backward points. The Gram–Schmidt orthogonalization procedure was used to eliminate the round-off error problem in cases where the growth of the solutions was so large as to destroy the eigenfunctions. Initially guessed values of c' were geared to convergence by the Secant method. This numerical scheme was adapted from that of Gustavsson (1981). The accuracy of the scheme was assured by comparing the calculated eigenvalues with those of Orszag (1971) and Mack (1976). Excellent agreement was observed with all but the unstable eigenvalue, which hardly converged. An increasing number of integration steps, between $y=0$ and $y=1$, were required for the convergence of c' as c'_i (the imaginary c') approached zero. In addition, convergence in this region demanded frequent orthogonalization steps when c'_r (the real c') was in the range of 0 to about $\frac{2}{3}$ and almost no orthogonalization when c'_r was in the range of about $\frac{2}{3}$ to unity.

3.2. *General behaviour of the eigenmodes*

The first set of eigenvalues were obtained at $k=0$ and at non-zero αR. This $k-\alpha R$ combination is physically absurd, but it served as a good starting point. Asymptotic expressions of the eigenvalue spectra at small αR-values, derived using regular perturbation expansions (see e.g. Drazin & Reid 1981, p. 158), at $k=0$ are

$$c'=\left(\frac{2}{3}-\frac{5}{2p_n^2}\right)-\mathrm{i}\left(\frac{p_n^2}{\alpha R}\right) \quad (n=0,2,4,\ldots),$$

with $p_n=(n+2)\pi/2$, in the symmetric case, and

$$c'=\left(\frac{2}{3}+\frac{5}{6q_n^2}\right)-\mathrm{i}\left(\frac{q_n^2}{\alpha R}\right) \quad (n=1,3,5,\ldots),$$

with $q_n \approx 1.430\pi,\ 2.459\pi,\ 3.471\pi, \ldots, \sim (n+2)\pi/2$ for larger n, in the antisymmetric case.

At $k=0$ and $\alpha R=25$, the eigenmodes are highly damped, and their streamwise phase velocities approach $\frac{2}{3}$ of the centreline velocity as the mode number increases. The eigenmodes have been numbered in the order of decreasing c'_i at a low αR-value. The locations of the symmetric (S) and the antisymmetric (A) eigenvalues in the c'-plane at $k=0$ and $\alpha R=5000$, traced by gradually increasing αR from about 25 to 5000, are shown in figures 2(*a*) and 2(*b*), respectively. As αR is increased from about 25 at $k=0$, the eigenvalues move in the direction of increasing c'_i, the higher modes moving almost along the S-branch (line $c'_r=\frac{2}{3}$), up to about $c'_i=-0.35$. With further increase in αR, the eigenvalues move either towards $c'=(1,0)$, that is along the P-branch, or towards the origin $c'=(0,0)$. In the latter direction, the symmetric

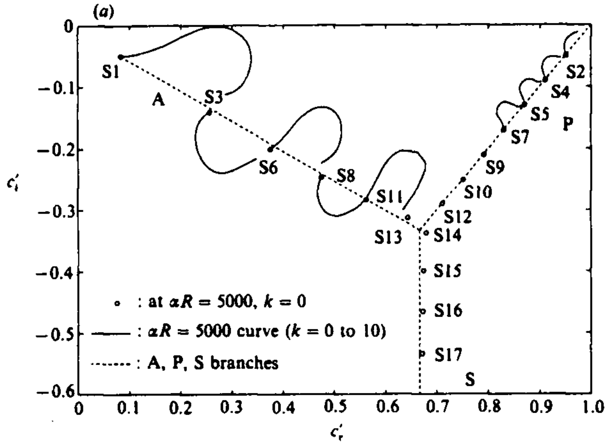

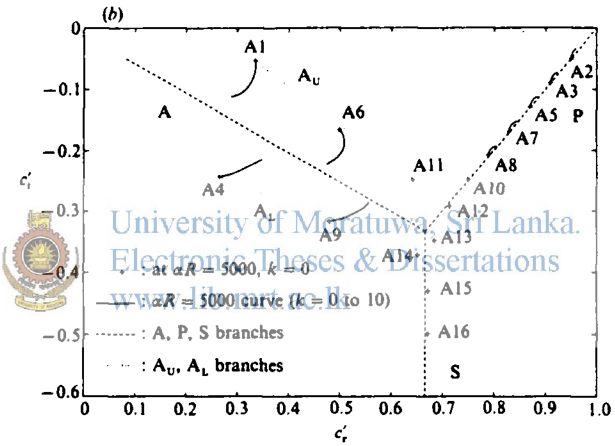

FIGURE 2. Locations of the least-damped OS (*a*) symmetric and (*b*) antisymmetric eigenmodes in the c'-plane, at $\alpha R = 5000$.

eigenvalues move along the A-branch whereas the antisymmetric eigenvalues move along the upper A-branch (A_U) or the lower A-branch (A_L). There exists a pattern in which the modes are distributed among the branches at increasing αR. This pattern, first found by Gustavsson (1986), is cyclic and has been confirmed in this study. The symmetric modes follow the order

$$A - P - A - P - P$$

for every 5-mode, and the antisymmetric modes follow the order

$$A_U - P - P - A_L - P$$

for every 5-mode. It is to be stressed here that even though the eigenmodes are grouped along three major branches A, P and S following the classification of Mack (1976), the grouping of this study has been carried out at $k = 0$, as in Gustavsson (1986), not at $k = 1$, as in Mack (1976).

As k increases from 0, the symmetric eigenvalues, which lie along the A-branch at $k = 0$ and at high αR ($= 5000$ in this case), move alternately to upper and lower sides of the A-branch, as shown in figure 2(a). With further increase in k, they curve back and move towards the A-branch. With increasing k, as shown in figure 2(b), the antisymmetric eigenvalues along the A_U and A_L branches at high αR ($= 5000$), also move towards the A-branch. Both the symmetric and antisymmetric eigenvalues along the P-branch at high αR curve back to the same branch in a simple manner, as k is increased. It is of relevance to realize that as $k \rightarrow \infty$, equation (25) approaches

$$D^2\phi_v - i\alpha R(U - c')\phi_v = 0.$$

This equation, with boundary conditions $\phi = 0$ at the wall $y = \pm 1$, yields the vertical vorticity eigenvalues which lie along the A, P and S branches. For more details about the vertical vorticity modes, the reader is referred to Gustavsson (1986).

In order to acquire a better insight into the behaviour of the eigenmodes, the first few of the symmetric as well as the antisymmetric eigenmodes are explored in detail in §§3.3 and 3.4.

3.3. *Symmetric modes*

Figure 3(a) shows how the eigenvalues corresponding to the first two symmetric modes S1 and S2 change their locations in the c'-plane with changing k and/or αR. Solid curves of figure 3(a) represent the $k = 0$ curves of both S1 and S2. The αR-curves of S1 are represented by the dashed curves and those of S2 by the dotted curves. (The curve along which k is a constant is referred to as the k-curve, and along which αR is a constant as the αR-curve.) The rings along each αR-curve represent $k = 2$, 3 and 10, respectively. When k increases from zero at constant αR, the higher αR ($= 500$ and 5000 for example)-curves of S1 curve back to the A-branch and those of S2 back to the P-branch, whereas the intermediate αR ($= 200$ and 100 for example)-curves extend across the c'-plane towards the opposite branch in either case. The αR-curves of both S1 and S2 not only characteristically change their shapes but also do so across the same range of αR. An enlarged view of this critical region, confined by the rectangle PQRS in figure 3(a), is given in figure 3(b) with a few more k-curves represented by solid lines. The $k = 2$ curve of S1 starting from $\alpha R = 200$ of S1 (point C) reaches $\alpha R = 500$ of S1 (point B), and then continue to move towards $c' = (0, 0)$ meeting the αR-curves of S1. The $k = 3$ curve of S1 starting from $\alpha R = 200$ of S1 (point D) reaches point E which lies on the $\alpha R = 500$ curve of S2 *not* of S1. With further increase in αR, this $k = 3$ curve moves towards $c' = (1, 0)$ meeting the αR-curves of S2, in contrast to the $k = 2$ curve of S1. Therefore one observes that the k-curves of S1 strikingly change their behaviour somewhere between $k = 2$ and $k = 3$ in the αR-range 200 to 500. Similar behaviour is also displayed by the k-curves of S2 as shown in figure 3(b), where points G, F, H and A are the counterparts of the points C, B, D and E, respectively.

The curious feature of figure 3(b) is what points A and E represent. Point A can represent either mode S1 at $k = 3$ and $\alpha R = 500$ or mode S2 at the same $k - \alpha R$ combination. The same is true for point E. These observations show that the modes S1 and S2, when put together, mutually complete each other. Consequently these modes lose or rather exchange their identities in the region enclosed by ABCDEFGHA in figure 3(b). The nature of this mode exchange suggests that it is connected with a mode coalescence, where two distinctly different eigenvalues degenerate into one single eigenvalue of order 2, i.e. to form a double pole. The k- and αR-ranges across which the eigenvalues degenerate are obviously the same ranges

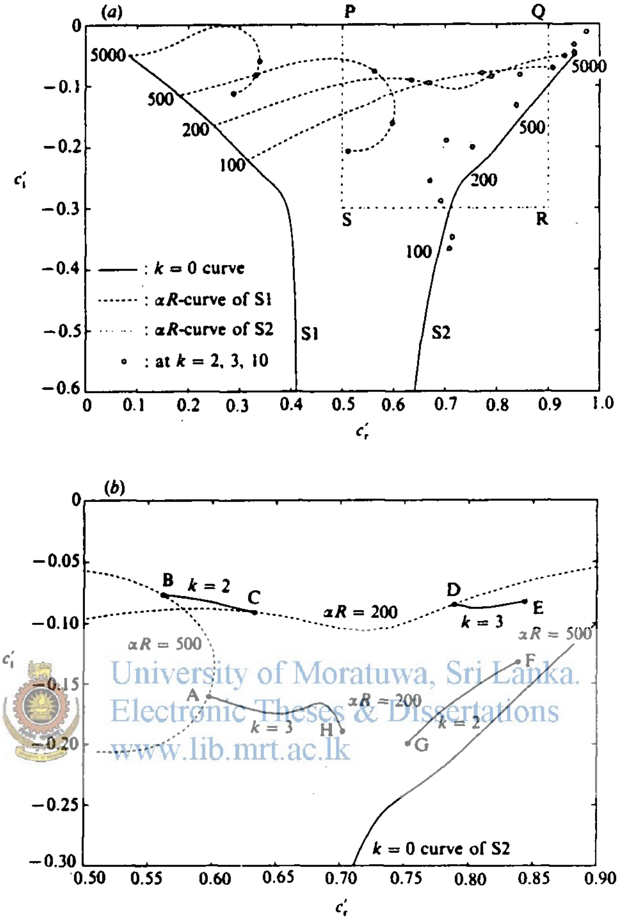

FIGURE 3. (*a*) Locations of the first two symmetric eigenmodes S1 and S2 in the c'-plane, and (*b*) a close look at the degenerating pattern, enlarged rectangle PQRS.

across which the k- and αR-curves significantly change their behaviour. Therefore the occurrence of a double pole and the k- and αR-ranges across which it occurs can easily be predicted by closely examining the detailed maps of the k- and αR-curves of the eigenmodes concerned.

Maps of the symmetric modes S3, S4 and S5 can be seen in figures 4(*a*), 4(*b*) and 4(*c*), respectively. The basic $k = 0$ curve and few αR-curves are shown. The maps of the first five symmetric modes S1 to S5 are different from each other; however, maps of the modes S6, S7, S8, S9 and S10, which are not produced in this paper, qualitatively resemble the maps of S1 to S5, respectively. This repetitive nature should not be surprising if one considers the cyclic nature in which the symmetric modes branch, as reported in §3.2.

The possible symmetric mode coalescences, obtained by carefully examining some of these maps, are reported in table 1. The degenerating mode pairs are joined by curves and the respective branches chosen by the modes at $k = 0$ are specified below

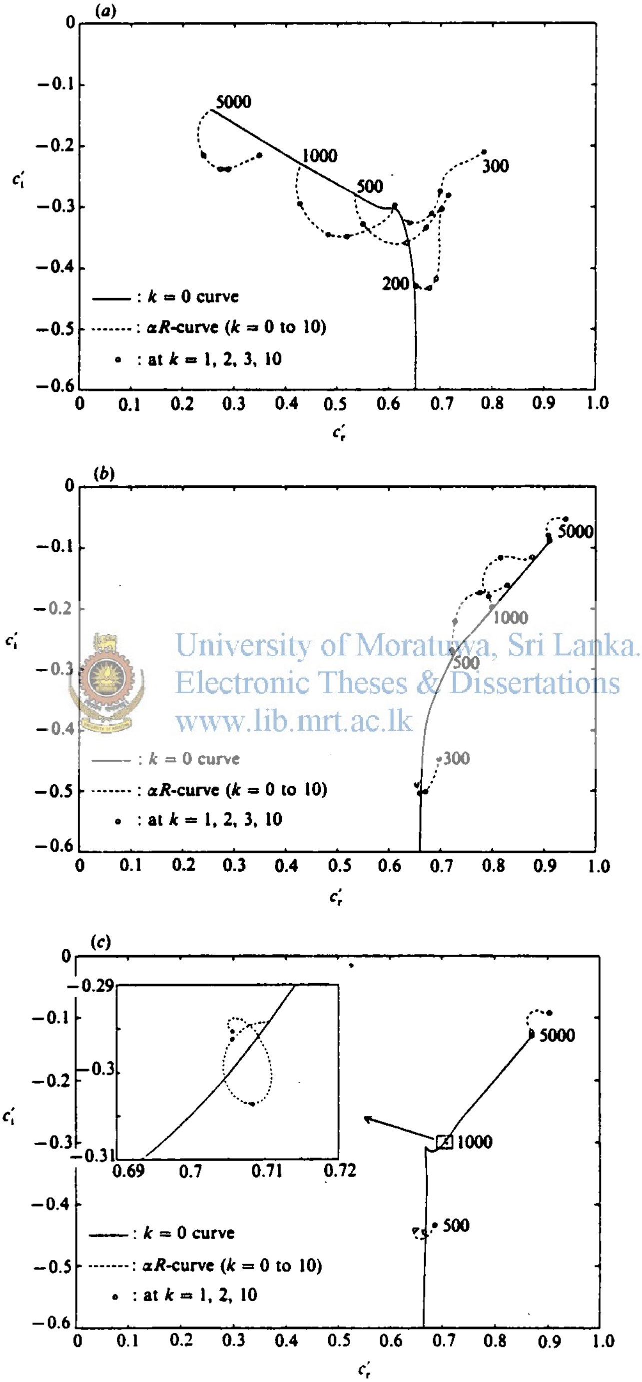

FIGURE 4. Locations of the symmetric modes (a) S3, (b) S4 and (c) S5 in the c'-plane.

Mode	S1	S2	S3	S4	S5	S6	S7	S8
Branch chosen at $k = 0$	A	P	A	P	P	A	P	A

TABLE 1. Degenerating symmetric mode pairs

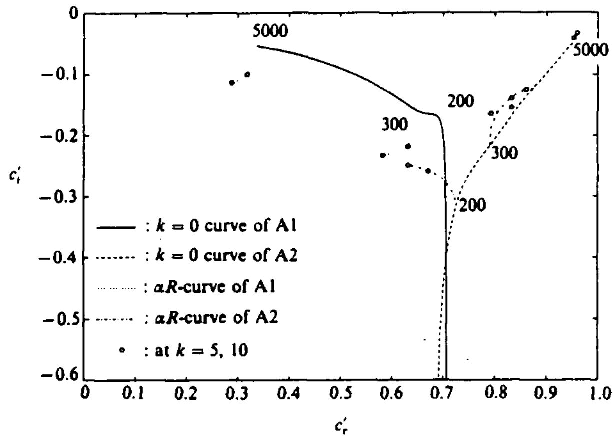

FIGURE 5. Degenerating pattern of the first two antisymmetric eigenmodes A1 and A2.

each mode. Table 1 provides a complete list of the degeneracies possible among the modes S1 to S7. The double curves between S5 and S6 reveal that it is possible for two modes to degenerate with each other more than once. Except for the bridging between modes S5 and S6, the pattern in which the modes degenerate seems to repeat for each 5-mode group, as indicated by table 1. The repetitive nature, already observed twice with the symmetric modes, strengthens the above speculation. Further discussion of the degeneracies follows a quick survey of the antisymmetric modes.

3.4. *Antisymmetric modes*

The first two antisymmetric eigenmodes A1 and A2 are shown in figure 5. The basic $k = 0$ curve and αR-curves at $\alpha R = 200$, 300 and 5000 of each mode are drawn. The characteristic changes in the shapes of αR-curves, shown in figure 5, and the associated k-curves behaviour are present with both A1 and A2. Consequently there is a degeneracy in the ranges $\alpha R = 200$–300 and $k = 0$–5.

Table 2 shows the degeneracies possible among modes A1 to A5. The fact that mode A3 does not degenerate at all can be explained by its map shown in figure 6, where the αR-curves of A3 more or less creep along the $k = 0$ curve. The k- and αR-curves of the antisymmetric modes, in general, span a smaller area of the c'-plane, as can be concluded from the maps of A1, A2 and A3 and the maps of A4 and A5, which are not produced here. This is probably why the number of degeneracies among the antisymmetric modes is comparatively smaller than the symmetric counterpart. In anticipation of a qualitative repetition of the maps as well as the degenerating pattern by each 5-mode group, no other antisymmetric modes were mapped.

Mode	A1	A2	A3	A4	A5
Branch chosen at $k = 0$	A_U	P	P	A_L	P

TABLE 2. Degenerating antisymmetric mode pairs

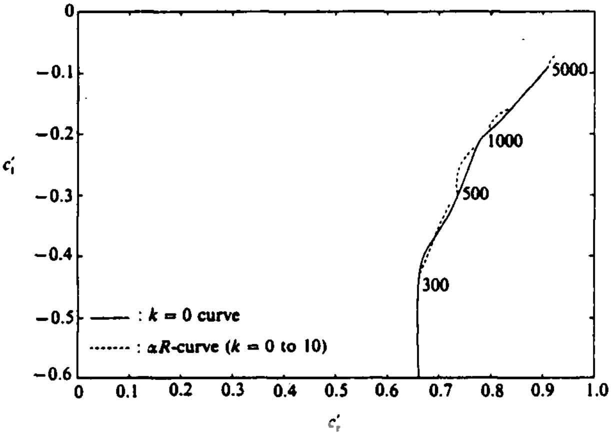

FIGURE 6. Location of the antisymmetric mode A3 in the c'-plane.

3.5. *Pin-pointing the double poles*

Having confined the first few degenerating mode pairs, we seek to pin-point the double poles with satisfactory accuracy. The poles c' are the zeros of the characteristic function $E(c', k, \alpha R)$, which is an entire function of c', k and αR. Its analytical properties can thus be exploited to obtain a dispersion relation in the vicinity of a double pole $(c_0', k_0, \alpha R_0)$. Both E and $\partial E/\partial c'$ are zero at a double pole so that a Taylor series expansion of E about such a point becomes

$$E(c', k, \alpha R) = (k-k_0)\frac{\partial E}{\partial k}\bigg|_0 + (\alpha R - \alpha R_0)\frac{\partial E}{\partial \alpha R}\bigg|_0 + (c'-c_0')^2\frac{\partial^2 E}{2\partial c'^2}\bigg|_0$$

$$+ (k-k_0)(c'-c_0')\frac{\partial^2 E}{\partial k\,\partial c'}\bigg|_0 + (\alpha R - \alpha R_0)(c'-c_0')\frac{\partial^2 E}{\partial \alpha R\,\partial c'}\bigg|_0 + \dots, \quad (26)$$

where $|_0$ represents the value at the double pole.

Since only the $(c', k, \alpha R)$ that are solutions to $E = 0$ are used in (26), $E(c', k, \alpha R)$ vanishes. Thus the dispersion relation obtained by the first approximation to (26) takes the following simple form:

$$(c'-c_0')^2 = A(k-k_0) + B(\alpha R - \alpha R_0), \quad (27)$$

where A and B are complex constants and can easily be deduced from (26).

The typical behaviour of the k- and αR-curves in the neighbourhood of a double pole is illustrated by figure 7, which displays the degenerating mode pair S1–S2. By knowing three points either along a constant αR-curve or along a constant k-curve, c_0' can readily be evaluated. With this c_0', and by exploiting the fact that the

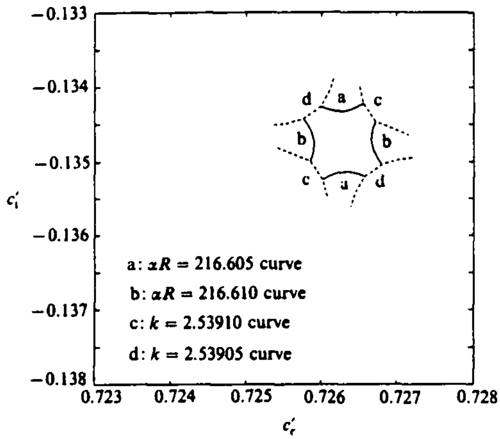

FIGURE 7. Behaviour of the degenerating modes S1 and S2 in the neighbourhood of the degeneracy S1–S2.

dispersion relation (27) is a mixture of real and complex entities, k_0 and αR_0 can easily be calculated. The reliance on these numerical values of c_0', k_0 and αR_0 to represent the double pole does of course increase as the curve concerned gets closer to the double pole. c_0' is then corrected by evaluating it from the eigenvalue relation $E = 0$, at the calculated k_0 and αR_0. The numerical zero of E is chosen to be $O(10^{-8})$. Since $\partial E/\partial c'$ also vanishes at the double pole, as a further check, $\partial E/\partial c'$ is numerically evaluated at the calculated c_0', k_0 and αR_0. Choosing a satisfactory numerical zero of $(\partial E/\partial c')|_{c_0'}$ can be achieved as follows. In the Taylor series expansion of E about the double pole, the terms $E|_{c_0'}$ and $(c'-c_0')(\partial E/\partial c')|_{c_0'}$ are dropped as they are identically zero. This step can numerically be justified when these terms are very small and of at least the same order. Since $E = O(10^{-8})$ and $(c'-c_0') \sim O(10^{-5})$, the numerical zero of $(\partial E/\partial c')|_{c_0'}$ can satisfactorily be chosen as $O(10^{-3})$. The dispersion calculations are repeated along curves closer and closer to the double pole until $(\partial E/\partial c')|_{c_0'}$ reaches the required order of magnitude. The $(c_0', k_0, \alpha R_0)$ at which it happens is taken to represent the double pole.

The major drawback in such a criterion to pin-point a double pole is the excessive number of eigenvalue computations required to pin-point one single double pole after it has been confined to coarse k- and αR-ranges. Dispersion relations obtained by higher approximations to the Taylor series expansion (26) seem to bring down the number of eigenvalue computations but, in reality, such relations led to either clumsy means or no means of pin-pointing c_0', k_0 and αR_0 and thus were discarded.

An elegant method of pin-pointing double zeros of a characteristic function has in fact been discussed by Gaster & Jordinson (1975). The function concerned was an analytical function of two complex variables, the streamwise wavenumber α and the frequency $\omega(=\alpha c)$. In the neighbourhood of the double zero, ω was expressed in terms of α as a sum of one regular series and the square-root of a second regular series. The rest of the calculations to pin-point the double zero was simple and rapid. An extension of such a method of series description to a more complicated problem, such as the one in this paper, is at the moment not clear. Nevertheless, an indirect and thus complicated way of employing the technique of Gaster & Jordinson to pin-point double zeros of a characteristic function in three variables has been discussed by

Mode pair	k_0	αR_0	c'_0	$R_{min} = \alpha R_0/K_0$	abs $(\partial E/\partial c')_{c'_0}$
		Symmetric degeneracies			
S1–S2	2.539076	216.6076	0.7263537 $-$ i0.1348152	85.3	0.0381
S3–S4	0.88582	363.7715	0.6406033 $-$ i0.3499482	410.6	0.0018
S3–S5	1.891178	527.6455	0.6357061 $-$ i0.3835066	279.0	0.0025
S5–S6	0.50635	904.2622	0.6691119 $-$ i0.3179580	1785.8	0.0028
		Antisymmetric degeneracies			
A1–A2	2.2574	230.29	0.7193432 $-$ i0.2073721	102.0	0.0031
A4–A5	2.8047	620.702	0.6444918 $-$ i0.3969629	221.3	0.0002

TABLE 3. The first four symmetric and the first two antisymmetric degeneracies pin-pointed in this study, see also figure 8

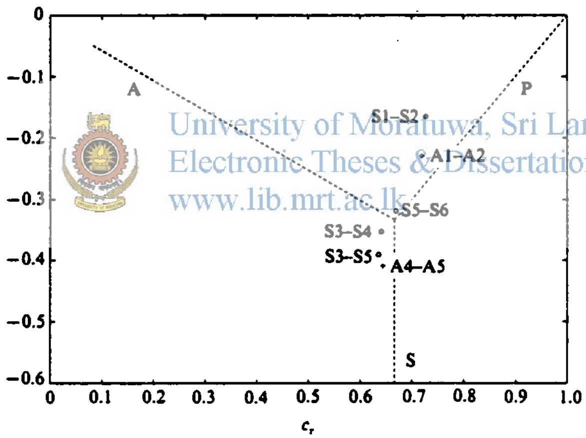

FIGURE 8. Locations of the first four symmetric (○) and the first two antisymmetric (+) degeneracies, listed in table 3, in the c-plane.

Koch (1986). However, we did not adapt Koch's procedure to our problem since Koch's method is not simpler than the method used in this work. A mathematically more elegant method of pin-pointing the double zeros of the characteristic function $E(c', k, \alpha R)$ is of interest since it will facilitate the analysis of more double poles of plane Poiseuille flow, and also the investigation of other flow systems, such as plane Couette flow.

The double poles pin-pointed in this study are listed in table 3 along with $R_{min} = \alpha R/k$ and the absolute value of $(\partial E/\partial c')|_{c'_0}$. It seems, from tables 1 and 2, that one necessary condition for two modes to degenerate is that at $k = 0$, one of these two modes should choose the A-branch and the other the P-branch. It is in the neighbourhood of the point where the S-branch splits into A and P branches that the αR-curves change shape. Hence, the eigenmodes always degenerate in this region as typically demonstrated by figure 8, in which the degeneracies are shown in the c-

plane (not in the c'-plane). As a consequence, the degeneracies have streamwise phase velocities around $\frac{2}{3}U_0$ and damping rates in the range of 0 to about $-\frac{1}{2}U_0$. Considering the repetitive nature of the eigenmode behaviour, it is reasonable to assume that there is an uncountable number of double poles occurring in the above-described region, among the infinitely many isolated poles of plane Poiseuille flow. A formal mathematical proof of this conjecture should be possible but it was not attempted in this work.

4. Excitation of degeneracies

In this section, we discuss the quantitative measures of the responses of the first few degeneracies listed in table 3, when subjected to external excitations. The contribution to $\hat{v}$ by a double pole c_0', written as $\hat{v}|_{c_0'}$, was derived in §2.2 and is expressed by (19*a–d*). Evaluation of $\hat{v}|_{c_0'}$ requires knowledge of F ((7*c*) or (7*d*)), E ((12*a*) or (12*b*)), and their derivatives with respect to c', at the double pole. Evaluation of F and E requires that the linearly independent solutions, $\{\phi_\nu\}_{\nu=1}^{4}$ and $\{K_\nu\}_{\nu=1}^{4}$, of the OS equation (25) and its adjoint equation (9) be known. These equations were thus solved by numerical methods similar to that described in §3.1. In addition, the forcing function Δ_b, where $b = \mathrm{s}$ in the symmetric case, and $b = \mathrm{a}$ in the antisymmetric case, should be specified. Δ, given by (4), is determined by $\hat{v}(t=0)$, the double Fourier-transformed vertical component of the *initial* perturbation velocity. For the sake of generality, the responses due to *any* but small disturbances are of interest. Therefore, $\hat{v}_b(t=0)$ is taken to be arbitrary and thus can be expanded in terms of a complete set of orthogonal symmetric (or antisymmetric) functions. This also applies to Δ_b. As a first attempt, Δ is expanded in terms of the Chebyshev polynomials of the first kind $\{T_n\}_{n=0}^{\infty}$ as

$$\Delta_{\mathrm{s}}(y) = \sum_{n=0,2,4,\ldots} b_n T_n(y) \tag{28a}$$

and

$$\Delta_{\mathrm{a}}(y) = \sum_{n=1,3,5,\ldots} b_n T_n(y), \tag{28b}$$

where

$$T_n(y) = \cos(n \cos^{-1} y). \tag{28c}$$

The symmetric polynomials are given by even n and the antisymmetric by odd n.

The responses due to different members of the Chebyshev family were independently investigated. With n specified for T_n, the integration in (7*c*) or (7*d*) was numerically performed using Simpson's extended rule. The c'-derivatives of F and E at the double pole c_0' were evaluated by perturbing the functions concerned about c_0' by a small amount $\delta_{c'}$ and then by using appropriate finite-difference formulas. The reliability of the numerical value of the derivative in question has been affirmed by carrying out numerical experiments with different lengths of $\delta_{c'}$ and in different directions. The numerical values of $r\,\mathrm{e}^{\mathrm{i}\theta}$ (19*b*) and $\rho\,\mathrm{e}^{\mathrm{i}\zeta}$ (19*c*) changed very little when the number of numerical steps between $y = 0$ and $y = 1$ were increased from 300 to 600 through 60 steps at a time. The amplitude R_r of (20), evaluated at different y-positions with specified αt, remained unchanged when Δ_b given by T_n, which is purely real, was replaced by $T_n\,\mathrm{e}^{\mathrm{i}\lambda}$, where λ was varied from 0 to 2π.

The first symmetric double pole S1–S2, when excited by the polynomial T_4, exhibits temporal growth of the amplitude R_r in the sense of cases (*a*) and (*c*) described in §2.2. Growth is observed around the centreline of the channel ($y = 0$) and is shown in figure 9, at chosen y-positions. The largest ratio of the maximum

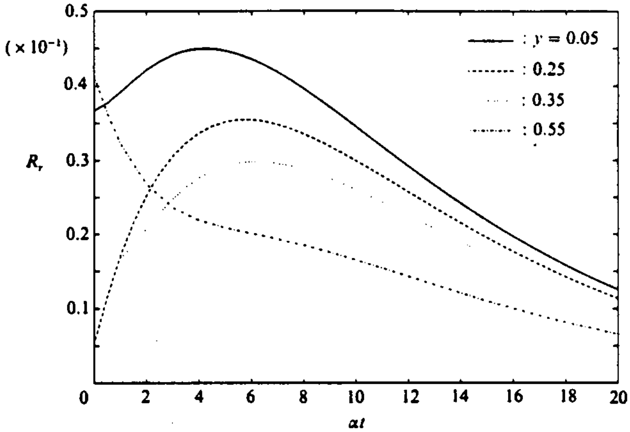

FIGURE 9. Temporal development of the amplitude R_r of the double pole S1–S2, at four different y-positions, when excited by T_4.

amplitude $(R_r)_m$ to the initial amplitude R_0 $(=\alpha R\rho)$, in this case, is about 6.605, occurring at $\alpha t = 5.743$, and is observed close to $y = 0.25$. However, the initial amplitude at $y = 0.05$, for instance, is greater than the maximum amplitude at $y = 0.25$, but the ratio of $(R_r)_m$ to R_0 at $y = 0.05$ is only 1.225. Thus, the chances of nonlinear consequences, initiated only by the magnitudes of $(R_r)_m$, seem slim in this case.

Nevertheless, the αt-values corresponding to $(R_r)_m$, at certain y-positions, suggest that the time-stretching phenomenon, discussed in §2.2, can be of importance. The (non-dimensional) time at which the maximum of R_r occurs at $y = 0.25$, for instance, is related to the Reynolds number, according to (23a), by

$$t_m = \frac{5.743}{216.6076} R = 0.0265R.$$

Despite of the smallness of the magnitude of (t_m/R), the characteristic time (t_m) spans the range 29.2 to 58.3 in the critical R range 1100–2200, discussed in the introduction. This means that the response of S1–S2, at $y = 0.25$, is in the growing phase until $t = 58.3$ at $R = 2200$, when excited by T_4. The numerical quantities above, however, should not be taken as final because T_4 alone is not Δ_s.

The first antisymmetric double pole A1–A2 also exhibits temporal growth in the sense of case (a), when excited by T_5. Growth is observed away from the centreline of the channel in contrast to that of S1–S2, and is shown in figure 10. The maximum amplitude at any y-position, in the case of A1–A2, does not exceed twice the corresponding initial amplitude.

The responses of S1–S2, when excited by the other symmetric Chebyshev polynomials, were also studied in detail and the results are demonstrated at a chosen y-position $(y = 0.25)$ in figure 11. Growth in the sense of case (a) is observed with T_4 as discussed earlier. $T_4 = 8y^4 - 8y^2 + 1$, bounded by ± 1, has two zero in the interval $y = [0, 1]$, and thus resembles a slightly distorted $\cos(2\pi y)$ function. Interestingly, the response of S1–S2 when excited by $\cos(2\pi y)$ is somewhat similar to the response due to T_4. The polynomials T_0 and T_2 give rise to higher initial

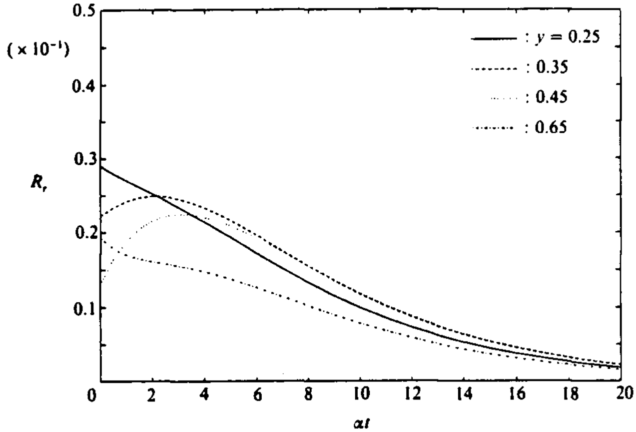

FIGURE 10. Temporal development of R_r of A1–A2, at four different y-positions, when excited by T_5.

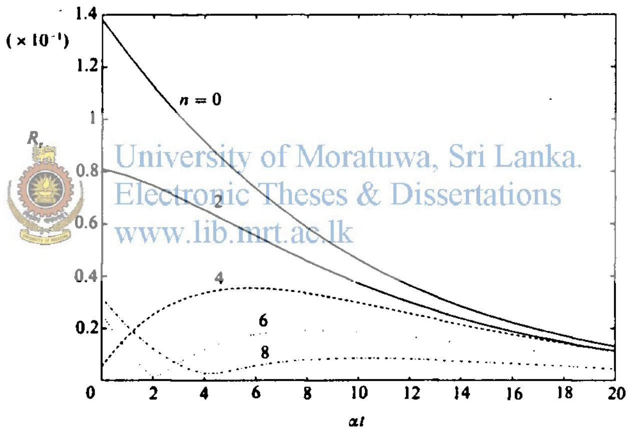

FIGURE 11. Temporal development of R_r of S1–S2, at $y = 0.25$, when excited by different T_n.

amplitudes than the other T_n do, but the amplitudes due to T_0 and T_2 monotonically decay to zero. In the interval $y = [0, 1]$, $T_0 = 1$ has no zero and $T_2 = 2y^2 - 1$ has one zero. When S1–S2 is excited by T_n ($n > 4$), growth in the sense of case (a) is seldom observed, but growth in the sense of case (c) is present. The time-stretching phenomenon is therefore in effect. As n increases, the number of zeros of T_n in $y = [0, 1]$ also increases, and the response of S1–S2 due to T_n becomes less and less pronounced as can be seen in figure 11.

The responses of A1–A2, when excited by the other antisymmetric Chebyshev polynomials are illustrated in figure 12 at a chosen y-position ($y = 0.35$). The polynomial $T_5 = 16y^5 - 20y^3 + 5y$, which causes growth in the sense of case (a), also has two zeros in $y = [0, 1]$. The qualitative behaviour of the responses of A1–A2 due to T_n ($n = 1, 3, 7, 9, \ldots$) resemble those of S1–S2 due to T_n ($n = 0, 2, 6, 8, \ldots$), respectively, and thus require no extra comments.

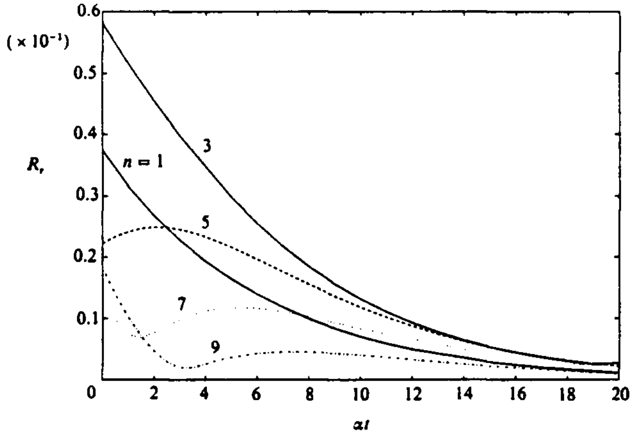

FIGURE 12. Temporal development of R_r of A1–A2, at $y = 0.35$, when excited by different T_n.

The overall response of a degeneracy due to the arbitrary forcing function Δ_b can, in principle, be evaluated by adding the responses due to different polynomials T_n, after weighting them by the corresponding constants b_n. The constants b_n can, though by a tedious means, be evaluated by substituting Δ_s and Δ_a, given by $(28a, b)$, into

$$\int_0^1 \Delta_s(y)\cosh(ky)\,dy = 0 \tag{29a}$$

and

$$\int_0^1 \Delta_a(y)\sinh(ky)\,dy = 0, \tag{29b}$$

respectively. These conditions are deduced (see Gustavsson 1986) from the fact that $\hat{v}_b(t = 0)$ is subjected to the boundary conditions

$$\hat{v}_b(t = 0) = D\hat{v}_b(t = 0) = 0 \quad \text{at} \quad y = \pm 1. \tag{30}$$

The responses of degeneracies other than the first symmetric and the first antisymmetric ones, listed in table 3, were also investigated by exciting them by the Chebyshev polynomials. The temporal development of the amplitude R_r in each of these cases is rapid, though not purely exponential, decay to zero, as illustrated by figure $13(a, b)$. This behaviour is not surprising if one considers the corresponding damping rates c_{i0} $(= c'_{i0} - k^2/\alpha R)$, given in figure $13(a, b)$, of these degeneracies. Therefore, it seems that the damping rate of a degeneracy could be used as an indicator in deciding whether or not that degeneracy be subjected to detailed analyses in search of growth and, hence, the consequences.

5. Discussion

Among the degeneracies listed in table 3, the first symmetric degeneracy S1–S2 and the first antisymmetric degeneracy A1–A2 exhibit temporal growth of the amplitudes. In the cases of the other four degeneracies, the amplitudes rapidly decay to zero. These results are, strictly speaking, valid only in the Fourier (wavenumber) space. But it is probable that the temporal histories of a degeneracy both in the Fourier space and in the real space are the same.

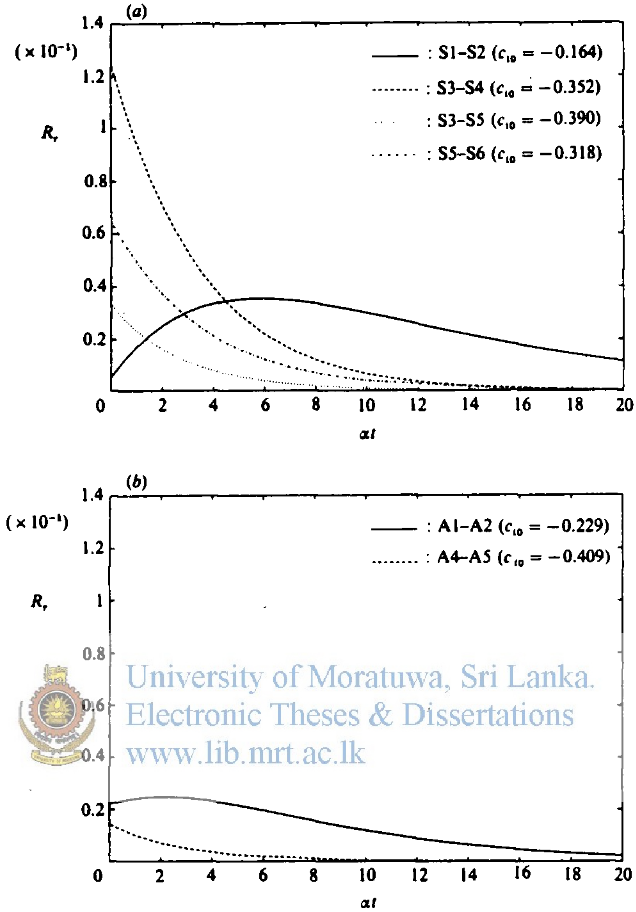

FIGURE 13. Temporal development of R_r corresponding to (a) the first four symmetric degeneracies, at $y = 0.25$, when excited by T_4, and (b) the first two antisymmetric degeneracies, at $y = 0.35$, when excited by T_5.

The damping rate of a degeneracy should, as a rule, be low enough for it to exhibit growth. In addition, R_{min} $(= \alpha R/k)$ of a degeneracy should correspond to the laminar region for it to contribute to the transition mechanism. We have, however, analysed only six of the infinitely many degeneracies of plane Poiseuille flow. It seems, from table 3, that degeneracies among the higher eigenmodes may have higher damping rates and higher values of R_{min}, and hence may be of marginal importance from the transition point of view, although we cannot prove that it is so.

The temporal (or spatial) responses of double poles rapidly developing into relatively large amplitudes, and their nonlinear consequences have also been the major concern of some past works, such as Benney & Gustavsson (1981), Koch (1986), Gustavsson (1986). None of these studies, including the present one, has so far given any *strong* evidence that the amplitudes of the double-pole responses can grow so large as to violate the assumptions of the linear theory.

However the time-stretching phenomenon discussed in this study, yet another facet of the degeneracy, can be active even if there is only a slight growth of the amplitude, as revealed by the degeneracy S1–S2 for instance. If the characteristic time, t_m of (23a), is stretched long enough, a new disturbance may see the basic profile not as parabolic but as parabolic plus the response of the degeneracy. Investigating the consequences of such a state is a natural development of the present study, and will be completed in due course. It seems that, among the degeneracies analysed in this study, S1–S2 and A1–A2 are the most suitable candidates to be subjected to further growth-related investigations.

We here digress to mention that strong linear waves, with wavenumber $k = 1.89$ and streamwise phase speed $c_r = 0.53$, accompanying turbulent spots in plane Poiseuille flow at $R = 1500$ were experimentally located by Henningson & Alfredsson (1987). The numerical simulations of a turbulent spot in plane Poiseuille flow, by Henningson (1988), also showed similar waves, having $k = 1.88$ and $c_r = 0.62$, at the same Reynolds number. Can these observations be accounted for by the degeneracy S3–S5, having $k = 1.891178$ and $c_r = 0.6357061$, despite the rapid decay of its response? A definite answer to this question awaits an enquiry into other possible aspects of degeneracies, such as their effects upon the disturbance energy.

I thank L. Håkan Gustavsson, my study supervisor, for suggesting the area of this research and for his continued interest. This work has in part been supported by the National Swedish Board for Technical Development through its program for basic research (STUF).

REFERENCES

ALAVYOON, F., HENNINGSON, D. S. & ALFREDSSON, P. H. 1986 Turbulent spots in plane Poiseuille flow – flow visualization. *Phys. Fluids* **29**, 1328–1331.

BENNEY, D. J. & GUSTAVSSON, L. H. 1981 A new mechanism for linear and nonlinear hydrodynamic instability. *Stud. Appl. Maths* **64**, 185–209.

BETCHOV, R. & CRIMINALE, W. O. 1966 Spatial stability of the inviscid jet and wake. *Phys. Fluids* **9**, 359–362.

CARLSON, D. R., WIDNALL, S. E. & PEETERS, M. F. 1982 A flow-visualization study of transition in plane Poiseuille flow. *J. Fluid Mech.* **121**, 487–505.

DRAZIN, P. G. & REID, W. H. 1981 *Hydrodynamic Stability*, Chap. 4. Cambridge University Press.

GASTER, M. 1968 Growth of disturbances in both space and time. *Phys. Fluids* **11**, 723–727.

GASTER, M. & JORDINSON, R. 1975 On the eigenvalues of the Orr–Sommerfeld equation. *J. Fluid Mech.* **72**, 121–133.

GUSTAVSSON, L. H. 1981 Resonant growth of three-dimensional disturbances in plane Poiseuille flow. *J. Fluid Mech.* **112**, 253–264.

GUSTAVSSON, L. H. 1986 Excitation of direct resonances in plane Poiseuille flow. *Stud. Appl. Maths* **75**, 227–248.

HENNINGSON, D. S. 1988 Wave growth associated with turbulent spots in plane Poiseuille flow. *Rep.* FFA-TN-1988-08. Aero. Res. Inst., Bromma, Sweden.

HENNINGSON, D. S. & ALFREDSSON, P. H. 1987 The wave structure of turbulent spots in plane Poiseuille flow. *J. Fluid Mech.* **178**, 405–421.

KOCH, W. 1986 Direct resonances in Orr–Sommerfeld problems. *Acta Mech.* **58**, 11–29.

MACK, L. M. 1976 A numerical study of the temporal eigenvalue spectrum of the Blasius boundary layer. *J. Fluid Mech.* **73**, 497–520.

ORSZAG, S. A. 1971 Accurate solution of the Orr–Sommerfeld stability equation. *J. Fluid Mech.* **50**, 689–703.

SCHENSTED, I. V. 1961 Contributions to the theory of hydrodynamic stability. PhD thesis, University of Michigan.

Paper II

Accepted for publication in *Studies in Applied Mathematics*

Degeneracies and Direct Resonances in Water Table Flow

By L. Håkan Gustavsson and R. Shanthini
Division of Fluid Mechanics, Luleå University of Technology, S-951 87 Luleå, Sweden

Degeneracies of the Orr-Sommerfeld eigenmodes and direct resonances between the Orr-Sommerfeld eigenmodes and vorticity eigenmodes are studied in water table flow. The sensitivity of the characteristics of these algebraic mechanisms to flow parameters, such as the Reynolds number (R), slope of the table (θ) and a material parameter (γ), are investigated. It is found that the mechanisms become operative at sub-transitional R, and their damping rates decrease with increasing R. When the mean flow profile is slightly distorted from the ultimate parabolic profile, the characteristics of the direct resonances show remarkable variations. Also, some of the algebraic mechanisms in water table flow are shown to have the same characteristics and model structures as some of those in plane Poiseuille flow.

1. Introduction

The linear stability theory of Orr [1] and Sommerfeld [2] has conventionally been employed to predict the Reynolds number, at which a small perturbation field imposed on a steady basic parallel flow starts to grow exponentially for all time (or space). The theoretical predictions, however, are not in agreement with the experimental transition Reynolds numbers for many wall-bounded shear flows. As a consequence, the use of linear theory to predict the onset of turbulence in this type of flows has been disputed, and the role of nonlinearities has instead become of primary interest.

The laminar-to-turbulent transition is inherently nonlinear, but as to the origin and character of the nonlinearities, and, in particular, as to the role of three–dimensionality, many unresolved questions still remain. The traditional approach to the nonlinear treatment of the stability problem is to consider secondary disturbances on a finite amplitude two-dimensional Tollmien-Schlichting wave (see e.g. [3] for a review). This approach models the experimental conditions for a vibrating ribbon, and good agreement is obtained between theoretical and experimental results (cf [4]).

On the other hand, in experiments where turbulence is initiated by *localized* disturbances, it can be questioned whether the relevant basis for secondary instabilities is a two-dimensional Tollmien-Schlichting wave. Rather, three-dimensional (3-D) mechanisms would be required at the primary level.

In studies of the development of 3–D disturbances, the possibility of algebraic growth has become apparent through the inherently 3-D mechanism of direct resonance [5] between the normal velocity and the normal vorticity of the (linear) perturbation field. The mechanism has been shown to exist in a variety of wall-bounded parallel shear flows, but its precise role in the laminar-to-turbulent transition is yet to be ascertained.

Another algebraic mechanism results from degenerating Orr-Sommerfeld eigenmodes. Degenerecies, also, have been recognized in many flows (see e.g. [6], [7]), but not until recently have more thorough investigations into their properties been conducted [8],[9].

Both direct resonance and degeneracy (of the temporal type) have the potential to cause algebraic growth with increasing time, but since they involve damped modes, the growth is limited to a short initial period, at least in the linear regime. Nonetheless, it is worthwhile to investigate these mechanisms, since they both start to operate at sub-transitional Reynolds numbers and provide definite predictions about characteristics such as wavelengths and propagation speeds, quantities which can be compared with experimental observations.

In this paper, we investigate into the two algebraic mechanisms in flow down an inclined plane (water table). In contrast to other flows investigated, this flow offers many changable parameters such as slope of the table and surface tension, besides flow rate and viscosity. In addition, the velocity profile itself may vary in the streamwise direction (though in a less controllable manner) due to the finite distance needed for the flow to attain the ultimate parabolic profile. Influences of changing these parameters, including the velocity profile, upon the characteristics of the algebraic mechanisms are discussed in section 3. The work has also been motivated by the affinity of water table flow to plane Poiseuille flow regarding the laminar velocity profile as well as the structure of the incipient turbulence. Hence, the characteristics of degeneracies and direct resonances in water table flow are compared to those in plane Poiseuille flow in section 4. Also, the theoretical results for the two flows are discussed with an experimental perspective in the last section.

2. Problem formulation

Consider the flow of a viscous, incompressible, liquid down an inclined plane. The coordinate system and the basic geometric parameters are defined in Figure 1.

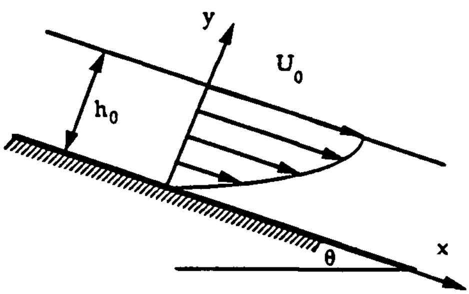

Figure 1. Flow geometry and mean flow configuration of water table flow.

The governing equations are made non-dimensional with the velocity at the free surface (U_0) and the water depth (h_0) as respective scales for velocity and length. The fully developed velocity profile of the flow is given in non-dimensional form by

$$U(y) = 2y - y^2 \ . \tag{1}$$

The (linear) stability of the flow is analysed by introducing small three-dimensional perturbations of velocity (u,v,w) and pressure (p), into the Navier-Stokes equations. After subtraction of the unperturbed flow solution, linearization and some reductions, the following set of equations are obtained:

$$\left(\frac{\partial}{\partial t} + U\frac{\partial}{\partial x}\right)\nabla^2 v - U''\frac{\partial v}{\partial x} = \frac{1}{R}\nabla^4 v \ . \tag{2}$$

$$\left(\frac{\partial}{\partial t} + U\frac{\partial}{\partial x}\right)\omega - \frac{1}{R}\nabla^2\omega = -U'\frac{\partial v}{\partial z} \ . \tag{3}$$

$$\left(\frac{\partial^2}{\partial x^2} + \frac{\partial^2}{\partial z^2}\right)p = \left(\frac{\partial}{\partial t} + U\frac{\partial}{\partial x} - \frac{1}{R}\nabla^2\right)\frac{\partial v}{\partial y} - U'\frac{\partial v}{\partial x} \tag{4}$$

Here,

$$\omega = \frac{\partial u}{\partial z} - \frac{\partial w}{\partial x}$$

is the perturbation vorticity in the y-direction, ∇^2 is the three-dimensional Laplacian and the prime represents d/dy. The Reynolds number R is defined as

$$R = U_0 h_0 / \nu \ , \tag{5}$$

where ν is the kinematic viscosity. The set of quations (2-4) is identical to that obtained in other parallel shear flows. However, differences appear when the boundary conditions are considered. To obtain the boundary conditions at the free surface, it is necessary to realize that the perturbations of the flow field lead to a deflection of the free surface (η). With the assumption that also η is small, the dynamic and kinematic boundary conditions at the inclined plane and at the free surface are reduced to the following, respectively:

At the inclined plane (i.e. at $y = 0$),

$$v = \frac{\partial v}{\partial y} = \omega = 0. \tag{6a-c}$$

At the free surface (i.e. at $y = 1$),

$$-p + \frac{\cos\theta}{F^2}\eta + \frac{2}{R}\frac{\partial v}{\partial y} - \frac{1}{We}\left(\frac{\partial^2\eta}{\partial x^2} + \frac{\partial^2\eta}{\partial z^2}\right) = 0, \tag{7a}$$

$$\frac{\partial w}{\partial y} + \frac{\partial v}{\partial z} = 0, \tag{7b}$$

$$\frac{\partial u}{\partial y} + \frac{\partial v}{\partial x} - 2\eta = 0 \tag{7c}$$

and

$$\frac{\partial\eta}{\partial t} + \frac{\partial\eta}{\partial x} = v. \tag{7d}$$

Here,

$F \equiv U_0/\sqrt{gh_0}$ is the Froude number,

$We \equiv \rho U_0^2 h_0/\sigma$ is the Weber number,

and g, ρ and σ are the gravity acceleration, the density and the surface tension, respectively. Condition (7a) is that of continuous normal stress, (7b-c) zero tangential stress, and (7d) is the kinematic condition at the surface. (A derivation of these conditions can be found on page 502 of [10].)

Elimination of the pressure between (4) and (7a) leads to one relation between v and η at $y = 1$. Another is obtained by using continuity on (7b) and (7c) to eliminate u and w. Together with (7d), these relationships can be used to eliminate η to obtain two homogeneous conditions for v at $y=1$. The algebraic manipulations are simplified if Fourier transformation is applied to the homogeneous coordinates x and z. In terms of the respective transform variables α and β, the two conditions for v at y = 1 can be written as

$$\left(\frac{\partial}{\partial t} + i\alpha\right)\left(\frac{\partial^2}{\partial y^2} + k^2\right)\hat{v} + 2i\alpha\hat{v} = 0 \ , \tag{8a}$$

and

$$\left(\frac{\partial}{\partial t} + i\alpha\right)\left[\frac{1}{R}\left(\frac{\partial^2}{\partial y^2} - 3k^2\right) - \frac{\partial}{\partial t} - i\alpha\right]\frac{\partial}{\partial y}\hat{v} = k^2\left(\frac{\cos\theta}{F^2} + \frac{k^2}{We}\right)\hat{v} \ . \tag{8b}$$

Here, $\hat{v}(\alpha,y,\beta,t)$ is the Fourier transform of $v(x,y,z,t)$, and $k^2 = \alpha^2 + \beta^2$. Alternatively, $\hat{v}$ can also be considered as the amplitude of the wave whose modulus of wave-vector is k.

Once the initial conditions are specified, $\hat{v}$ can be determined by solving the Fourier transformed versions of (2) and (6a-b) together with (8a-b), using Laplace transform techniques. As can be inferred from the related case of plane Poiseuille flow discussed by Shanthini [9], the explicit form of the solution is necessary if one is interested in evaluating the temporal development of the response of the algebraic mechanism of degeneracy. But if, as in this study, the interest are the characteristics of degeneracies, and not their responses, then it suffices to know the parameter-combinations at which singularities of the Laplace transformed $\hat{v}$ (denoted by $\tilde{\hat{v}}$) exist. It can easily be shown that the singularities of $\tilde{\hat{v}}$ are in fact eigenvalues of the following eigenvalue problem obtained simply by substituting $\hat{v} = \phi(y)e^{-i\alpha ct}$ in the relevant equations:

$$(D^2 - k^2)^2\phi - i\alpha R(U - c)(D^2 - k^2)\phi + i\alpha R\, U''\phi = 0 \ , \tag{9}$$

with

$$\phi = D\phi = 0 \qquad \text{at } y = 0, \quad \text{(10a-b)}$$

and

$$\left.\begin{aligned} &(1 - c)(D^2 + k^2)\phi + 2\phi = 0 \\ &[D^2 - 3k^2 + i\alpha R(c-1)]D\phi + \frac{k^2 R}{2i\alpha}\left(\frac{\cos\theta}{F^2} + \frac{k^2}{We}\right)(D^2 + k^2)\phi = 0 \end{aligned}\right\} \text{at } y = 1, \quad \text{(10c-d)}$$

where D is the operator d/dy. If this problem produces two eigenvalues which coalesce for a certain parameter combination (α, k, R, θ, F, We), then a degeneracy is obtained. The degeneracy, which is a second order pole of $\tilde{\hat{v}}$, is what is responsible for the algebraic temporal term in the expression for $\hat{v}$. (For details of this phenomenon, the reader is referred to [9].)

Once $\hat{v}$ is known, the other velocity components can be obtained from (3) and continuity. Solving the forced problem (3) requires two boundary conditions for ω, of which (6c) is one. The other, derived from (7b) and (7c) using the definition of ω as well as continuity, is

$$\frac{\partial}{\partial y}\hat{\omega} = -\frac{\beta}{\alpha}\left(\frac{\partial^2}{\partial y^2} + k^2\right)\hat{v} \qquad \text{at } y = 1, \qquad (11)$$

where $\hat{\omega}(\alpha,y,\beta,t)$ is the Fourier transform of $\omega(x,y,z,t)$. The forcing of ω is thus conducted both through the equation (3) as well as through the boundary condition (11). The specific form of the response, obtained by solving the initial value problem for ω using Laplace transform techniques, is as follows:

$$\tilde{\hat{\omega}} = -i\beta R\left\{\psi_1\int_0^y \psi_2 U'\tilde{\hat{v}}\,d\xi + \psi_2\int_y^1 \psi_1 U'\tilde{\hat{v}}\,d\xi\right\}$$

$$+\, i\beta R\frac{\psi_2}{\psi'_{21}}\left\{\psi'_{11}\int_0^1 \psi_2 U'\tilde{\hat{v}}\,d\xi - \frac{1}{i\alpha R}\left[(D^2+k^2)\tilde{\hat{v}}\right]_{y=1}\right\}$$

$$+\, R\left\{\psi_1\int_0^y \psi_2\hat{\omega}_0\,d\xi + \psi_2\int_y^1 \psi_1\hat{\omega}_0\,d\xi - \psi_2\frac{\psi'_{11}}{\psi'_{21}}\int_0^1 \psi_2\hat{\omega}_0\,d\xi\right\}, \qquad (12)$$

where $\tilde{\hat{\omega}}$ is the Laplace transform of $\hat{\omega}$, and $\hat{\omega}_0$ is the initial value of $\hat{\omega}$. The functions ψ_1 and ψ_2 are the linearly independent solutions to the normal vorticity operator of the Fourier-Laplace transformed (3). These functions are normalized such that at y = 0, $\psi_1 = \psi'_2 = 1$ and $\psi'_1 = \psi_2 = 0$. The values of ψ_1 and ψ_2 at y = 1 are denoted by ψ_{11} and ψ_{21}, respectively. The prime denotes the y-derivative.

It follows from (12) that a resonant forcing occurs when a zero of ψ_{2i}' coincides with a pole of $\tilde{\hat{v}}$ in the Laplace-plane. The zero of ψ_{2i}' is determined by solving the following eigenvalue problem (which is obtained by substituting $\hat{\omega} = \psi(y)e^{-i\alpha ct}$ in the relevant equations):

$$(D^2 - k^2)\psi - i\alpha R(U - c)\psi = 0 \ , \tag{13}$$

with

$$\psi = 0 \qquad \text{at } y = 0 \ , \tag{14a}$$

and

$$D\psi = 0 \qquad \text{at } y = 1 \ . \tag{14b}$$

If the eigenvalue problem of ω and that of v produce identical values of c for a given parameter combination (α, k, R, θ, F, We), a direct resonance is present.

The comparison of numerical results with experimental observations can be facilitated by the use of non-dimensional parameters which are related to primary experimental quantities such as flow rate, viscosity, surface tension and slope of water table. By introducing a material parameter [11], defined as

$$\gamma = \frac{2\sigma}{\rho(9g\nu^4)^{1/3}} \ , \tag{15}$$

we can replace the parameter set (α, k, R, θ, F, We) by (α, k, R, θ, γ), in terms of which the Froude and the Weber numbers are expressed as

$$F = \sqrt{\frac{R\sin\theta}{2}} \tag{16}$$

and

$$We = \frac{1}{\gamma}\left(\frac{4R^5\sin\theta}{9}\right)^{1/3} . \tag{17}$$

These expressions are obtained by using the relation $U_0 = h_0^2\ g\sin\theta/2\nu$ (see [10]) and the definition for γ.

For a developing water table flow, the set of parameters R, θ and γ is not complete without a parameter which characterizes the velocity profile. The developing flow is subject to two counteracting processes: the acceleration due to gravity and the retardation due to viscosity. When the effect of viscosity has penetrated the liquid layer the two processes balance each other and the velocity profile becomes parabolic and the liquid depth a constant. Using a similarity-type of assumption (cf [12]), an asymptotic expression for the developing profile of the water table flow can be obtained. With the first order correction, this profile becomes

$$\bar{U} = 2\bar{y} - \bar{y}^2 + \lambda_v (\bar{y} - 1.5\bar{y}^2 + 0.5\bar{y}^4), \tag{18}$$

which has been normalized with the local free surface velocity and local water depth.

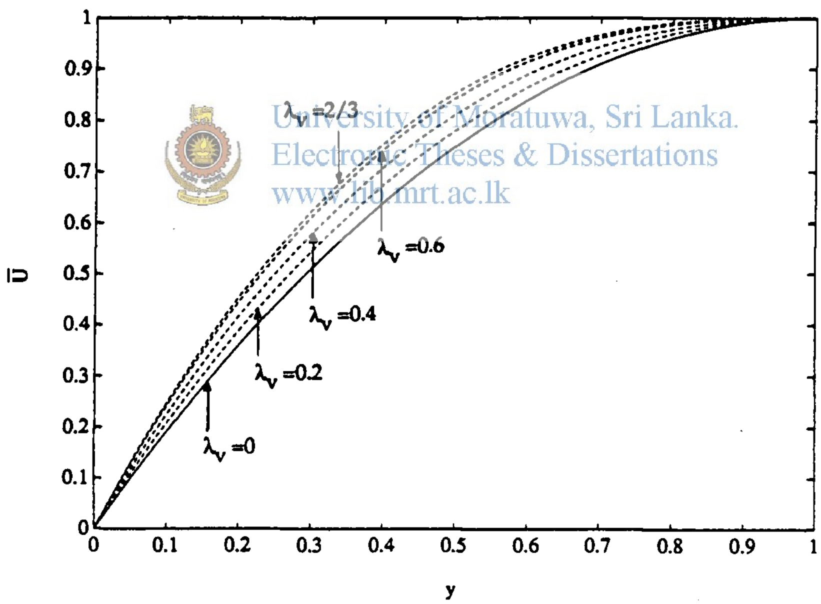

Figure 2. Developing velocity profile, described by $\bar{U}$ of (18), for diferent values of the velocity parameter λ_v ranging from 0 to 2/3. (The case of $\lambda_v = 0$ represents the fully developed parabolic profile.)

The parameter λ_v of (18), which will be referred to as the velocity parameter, is limited to the range

$$0 \le \lambda_v \le 2/3 \ ,$$

where the lower limit corresponds to the fully developed parabolic profile and the upper limit to the restriction that the maximum velocity is attained at the surface. Figure 2 displays the velocity profile (18) for values of λ_v = 0, 0.2, 0.4, 0.6, and 2/3. It is shown in the next section that these profiles, despite their apparent similarities, have quite drastic effects on degeneracies and, particularly, on direct resonances.

3. Characteristics of degeneracies and direct resonances

The first set of degeneracies and direct resonances were searched at $R = 1000$, $\theta = 3^\circ$, $\gamma = 3000$ and $\lambda_v = 0$. This parameter combination is chosen as the standard one owing to its proximity to experimental conditions (see e.g. [12], [13], [14]). The minimum R at which externally initiated isolated regions of turbulence (turbulent spots) are sustained by water table flows is about 1000. A ripple-free parabolic profile is attained at a reasonable length of the water table when $\theta = 3^\circ$. And water at 18°C, which is usually close to the indoor operating conditions of a water table, corresponds to $\gamma \approx 3000$. Finally, a parabolic profile is parameterized by $\lambda_v = 0$.

At this standard parameter-set, we have located five degeneracies and five direct resonances, each of which exists only for certain values of the wavenumbers α and β. The degeneracies are listed in table 1 and the direct resonances in table 2, along with the following characteristics: streamwise wavenumber α, modulus of the wave-vector k ($\equiv \sqrt{\alpha^2+\beta^2}$), and complex phase speed c.

To characterize the degeneracies and the direct resonances, one could alternatively use experimentally observable quantities such as the streamwise phase speed of the wave, the wavelength, and the oblique angle that the wave crest makes with the streamwise direction. The streamwise phase speed is given by c_r (the real part of c), the wavelength by $(2\pi/k)$, and the oblique angle by $\sin^{-1}(\alpha/k)$. Furthermore, the product of

c_i (the imaginary part of c) and the streamwise wavenumber α gives the temporal damping rate of the associated exponential term, which indeed strongly influences the algebraic temporal development of the mechanism concerned (for details see [15], [9]). Since the complete responses of the mechanisms are not evaluated in this paper, we use the absolute value of inverse damping rate, $|1/\alpha c_i|$, as a *tentative* measure of the physical relevance of the mechanism concerned, (cf [8]). The numerical values of the characteristics c_r, $(2\pi/k)$, $\sin^{-1}(\alpha/k)$ and $|1/\alpha c_i|$ do of course vary as the parameter set $(R, \theta, \gamma, \lambda_v)$ deviates from the standard one, and the variations are reported below.

Name	α	k	$c = c_r + ic_i$
d1	0.25876	0.64388	0.723247-0.198954i
d2	0.23007	2.25628	0.719087-0.229728i
d3	0.50452	0.75413	0.674214-0.235307i
d4	0.53353	0.69242	0.620812-0.298842i
d5	0.62051	2.80166	0.644693-0.409804i

Table 1. Five degeneracies in water table flow at R=1000, $\theta=3^\circ$ and $\gamma=3000$.

Name	α	k	$c = c_r + ic_i$
r1	0.07354	0.3891	0.6718-0.8196i
r2	0.1451	5.7970	0.6926-0.5750i
r3	0.13889	33.447	0.6118-8.3439i
r4	0.1314	1.0607	0.6710-0.9077i
r5	0.4801	0.8476	0.6991-0.2867i

Table 2. Five direct resonances in water table flow at R=1000, $\theta=3^\circ$ and $\gamma = 3000$.

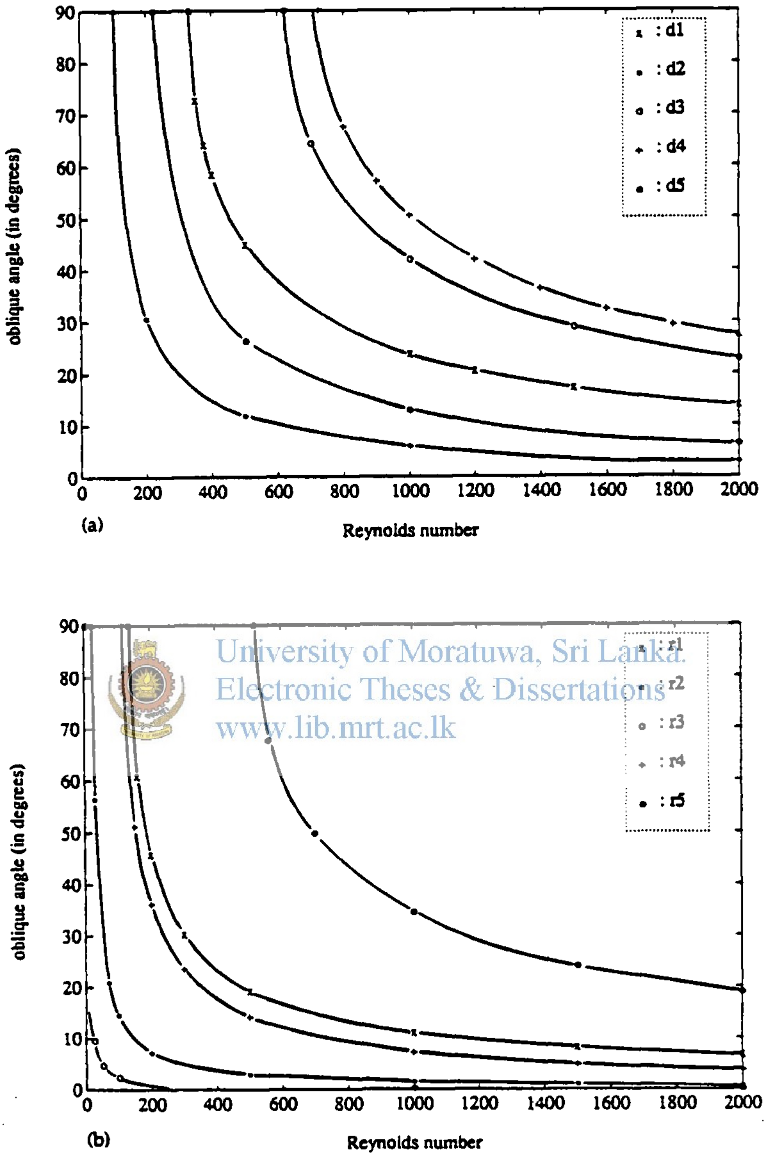

Figure 3. Variation in the oblique angle $\sin^{-1}(\alpha/k)$ with the Reynolds number R at $\theta=3^{\circ}$, $\gamma=3000$ and $\lambda_v=0$: (a) for degeneracies, and (b) for direct resonances.

Varying the Reynolds number (R)

With θ, γ and λ_v at their standard values, R was varied in the range of 0 to 2000. The upper limit of 2000 corresponds to the R about which the turbulent spots first appear spontaneously in the flow [12].

It is found in both cases of degeneracies and of direct resonances that, with varying R, the streamwise phase speeds remain almost constants and the wavelengths vary slightly, whereas the oblique angles and the inverse damping rates vary considerably, as shown in figures 3a-b and 4a-b.

Figure 3a shows that each of the five degeneracies takes the oblique angle of 90° at some R-value. (An oblique angle of 90° implies that $\alpha=k$ and therefore $\beta = 0$, which corresponds to the traditional two-dimensional stability case.) Further reduction in R-value, as can be gathered from figure 3a, would result in α-values which are higher than the corresponding k-value of the degeneracy, which is impossible. Thus we conclude that the R-value corresponding to the oblique angle of 90° is the minimum value of R at which a degeneracy may exist. It will therefore be referred to as the R_{min} of the respective degeneracy. The R_{min} - values of the degeneracies d2, d5, d1, d3 and d4 (the order is that of figure 3a) are approximately 102, 221, 331, 620 and 726, respectively. (These values pertain to $\theta = 3°$, $\gamma = 3000$ and $\lambda_v = 0$, and will change as either θ or γ or λ_v is altered.) At $R=R_{min}$, the wave crest is aligned with the spanwise direction. If R is increased above R_{min}, as seen in figure 3a, the oblique angles decrease, which means that the wave-crests tend to align themselves with the streamwise direction with increasing R. Similar behaviour is exhibited also by all the five direct resonances, which appear in the order of r3, r2, r4, r1 and r5 in figure 3b with approximately 4, 25, 116, 137 and 517 as their respective R_{min} -values.

The shapes of the curves in figure 3a-b suggest that the corresponding αR-values of both degeneracies and direct resonances may remain more or less constants with varying R, since the k-values change only slightly with R. This implies that α-values decrease almost linearly with increasing R in cases of both degeneracies and direct resonances. The expected linear decrease in α-values leads to almost linear increase in $|1/\alpha c_i|$-values with increasing R, as shown in figure 4a-b, since c_i-values of both degeneracies and direct resonances are practically constants with

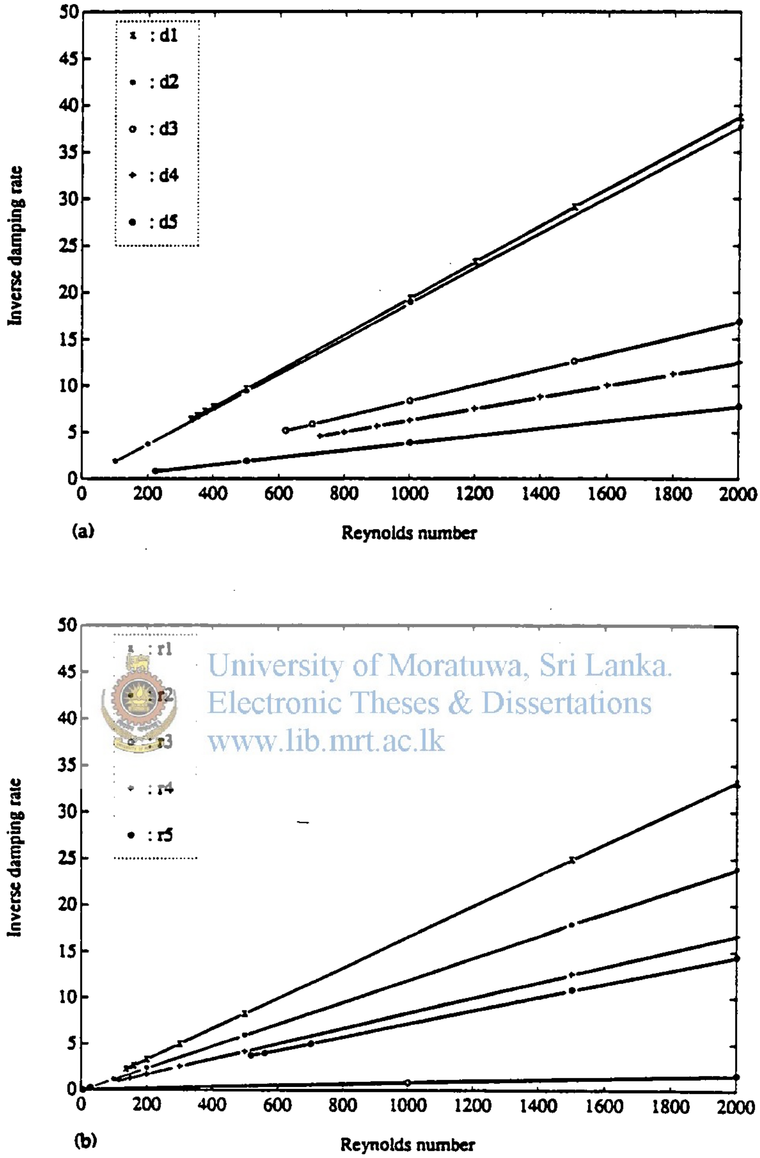

Figure 4. Variation in the inverse of damping rate $|1/\alpha c_i|$ with the Reynolds number R at $\theta=3^\circ$, $\gamma=3000$ and $\lambda_v=0$: (a) for degeneracies, and (b) for direct resonances.

increasing R. One can conclude from figure 4a-b that, in general, the physical relevance of the algebraic mechanisms increases with increasing Reynolds number, and that at high Reynolds numbers some become more important than the others.

Varying the slope of the table (θ)

Keeping R, γ and λ_v at the standard values, θ was decreased from 3° to 0.1°. This range of θ was chosen since the only problem encountered at smaller values of θ is that the flow requires a longer length of the table to become fully developed. Larger values of θ introduces a more serious problem of the flow becoming dominated by the unstable surface mode (discussed by Yih [10] and others), and thus are avoided. The slope θ is not lowered below 0.1° since the driving force due to the gravity becomes insignificant as the table is moved towards a horizontal position.

As for R, with changing θ the streamwise phase speeds remain practically unchanged, but the other characteristics respond differently. Variations in the wavelengths are shown in figure 5a-b, in which one observes that the shorter the wavelength the less sensitive is it to varying θ (in the range of θ=3° to 0.1°). The degeneracies d2 and d5 and the direct resonances r2 and r3, which have the shortest wavelengths (=highest wavenumbers) at θ=3° (see tables 1 and 2), remain unchanged as θ is reduced to 0.1°. Also, it seems that further reduction in θ has no influence upon the wavenumbers of these degeneracies and direct resonances. We can thus name this group of degeneracies and direct resonances as the H-group (where H represents the horizontal limit). The group of remaining degeneracies (d1, d3 and d4) and direct resonances (r1, r4 and r5) is named the V-group (V for vertical). A common feature among the members of V-group is that their respective k-values are of order unity, or less, at θ=3° (see tables 1 and 2), and hence they have long wavelengths. Moreover, their wavelengths increase when θ is decreased from 3°, as shown in figure 5a-b. Some V-group members (d1, d3, d4 and r5) even disappear at some critical slopes, each of which is marked by an additional bar in figure 5a-b.

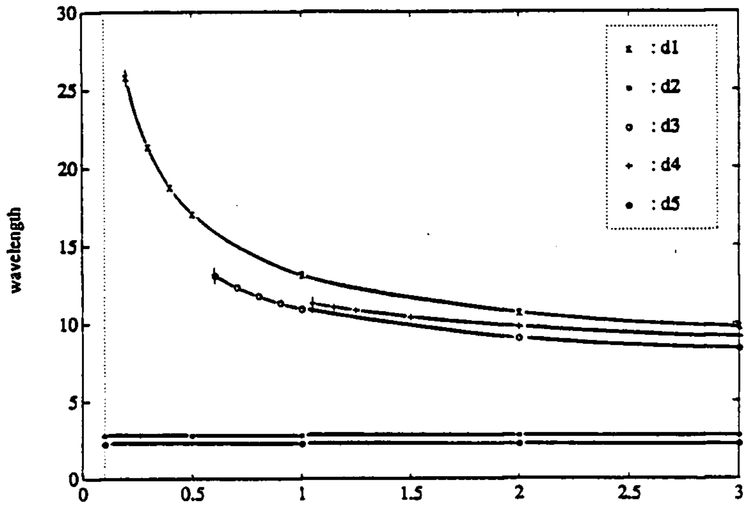

(a) slope of the table (in degrees)

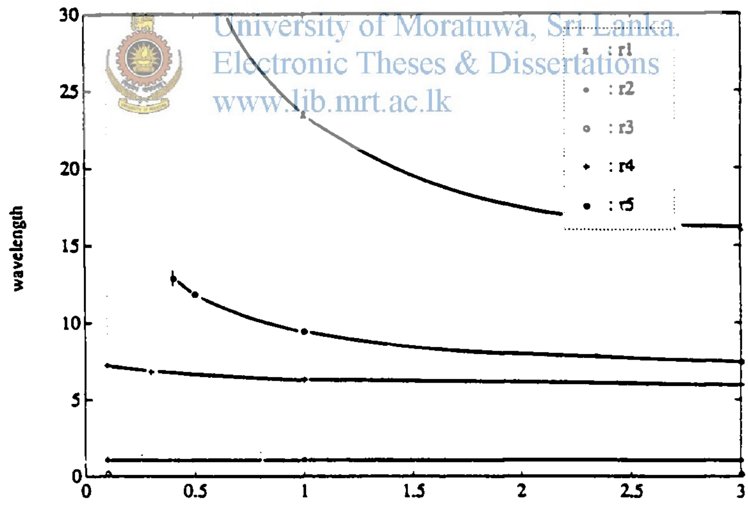

(b) slope of the table (in degrees)

Figure 5. Variation in the wavelength $2\pi/k$ with the slope of the table θ at R=1000, γ=3000 and λ_v=0: (a) for degeneracies, and (b) for direct resonances.

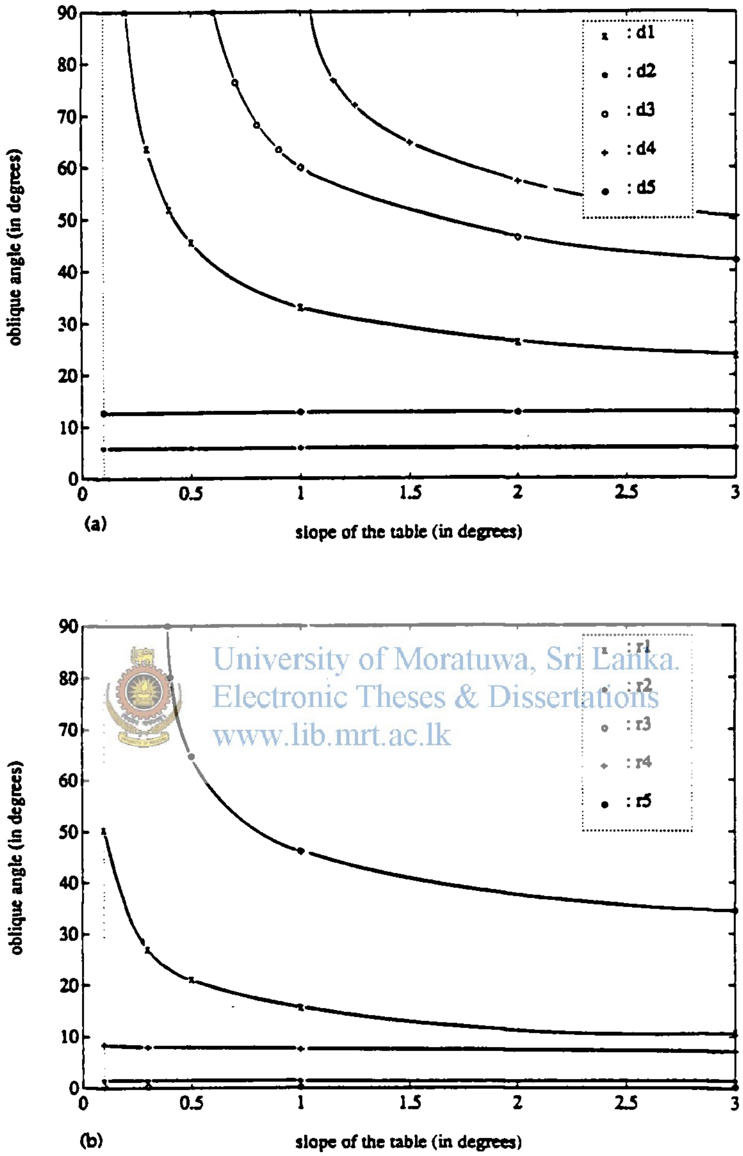

Figure 6. Variation in the oblique angle $\sin^{-1}(\alpha/k)$ with the slope of the table θ at R=1000, γ=3000 and λ_v=0: (a) for degeneracies, and (b) for direct resonances.

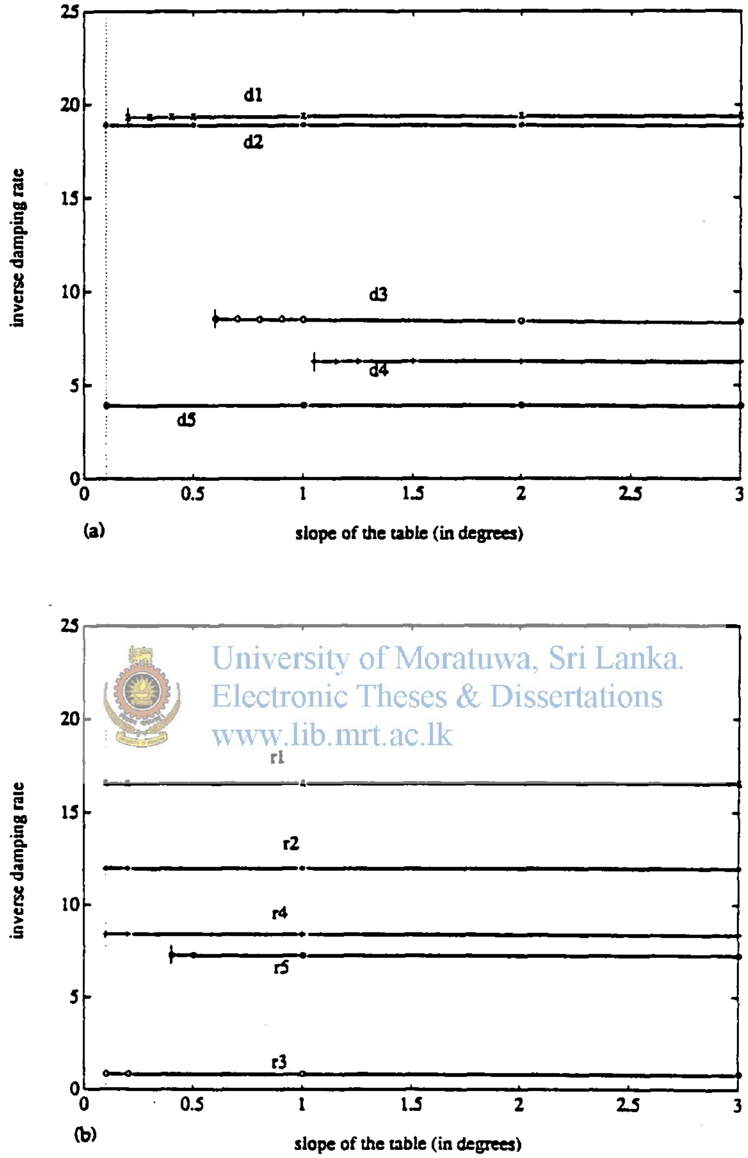

Figure 7. Variation in the inverse of damping rate $|1/\alpha c_i|$ with the slope of the table θ at R=1000, γ=3000 and λ_v=0: (a) for degeneracies, and (b) for direct resonances.

At the critical slopes, the oblique angle of the respective V-group members is 90°, as can be seen in figure 6a-b. It is found that r1, which belongs to the V-group, also reaches the oblique angle of 90°, and hence disappears, at about $\theta=0.058°$ at which its wavelength is about 70. The oblique angle of the remaining V-group member r4, whose k-value is about unity at $\theta=3°$, seems to be insensitive to varying θ in figure 6b. However, at close look, one observes that the oblique angle does increase as θ approaches 0.1°. Like the wavelengths, also the oblique angles of the H-group members are insensitive to θ as it is lowered from 3°.

The most interesting result of varying θ is, perhaps, the insensitiveness of the damping rates of the algebraic mechanisms, as shown in figure 7a-b.

Varying the material parameter (γ)

With R, θ and λ_v kept at their standard values, γ was varied from 1 to 50000. This range of γ corresponds to values for some common liquids as listed in table 3.

Liquid	water				glycerol	glycol	mercury
Temperature (in °C)	0	20	50	100	20	20	20
γ	1569	3267	6782	14030	0.178	41.6	28560

Table 3. Values of material parameter γ for some common liquids.

As in the previous cases, the streamwise phase speeds do not vary noticeably with varying γ. The wavelengths (figure 8a-b) and the oblique angles (figure 9a-b) remain almost insensitive at low values of γ, whereas, at high values of γ, only those of the H-group members are unaffected. In fact, some of the V-group members, d3, d4 and r5, even disappear in the studied interval.

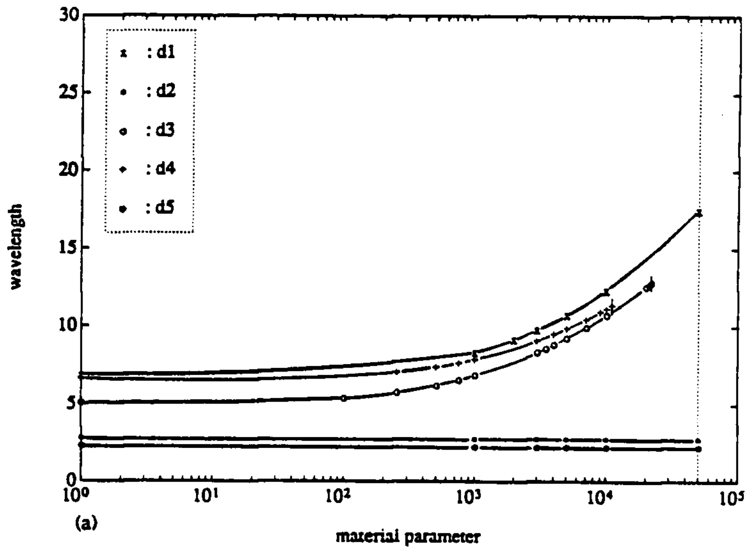

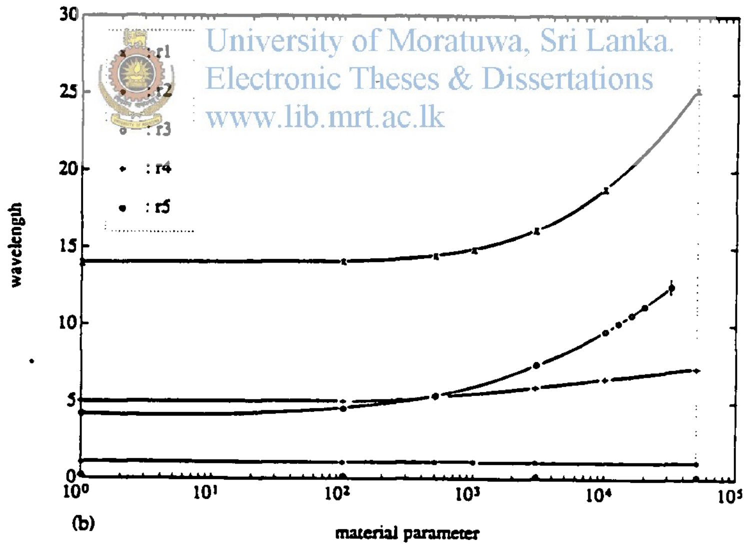

Figure 8. Variation in the wavelength $2\pi/k$ with the material parameter γ at R=1000, $\theta=3^{\circ}$ and $\lambda_v=0$: (a) for degeneracies, and (b) for direct resonances.

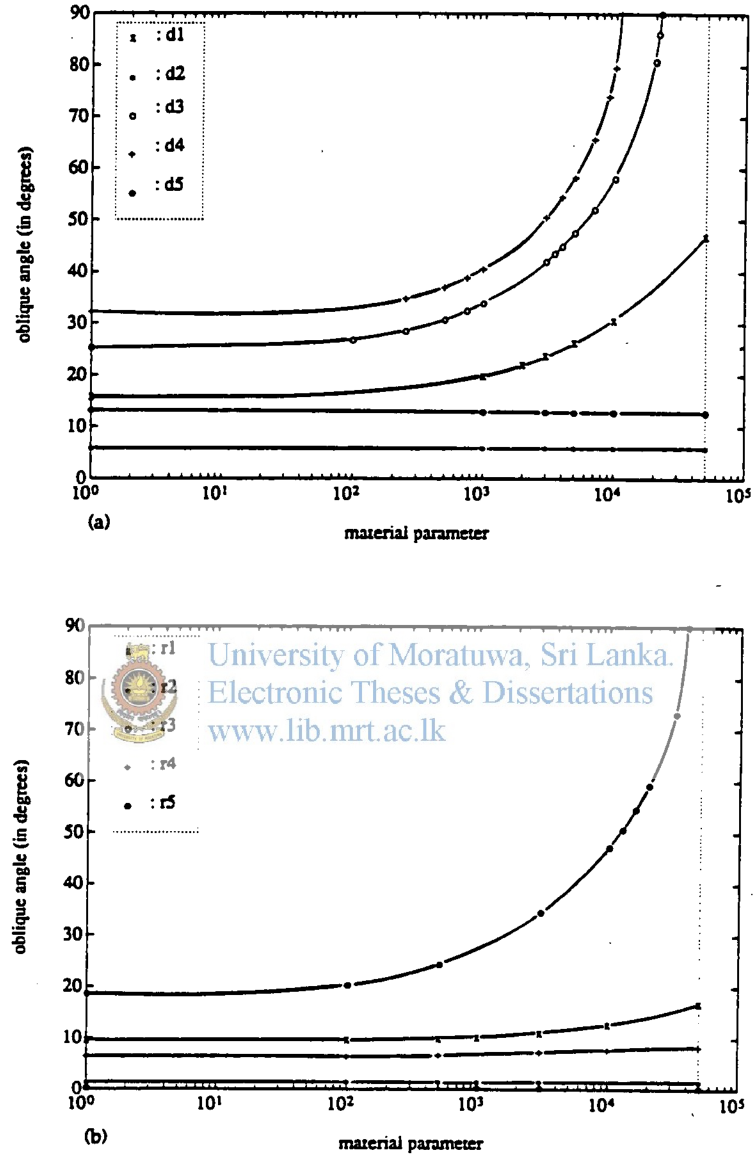

Figure 9. Variation in the oblique angle $\sin^{-1}(\alpha/k)$ with the material parameter γ at R=1000, θ=3° and λ_v =0: (a) for degeneracies, and (b) for direct resonances.

Like in the case of varying θ, with varying γ, the α-values and the c_i-values of both the degeneracies and the direct resonances change so little that the respective $|1/\alpha c_i|$-values remain practically unaffected in the γ-range considered.

Varying the velocity parameter (λ_v)

The results of varying R, θ and γ were all obtained assuming that the basic velocity profile is parabolic, i.e. $\lambda_v = 0$. In experiments, this profile is generally attained far downstream with the required distance increasing as θ decreases. It is therefore of interest to know the influences of the intermediate (developing) velocity profiles upon the characteristics of degeneracies and of direct resonances.

To study this, the velocity profile U of (1) is replaced by $\bar{U}$ of (18) in equations (9) and (13). This replacement modifies the free surface boundary conditions of the normal velocity given by (10c-d) such that the factor 2 in 2ϕ, and in $2i\alpha$, is changed to (2-3b). The range of λ_v, as pointed out at the end of section 2, is bounded by 0 and 2/3.

In case of degeneracies, the values of the streamwise phase speeds seemingly increase with increasing λ_v, as shown in figure 10a. Actually, the phase velocities only tend to redistribute themselves around the mean velocity of the developing flow, given by $(2/3 + \lambda_v/10)$, which is represented by the dashed-dotted line in this figure. Figure 10b shows that the wavelengths of all degeneracies, except d2, vary slightly in the range of λ_v investigated. Figure 10c shows that the oblique angles of all degeneracies, except d2, increase with increasing λ_v, but no degeneracy disappears. It is perhaps not surprising that d2 is insensitive to varying λ_v since it is an H-group degeneracy. However, the other H-group degeneracy (d5) shows variations in the wavelength (figure 10b) as well as in the oblique angle (figure 10c). Thus it seems that the developing velocity profile does not differentiate the degeneracies of the H-group from those of the V-group, and influences each degeneracy distinctively, though not significantly. Moreover, the $|1/\alpha c_i|$-values of all the degeneracies considered are essentially constants with varying λ_v, according to figure 10d.

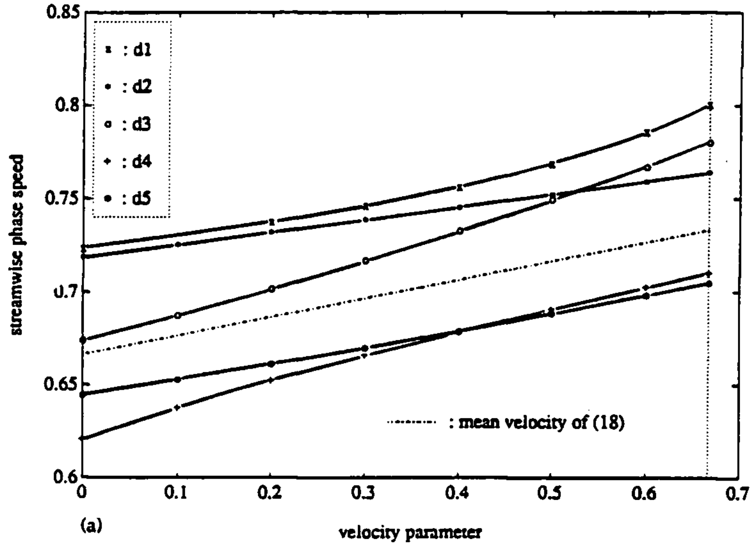

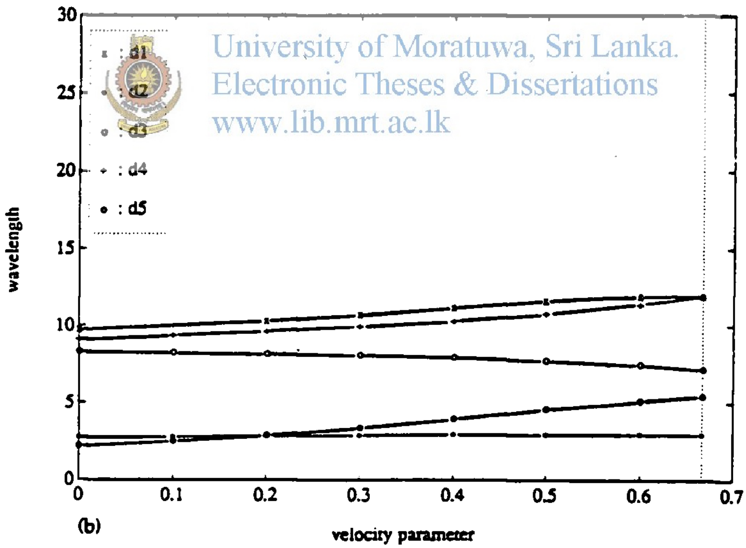

Figure 10. Influences of the velocity parameter λ_v upon the characteristics of the degeneracies at R=1000, θ=3°, and γ=3000: (a) the streamwise phase speed c_r, (b) the wavelength $2\pi/k$, (c) the oblique angle $\sin^{-1}(\alpha/k)$, and (d) the inverse of damping rate $|1/\alpha c_i|$.

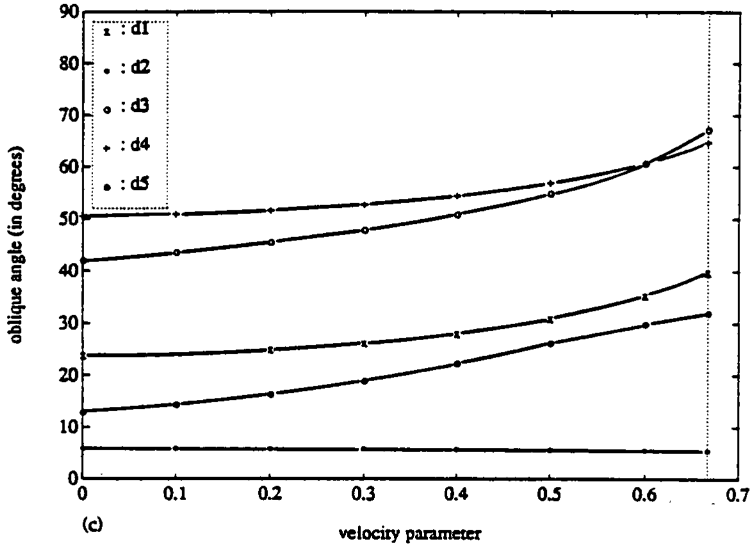

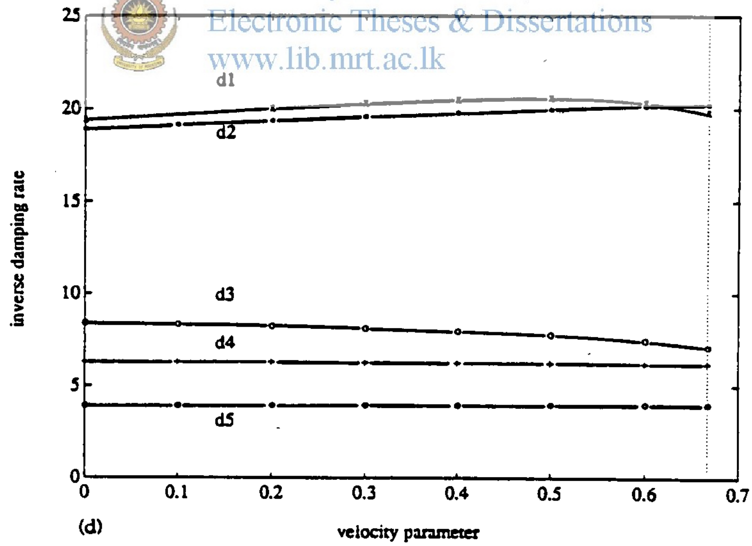

Figure 10. Continued.

In case of the direct resonances, only r4, whose k-value is about unity, is unaffected by variations in λ_v , as shown in figure 11a-f. Its streamwise phase speed increases with increasing λ_v along with the mean velocity represented by the dashed-dotted line in figure 11a. A similar trend is displayed by r1 which exists only in the range of $0 \le \lambda_v \le 0.485$. Other characteristics of r1, the wavelength (figure 11b) and the oblique angle (figure 11d), are insensitive to varying λ_v at smaller values, but they increase sharply when λ_v approaches 0.485, at about which r1 vanishes.

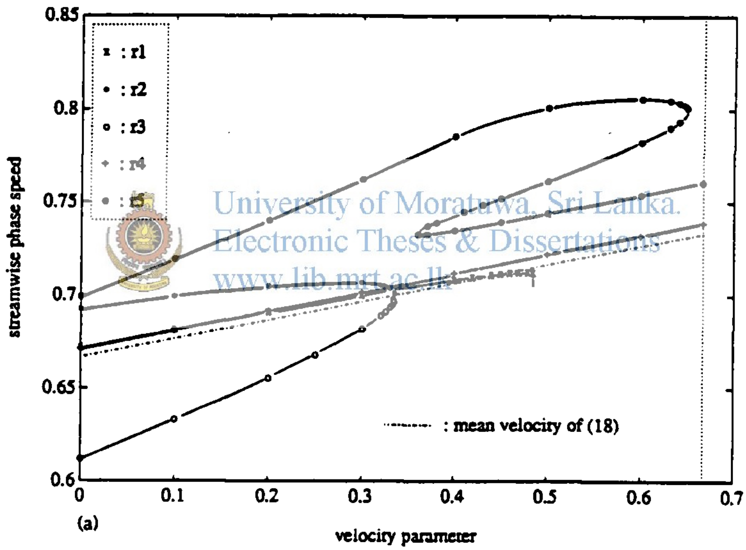

Figure 11. Influences of the velocity parameter λ_v upon the characteristics of the direct resonances at R=1000, $\theta=3^\circ$, and $\gamma=3000$: (a) the streamwise phase speed c_r, (b-c) the wavelength $2\pi/k$, (d-e) the oblique angle $\sin^{-1}(\alpha/k)$, and (f) the inverse of damping rate $|1/\alpha c_i|$.

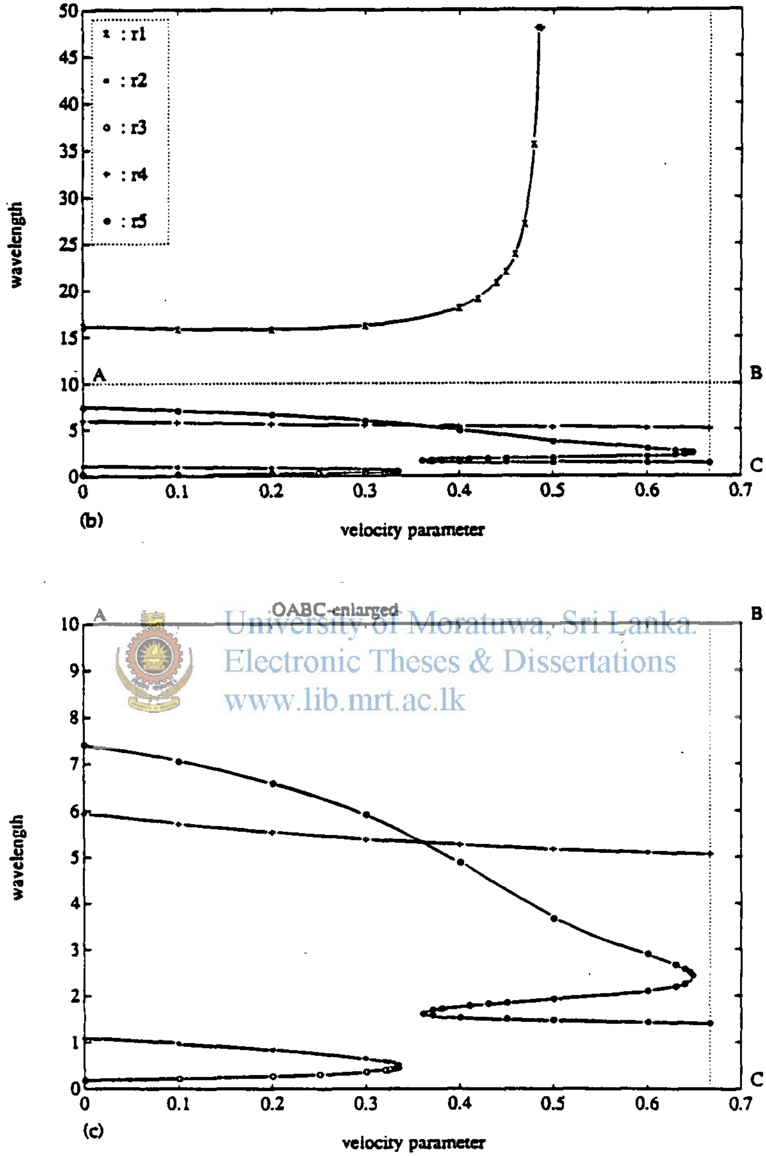

Figure 11. Continued.

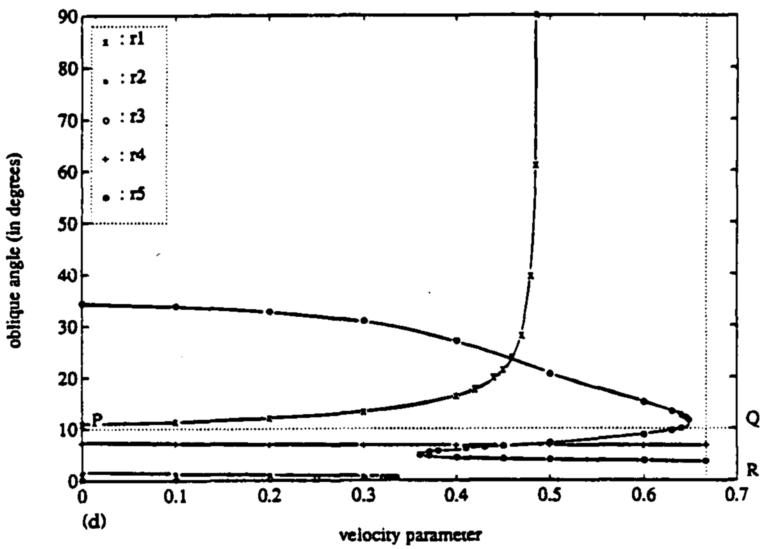

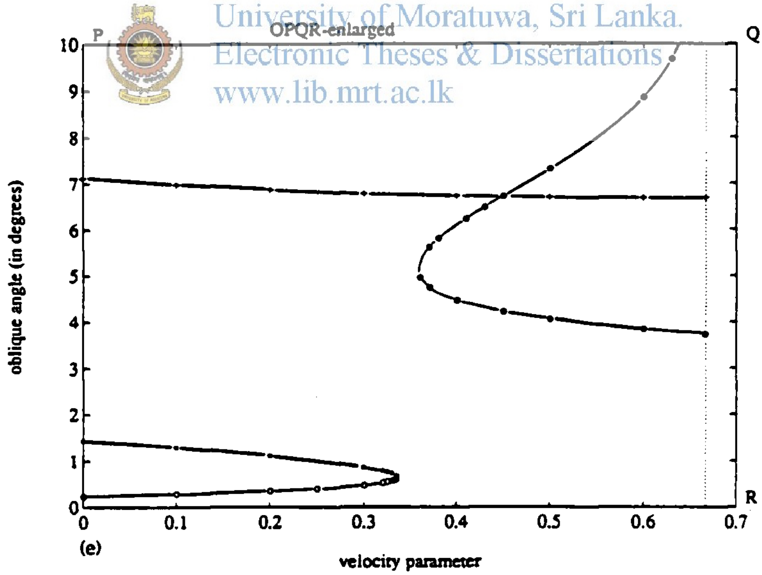

Figure 11. Continued.

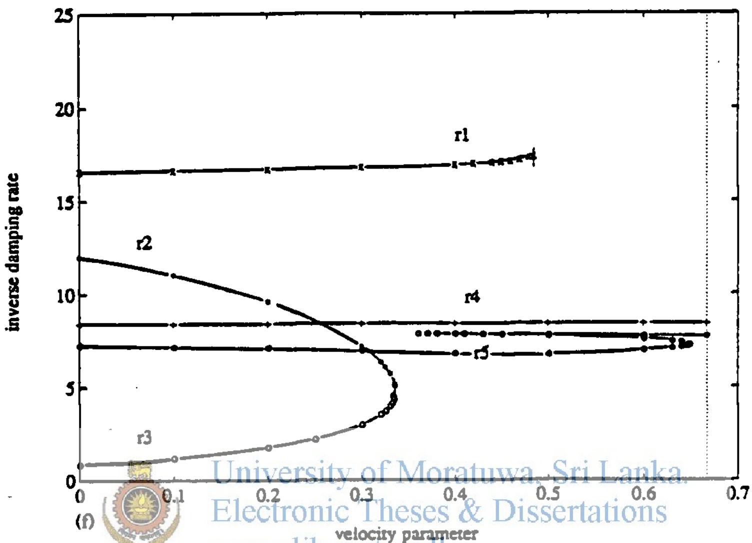

Figure 11. Continued.

With increasing λ_v, the variations in the characteristics of r2, r3 and r5 are spectacular, as can be seen in figure 11a-f. The resonances r2 and r3 exist only in the range of $0 \le \lambda_v \lesssim 0.335$, and interestingly these two resonances describe the upper and the lower branches of a continuous curve as displayed in each of figures 11a-f. According to these figures, the curve of r5 has a fold in the interval about $0.36 \le \lambda_v \le 0.65$ revealing the presence of three resonances, in place of one, in that interval. The $|1/\alpha c_i|$-values of the resonances r1, r4 and r5 are more or less the same at any λ_v-value considered, but that of r2 decreases and of r3 increases until they merge at about λ_v=0.335, as shown in figure 11f.

Over all, the developing velocity profile seems to have insignificant influences upon the characteristics of the degeneracies, whereas its influences on the direct resonances are remarkable. This difference may be attributed to the fact that degeneracies are double zeros of a single function which changes smoothly as the mean flow changes, whereas direct resonances result from coinciding zeros of two independent functions. Another important observation is that, in both cases of degeneracies and direct resonances, the variations in the streamwise phase velocities are confined to the range of 0.61 to 0.81, (see figures 10a and 11a), which is below the maximum velocity of the basic flow, which is unity. (The significance of this observation will be discussed later.) Finally, it should be remembered that the curves of figures 10 and 11 belong to the combination of $R = 1000$, $\theta = 3^{\circ}$ and $\gamma = 3000$, and any change in this combination may alter the shapes of these curves. Particularly, the consequences of varying R could be of interest but is not pursued in this study.

4. Comparison with plane Poiseuille flow

The results obtained so far, interesting in their own right, may be given further significance when compared to degeneracies and direct resonances in plane Poiseuille flow. This flow, shown in figure 12, is simpler to treat analytically than the water table flow since the boundary conditions are those at solid walls. However, the symmetry of the basic flow and the homogeneity of the boundary conditions allow both symmetric and anti-symmetric solutions for the eigenvalue problems of interest, and thus add more complexity to the modal structure.

The eigenvalue problem of the normal *velocity* in plane Poiseuille flow is described by equation (9), with the basic flow U defined by (1) in the interval y=0 to 2. (The scales used for non-dimensionalization are centreline velocity and channel half-height, which are equivalent to the scales used for water table flow.) The conditions at the lower boundary (at y=0) are the same as those at the inclined plane of the water table flow, and thus are described by (10a-b) as $\phi = D\phi = 0$. The remaining conditions at the upper boundary (at y=2) are also $\phi = D\phi = 0$, and can be replaced by conditions related to the symmetric properties of the eigenfunctions at the centreline (at y=1), as follows:

For the symmetric case

$$D\phi = D^3\phi = 0 \qquad \text{at } y = 1\,, \qquad (19a\text{-}b)$$

and for the antisymmetric case

$$\phi = D^2\phi = 0 \qquad \text{at } y = 1\,. \qquad (20a\text{-}b)$$

The degneracies obtained using (19a-b) are thus known as the symmetric degeneracies and those obtained with (20a-b) as the antisymmetric degeneracies; some of these degeneracies are listed in table 4. (The numerical values were first presented in [9])

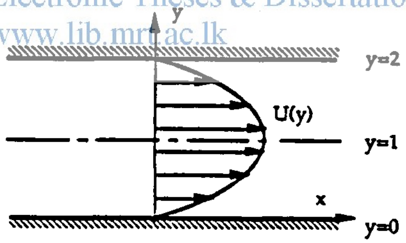

Figure 12. Mean flow configuration of plane Poiseuille flow.

For the normal *vorticity* , the eigenvalue problem (13)-(14) in water table flow is identical to the symmetric problem in plane Poiseuille flow, which is obvious from the boundary conditions at the centreline (at y=1). When an eigenvalue of this problem coincides with an eigenvalue of the normal velocity (antisymmetric) problem, there forms a direct resonance known as the symmetric direct resonance of plane Poiseuille flow (see e.g. [16]). Few of these direct resonances computed by Gustavsson [15] are re-listed in table 5 for comparison's sake.

Name	α	k	$c = c_r + ic_i$
sd1	0.216608	2.539077	0.726284-0.164493i
sd2	0.363772	0.885820	0.640595-0.352177i
sd3	0.527646	1.891179	0.635669-0.390237i
sd4	0.904262	0.506350	0.669154-0.318220i
ad1	0.230289	2.257373	0.719016-0.229603i
ad2	0.620702	2.804728	0.644522-0.409711i

Table 4. Four of the symmetric degeneracies (sd) and two of the antisymmetric degeneracies (ad) in plane Poiseuille flow at R=1000.

Name	α	k	$c = c_r + ic_i$
sr1	0.13889	33.4455	0.61180-8.34338i
sr2	0.14507	5.7942	0.69256-0.57474i
sr3	0.34576	1.0152	0.80941-0.19269i
sr4	0.12392	0.8165	0.67090-0.96110i
sr5	0.34421	3.7555	0.67187-0.58756i
sr6	0.13985	6.8108	0.68073-0.37505i
sr7	0.89448	0.6313	0.67137-0.58806i

Table 5. Seven of the symmetric direct resonances (sr) in plane Poiseuille flow at R=1000.

A comparison between table 4 and table 1 shows that the two antisymmetric degeneracies ad1 and ad2 are quite close to the water table degeneracies d2 and d5, respectively. According to the results of section 3, in the parameter ranges studied, it is d2 and d5 which are most insensitive to changes in θ and γ, and thus belong to the H-group. These degeneracies also have large k-values, which can in fact be used to tentatively motivate this behaviour. Considering (10d), it is seen that, for large k together with small θ, an approximation for this equation becomes $(D^2+k^2)\phi = 0$, which together with (10c) implies that the eigenfunction will have $\phi = D^2\phi = 0$ at $y = 1$. This is exactly the conditions for an antisymmetric eigenfunction in plane Poiseuille flow (cf 20a-b), and thus it may not be surprising that d2 and d5 are comparable to the antisymmetric degeneracies of plane Poiseuille flow. The other water table degeneracies listed in table 1, which have small k-values, seem to have no obvious connection with the remaning degeneracies of plane Poiseuille flow listed in table 4. Comparing table 5 to table 2 reveals that the H-group water table direct resonances r2 and r3, which have large k-values, are related to the plane Poiseuille flow direct resonances sr2 and sr1, respectively. Among the rest of the direct resonances, no obvious connection is observed. We therefore conclude that the degeneracies and direct resonances which are common to both flows have short wavelengths, and that the corresponding eigenmodes of the normal velocity are antisymmetric about $y=0$ and those of the normal vorticity are symmetric about $y=0$.

Moreover, with varying R, the k-values and the c-values of the degeneracies and direct resonances in plane Poiseuille remain absolute constants, while the α-values vary such that the corresponding αR-values remain constants. Consequently the streamwise phase velocities, the wavelengths, the oblique angles and the $|1/\alpha c_i|$-values of these algebraic mechanisms in plane Poiseuille flow vary with R in a manner very similar to those in water table flow. Further more, the range that the streamwise phase speeds of these mechanisms in plane Poiseuille flow spans (see table 4 and 5) is the same as that spanned by those in water table flow.

5. Concluding remarks

Of the infinitely many degeneracies and direct resonances in water table flow, we have here analysed only those with R_{min}-values lower than the R (~1000) at about which the flow can first sustain turbulence. It is shown in section 3 that with increasing R, the inverse damping rates of the algebraic mechanisms increase almost linearly. This result indicates that the algebraic mechanisms should become more physically relevant with increasing R; which is indeed the kind of behaviour that one would expect from mechanisms which may play an active role in laminar-to-turbulent transition. It is possible that the increasing physical relevance of each of these mechanisms be associated with a threshold value at some Reynolds number above which the flow becomes unstable to secondary disturbances. This possibility is at present investigated with the degeneracies in plane Poiseuille flow, since this flow is simpler to treat analytically, and in the future will be extented to water table .

To establish the capacity of the algebraic mechanisms to account for observable quantities, such as propagation-speeds, wavelengths, and oblique angles, one should at this stage compare the theoretical predictions with relevant experimental information. Unfortunately, no data are yet available that strictly pertain to the assumptions of the theory; that is, small three-dimensional perturbations in the sub-transitional Reynolds number range. What is needed is therefore carefully measured properties of the pre-turbulent-spot environments at various slopes of the table and at various values of the material parameters, and also along the developing velocity profile. These measurements could then be compared to the results of this study to determine the role played by the algebraic mechanisms in laminar-to-turbulence transition.

Nevertheless, additional information could be gained for a proper assessment of the mechanisms by considering the experimental and theoretical similarities, and differences, between water table flow and plane Poiseuille flow. It is concluded in section 4 that the symmetric vorticity modes and the antisymmetric velocity modes of plane Poiseuille flow are represented in water table flow, whereas the antisymmetric vorticity- and symmetric velocity-modes of plane Poiseuille flow are not. In terms of the direct resonance mechanism, this indicates that phenomena associated with antisymmetric vorticity in plane Poiseuille flow should not be detected in water table flow. It is indeed experimentally observed that the characteristic waves found at the wing tips of the turbulent spots in plane Poiseuille flow are associated with antisymmetric streamwise velocity, and hence vertical vorticity, disturbances [17]. The absence of these waves in water table flow [13] is consistent with the lack of these vorticity modes in that flow. The observed similarities between the two flows are the transitional Reynolds numbers and the propagation speeds of the centre part of the spots [18], [12]. The propagation velocities of the spots in both flows are in fact comparable with the range of c_r spanned by the mechanisms, which is about 0.61 to 0.81 (of the free surface velocity in water table flow and of the centre-line velocity in plane Poiseuille flow). Nonetheless, it remains to be seen how the algebraic mechanisms described here can be related to the turbulent spots.

References

1. W. M'F. ORR, The stability or instability of the steady motions of a perfect liquid and a viscous liquid, *Proc. Roy. Irish Acad.* A 27:9-138 (1907).
2. A. SOMMERFELD, Ein bietrag zur hydrodynamischen erklarung det turbulenten flussigkeitsbewegungen, in *Atti. del 4. Congr. Internat. dei Mat. III*, Roma, 116-124 (1908).
3. T. HERBERT, Stability of plane Poiseuille flow - theory and experiment, *Fluid Dyn. Trans.* 11:77-126 (1983).
4. J. KIM and R. D. J. MOSER, On the secondary instability in plane Poiseuille flow, *Phys. of Fluids* A 1:775-777 (1989).
5. L. H. GUSTAVSSON and L. S. HULTGREN, A resonance mechanism in plane Couette flow, *J. Fluid Mech.* 98:149-159 (1980).
6. C. E. GROSCH and H. SALWEN, The stability of steady and time-dependent plane Poiseuille flow, *J. Fluid Mech.* 34:177-205 (1968).
7. L. M. MACK, A numerical study of the temporal eigenvalue spectrum of the Blasius boundary layer, *J. Fluid Mech.* 73:497-520 (1976).
8. W. KOCH, Direct resonances in Orr-Sommerfeld problems, *Acta Mechanica* 58:11-29 (1986).

9. R. SHANTHINI, Degeneracies of the temporal Orr-Sommerfeld eigenmodes in plane Poiseuille flow, *J. Fluid Mech.* 201:13-34 (1989).

10. C.-S. YIH, *Fluid Mechanics*, West River Press, Ann Arbor, Michigan, 1977.

11. M. GRAEF, Zur Instabilität ebener Riselfilme bei Berücksichtung der Oberflächenspannung. Max-Plank Institut für strömungsforschung, Bericht 1 (1961).

12. L. H. GUSTAVSSON and J.-E. ÖGREN, Observations of turbulent spots on a water table, in *Noise Radiation from drill steels*, by J.-E. Ögren, Doctoral Thesis 1983:23D, Luleå University of Technology, Sweden (1983).

13. P.-A. LINDBERG, E. M. FAHLGREN, P. H. ALFREDSSON and A. V. JOHANSSON, An experimental study of the structure and spreading of turbulent spots, in *laminar-turbulent transition*, ed. Kozlov, Springer, 617-624 (1985).

14. P. GREN, Laser Doppler Measurement of turbulent spots on a water table, in *Structured Surfaces and Turbulence*, Licentiate Thesis 1987:04L, Luleå University of Technology, Sweden (1987).

15. L. H. GUSTAVSSON, Excitation of direct resonances in plane Poiseuille flow, *Stud. Appl. Maths* 75:227-248 (1986).

16. L. H. GUSTAVSSON, Resonant growth of three-dimesional disturbances in plane Poiseuille flow, *J. Fluid Mech.* 112:253-264 (1981).

17. D. S. HENNINGSON and P. H. ALFREDSSON, The wave structure of turbulent spots in plane Poiseuille flow. *J. Fluid Mech.* 178:405-421 (1987).

18. F. ALAVYOON, D. S. HENNINGSON and P. H. ALFREDSSON, Turbulent spot in plane Poiseuille flow - flow visualization, *Phys. of Fluids* 29:1328-1331 (1986).

Paper III

Submitted to *Journal of Fluid Mechanics*

Influence of temporal degeneracies upon the development of perturbation field - in plane Poiseuille flow

By Rajaratnam Shanthini

Division of Fluid Mechanics, Luleå University of Technology, S-951 87 Luleå, Sweden.

The local and the global temporal developments of the perturbation field are studied for plane Poiseuille flow, in the presence of temporal degeneracies. The initial perturbation velocity normal to the walls is chosen to be described by the generalized Orr-Sommerfield eigenfunction in the normal direction. The subsequent temporal development of the amplitude of this normal velocity is shown to be that of monotonical decay, in the linear regime. None the less, notable initial growth is exhibited by the streamwise velocity of the *two-dimensional* perturbation flow in the case of first symmetric degeneracy. However, in all cases of degeneracies investigated, the two-dimensional perturbation flow looses its kinetic energy with increasing time.

In the case of a *three-dimensional* perturbation flow, the spanwise variations in the normal velocity induce normal vorticity, whose amplitude is shown to increase with increasing Reynolds number. The presence of normal vorticity causes the perturbation flow to gain kinetic energy from the basic Poiseuille flow. This gain is so great that the perturbation flow overcomes its energy loss due to viscous dissipation and exhibits significant initial growth of its kinetic energy, at crucial Reynolds numbers.

1. Introduction

It is well known that the characteristic equation of the temporal Orr-Sommerfeld eigenvalue problem in plane Poiseuille flow has infinitely many isolated zeros in the plane of complex phase-speed (c); see e.g Schensted (1961). These zeros were thought to be simple until Grosch & Salwen (1968) pointed out the possibility of a double zero, the presence of which was later confirmed by Gustavsson (1981). A detailed study of the double zeros of temporal type, termed temporal degeneracies, was carried out recently by Shanthini (1989). It was shown that there are in fact more than one degeneracy in plane Poiseuille flow, and that each of these degeneracies appears *only* at a certain combinations of k (the modulus of wave vector) and αR (the streamwise wavenumber times the Reynolds number). This implies that a temporal degeneracy takes unique values for α and β (the spanwise wavenumber) at a chosen Reynolds number, and that it disappears at Reynolds numbers below the ratio ($\alpha R/k$) corresponding to that degeneracy. At this minimum Reynolds number, the degeneracy concerned corresponds to the two-dimensional case (β=0 and α=k).

Degeneracies are of interest in hydrodynamic stability since they lead to the possibility of algebraic growth. A formal solution describing the development of the perturbation velocity *normal* to the walls, corresponding to a degeneracy, was obtained in Shanthini (1989), and is further simplified to a convenient form in this paper (§3). This expression shows the probable initial temporal growth of the normal velocity and its eventual exponential decay in the linear regime - owing to the fact that the degeneracies considered are damped. Degeneracies influence not only the normal component, but also the streamwise and the spanwise components, of the perturbation velocity field. Analytical expressions, as well as their quantitative representations, describing the temporal development of the entire perturbation velocity field have been obtained for both the two-dimensional case (§4) and the three-dimensional case (§5).

Having obtained the histories of individual velocity components of the perturbation flow, it is straight forward to evaluate its kinetic energy (§6), which yields a global vision of the development of the perturbation flow. The temporal development of the kinetic energy is discussed also in the light of *Reynolds-Orr energy equation*, which gives specific information about the energy transfer between the basic flow and the perturbation flow.

2. Problem Formulation

2.1. *Description of the perturbation field*

The incompressible flow of a viscous fluid between two infinite plates, driven by a constant pressure gradient, is known as plane Poiseuille flow. Normalized with the centreline velocity (U_0) and the channel half-height (h_0), the fully developed velocity profile can be written as

$$U(y) = 1-y^2 . \tag{2.1}$$

Here, y represents the direction normal to the plates, and the streamwise and the spanwise directions are represented by x and z, respectively. On this basic flow imposed is a three-dimensional infinitesimal perturbation velocity (u, v, w). Our interest is to analyse the linear development of this perturbation field in the presence of temporal degeneracies, as described in the introduction. To study this, we choose the perturbation field to be spatially periodic in x- and z- directions such that the respective (real) wavenumbers α and β are the same as those at which a degeneracy can be activated. This step leads to the following description of the perturbation field:

$$\begin{Bmatrix} u(x,y,z,t) \\ v(x,y,z,t) \\ w(x,y,z,t) \end{Bmatrix} = \frac{1}{2}\left(\begin{Bmatrix} \hat{u}(y,t) \\ \hat{v}(y,t) \\ \hat{w}(y,t) \end{Bmatrix} e^{i\alpha x + i\beta z} + complex\ conjugate \right). \quad (2.2a-c)$$

The absolute values of ($\hat{u}$, $\hat{v}$, $\hat{w}$) represent the amplitudes of (u, v, w), and it is the temporal development of these amplitudes that is of our concern. Note that had a double Fourier transformation been carried out on the homogeneous spatial coordinates x and z, with α and β as transform variables, the components ($\hat{u}$, $\hat{v}$, $\hat{w}$) would have represented the Fourier transformed (u, v, w). However, in either representation, the components ($\hat{u}$, $\hat{v}$, $\hat{w}$) are related through continuity as follows:

$$i\alpha\hat{u} + \frac{\partial \hat{v}}{\partial y} + i\beta\hat{w} = 0. \quad (2.3)$$

Using (2.2) and (2.3) together with the *normal vorticity* component of the perturbation flow, defined as

$$\omega = \frac{\partial u}{\partial z} - \frac{\partial w}{\partial x}, \quad (2.4)$$

it can be shown that

$$\hat{u} = i\left\{\frac{\alpha}{k}\left(\frac{1}{k}\frac{\partial \hat{v}}{\partial y}\right) - \frac{\beta}{k}\left(\frac{\hat{\omega}}{k}\right)\right\}, \quad (2.5a)$$

and that

$$\hat{w} = i\left\{\frac{\beta}{k}\left(\frac{1}{k}\frac{\partial \hat{v}}{\partial y}\right) + \frac{\alpha}{k}\left(\frac{\hat{\omega}}{k}\right)\right\}. \quad (2.5b)$$

Hence, the development of the perturbation field can also be studied by analyzing the temporal development of the following amplitudes:

$$\left(|\hat{v}|\,,\ \left|\frac{1}{k}\frac{\partial \hat{v}}{\partial y}\right|\,,\ \left|\frac{\hat{\omega}}{k}\right| \right). \tag{2.6}$$

In case of the two-dimensional perturbation field, where β=0, the second component of (2.6) is simply the amplitude of the streamwise velocity. The third component of (2.6) is non-vanishing only in case of the three-dimensional perturbation field. In either case, the first component of (2.6) is the amplitude of the normal velocity. This description is favoured since, among other reasons, we choose to investigate the development of the initial perturbation field which is free of *initial normal vorticity.*

2.2. *Initial perturbation field*

The x- and z- dependence of the initial perturbation filed is described by (2.2), and the y-dependence is chosen such that

$$\hat{v}_0 = \frac{d\hat{v}_0}{dy} = 0 \quad \text{at} \quad y = \pm 1, \tag{2.7a}$$

and that

$$\hat{\omega}_0 = 0 \quad \forall\, y. \tag{2.7b}$$

Here, the subscript 0 indicates the initial values (i.e. the functional values at t=0). Condition (2.7a) results from boundary conditions at rigid walls and condition (2.7b) corresponds to zero initial normal vorticity. A suitable functional form for $\hat{v}_0$ is given in §3.2, where also the reasons for such a choice have been discussed. In the oncoming analyses, $\hat{v}_0$ is chosen to be *either* symmetric, *or* antisymmetric, about the centreline of the channel (i.e. at y=0) since any disturbance can be split into a symmetric part and an antisymmetric part.

3. Development of normal (perturbation) velocity amplitude

3.1. *Analytical expression for $|\hat{v}(y,t)|$ in the presence of degeneracy*

The normal velocity component of the perturbation field is governed by the following (linear) equation:

$$\left(\frac{\partial}{\partial t} + U\frac{\partial}{\partial x}\right)\nabla^2 v \; - \; \frac{d^2U}{dy^2}\frac{\partial v}{\partial x} \; - \; \frac{1}{R}\nabla^4 v \; = \; 0 \, . \tag{3.1a}$$

$$v \; = \; \frac{\partial v}{\partial y} \; = \; 0 \quad \text{at} \quad y = \pm 1 \, . \tag{3.1b}$$

Here, ∇^2 is the three-dimensional Laplacian and R is the Reynolds number defined in terms of U_0 and h_0. Substituting (2.2) in (3.1) leads to the following partial differential equation for $\hat{v}(y,t)$:

$$\left(\frac{\partial}{\partial t} + i\alpha U\right)\left(\frac{\partial^2}{\partial y^2} - k^2\right)\hat{v} \; - \; i\alpha\frac{d^2U}{dy^2}\hat{v} \; - \; \frac{1}{R}\left(\frac{\partial^2}{\partial y^2} - k^2\right)^2\hat{v} \; = \; 0 \, . \tag{3.2a}$$

$$\hat{v} \; = \; \frac{\partial \hat{v}}{\partial y} \; = \; 0 \quad \text{at} \quad y = \pm 1 \, . \tag{3.2b}$$

Equation (3.2) can then be subjected to Laplace transformation on the time coordinate t, with s as the transform variable, to obtain an ordinary differential equation which permits formal solution to $\hat{v}(y,t)$. Introducing

$$c = -\frac{s}{i\alpha} \, , \tag{3.3}$$

the transformed equation can be written as follows:

$$\left\{\left(D^2 - k^2\right)^2 \; - \; i\alpha R\,(U - c)\left(D^2 - k^2\right) \; + \; i\alpha R\left(D^2 U\right)\right\}\phi \; = \; -R\,\Delta \, . \tag{3.4a}$$

$$\phi \; = \; D\phi \; = \; 0 \quad \text{at} \quad y = \pm 1 \, . \tag{3.4b}$$

Here, ϕ is the Laplace transformed $\hat{v}(y,t)$, D is the operator d/dy , and

$$\Delta \; = \left(D^2 - k^2\right)\hat{v}_0 \, . \tag{3.5}$$

Equation (3.4) can be solved formally, at a k-αR combination of a degeneracy, using the method of variation of parameters. The solution is then inverse Laplace transformed to recover the following analytical expression for $\hat{v}(y,t)$:

$$\hat{v}\,(y,t) \;=\; \sum_{\substack{m=1 \\ m \neq l}}^{\infty} \frac{i\alpha R\, F_m}{\left(\frac{\partial E}{\partial c}\right)_m}\, exp\left(-i\alpha R c_m \,\frac{t}{R}\right)$$

$$+\; \frac{2 i\alpha R}{\left(\frac{\partial^2 E}{\partial c^2}\right)_l} \left[-i\alpha R F_l\, \frac{t}{R} + \left(\frac{\partial F}{\partial c}\right)_l - \frac{1}{3}\, \frac{\left(\frac{\partial^3 E}{\partial c^3}\right)_l}{\left(\frac{\partial^2 E}{\partial c^2}\right)_l}\, F_l \right] exp\left(-i\alpha R c_l \,\frac{t}{R}\right). \qquad (3.6)$$

Details of the derivation of (3.6) are available in Shanthini (1989) and hence are not repeated here. We now go on to describe the notations used in (3.6).

For *symmetric* $\hat{v}_0$,

$$F = -\phi_1 \int_0^1 \left(E_{23}\,\phi_2^\dagger + E_{43}\,\phi_4^\dagger\right)\Delta\; d\eta \;-\; \phi_3 \int_0^1 \left(E_{12}\,\phi_2^\dagger + E_{14}\,\phi_4^\dagger\right)\Delta\; d\eta \qquad (3.7a)$$

and

$$E \;=\; E_{13}\;. \qquad (3.7b)$$

For *antiymmetric* $\hat{v}_0$,

$$F = -\phi_2 \int_0^1 \left(E_{14}\,\phi_1^\dagger + E_{34}\,\phi_3^\dagger\right)\Delta\; d\eta \;-\; \phi_4 \int_0^1 \left(E_{21}\,\phi_1^\dagger + E_{23}\,\phi_3^\dagger\right)\Delta\; d\eta \qquad (3.8a)$$

and

$$E \;=\; E_{24}\;. \qquad (3.8b)$$

Here, the functions $\{\phi_\upsilon\}_{\upsilon=1}^{4}$ are the linearly independent solutions to the Orr-Sommerfeld (OS) operator, which is in the left-hand side of (3.4a). The functions $\left\{\phi_\upsilon^\dagger\right\}_{\upsilon=1}^{4}$ are the linearly independent solutions to its adjoint operator,

$$\left(D^2-k^2\right)^2 \;-\; i\alpha R\,(U-c)\left(D^2-k^2\right) - \;2 i\alpha R\,(DU)D\,. \qquad (3.9)$$

These functions are ordered such that $(\phi_1,\, \phi_3,\, \phi_2^\dagger,\, \phi_4^\dagger)$ are symmetric and $(\phi_2,\, \phi_4,\, \phi_1^\dagger,\, \phi_3^\dagger)$ are antisymmetric about the centreline of the channel, (see appendix A). The symbol E_{pq} is defined by

$$E_{pq} \;=\; \phi_{pw} D\phi_{qw} \;-\; \phi_{qw} D\phi_{pw}\;, \qquad (p,q \;=\; 1,2,3,4)\,, \qquad (3.10)$$

where the second subscript w represents values at the wall at y=1. Also in (3.6), index m indicates values at $c=c_m$, which are the simple zeros of the characteristic function E. These are also the OS eigenmodes. Finally, the subscript l represents the degeneracy

The underlying assumption in obtaining (3.6) is that, at the k-αR combination chosen, there is only one degeneracy among the infinitely many isolated OS eigenmodes, which is the case for the degeneracies investigated in this paper.

The material presented so far in this section, which is somewhat a repetition of parts of Shanthini (1989), lays the basis for simplifying (3.6) as follows. It is straight forward to show that the expression for F (3.7a or 3.8a) can be reduced to the following *at a zero* of E (3.7b or 3.8b):

$$F = \Phi \int_0^1 \Phi^\dagger \, \Delta \, d\eta \, . \tag{3.11}$$

Here

$$\Phi = A\phi_1 - \phi_3 \tag{3.12a}$$

and

$$\Phi^\dagger = E_{12}\,\phi_2^\dagger + E_{14}\,\phi_4^\dagger = -\frac{1}{A}\left(E_{23}\,\phi_2^\dagger + E_{43}\,\phi_4^\dagger\right) , \tag{3.12b}$$

with

$$A = \frac{\phi_{3w}}{\phi_{1w}} = \frac{D\phi_{3w}}{D\phi_{1w}} , \tag{3.12c}$$

when $\hat{v}_0$ is symmetric about the centreline of the channel and E is represented by E_{13}. For opposite symmetry for $\hat{v}_0$, E is represented by E_{24} and

$$\Phi = A\phi_2 - \phi_4 \tag{3.13a}$$

and

$$\Phi^\dagger = E_{21}\,\phi_1^\dagger + E_{23}\,\phi_3^\dagger = -\frac{1}{A}\left(E_{14}\,\phi_1^\dagger + E_{34}\,\phi_3^\dagger\right) , \tag{3.13b}$$

with

$$A = \frac{\phi_{4w}}{\phi_{2w}} = \frac{D\phi_{4w}}{D\phi_{2w}} . \tag{3.13c}$$

Note that the expressions for Φ and $\Phi^\dagger$ in both (3.12) and (3.13) are also solutions to the OS and its adjoint equations, respectively. Moreover, it is straight forward to show that Φ satisfies the condition

$$\Phi = D\Phi = 0 \quad \text{at} \quad y = \pm 1 \tag{3.14a}$$

at a zero of E. Also, using the relationship between $\{\phi_{\upsilon}^{\dagger}\}_{\upsilon=1}^{4}$ and $\{\phi_{\upsilon}\}_{\upsilon=1}^{4}$ (stated in appendix A), it can be shown that $\Phi^{\dagger}$ satifies the condition

$$\Phi^{\dagger} = D\Phi^{\dagger} = 0 \quad \text{at} \quad y = \pm 1 \tag{3.14b}$$

at a zero of E. Hence, Φ and $\Phi^{\dagger}$ are indeed the OS eigenfunction and its adjoint function, respectively. With this realization, utilizing expression (3.5) for Δ and using the relationships (B1-B3) given in appendix B, equation (3.6) can be rewritten as

$$\begin{aligned} \hat{v}(y,t) = & \sum_{\substack{m=1 \\ m \neq l}}^{\infty} \frac{(\Phi_m^{\dagger}, \hat{v}_0)}{(\Phi_m^{\dagger}, \Phi_m)} \Phi_m \, exp\left(-i\alpha R c_m \frac{t}{R}\right) \\ & + \frac{1}{\left(\Phi_l^{\dagger}, \frac{\partial \Phi_l}{\partial c}\right)} \left[(\Phi_l^{\dagger}, \hat{v}_0)\left(-i\alpha R \, \Phi_l \frac{t}{R} + \frac{\partial \Phi_l}{\partial c}\right) \right. \\ & \left. + \left(\frac{\partial \Phi_l^{\dagger}}{\partial c} - \frac{\left(\frac{\partial \Phi_l^{\dagger}}{\partial c}, \frac{\partial \Phi_l}{\partial c}\right)}{\left(\Phi_l^{\dagger}, \frac{\partial \Phi_l}{\partial c}\right)} \Phi_l^{\dagger}, \hat{v}_0 \right) \Phi_l \right] exp\left(-i\alpha R c_l \frac{t}{R}\right). \end{aligned} \tag{3.15}$$

In this expression, the inner-product notation

$$(f, g) = \int_0^1 f(y) \left(D^2 - k^2\right) g(y) \, dy \tag{3.16}$$

is used. At this stage, we have the most general analytical expression to evaluate the response of $\hat{v}(y,t)$ in the presence of a degeneracy (cf. Schensted 1961) to an initial perturbation field chosen to fulfill (2.7a); conditon (2.7b) is irrelevent at this stage.

3.2. *Suitable functional form for* $\hat{v}_0$

Choosing a suitable functional form to describe $\hat{v}_0$ is guided by the following two conditions: the magnitude of $\hat{v}_0$ at any y-position should be small enough to justify the assumptions of linearization and boundary conditions given by (2.7a) should be satisfied. One obvious choice for $\hat{v}_0$ then becomes the OS eigenfunctions themselves.

At the k-αR combination of a degeneracy, the complete set of eigenfunctions are given by

$$\left\{ \Phi_m \;(m = 1, \infty \,;\, m \neq l),\; \Phi_l \,,\; \frac{\partial \Phi_l}{\partial c} \right\}, \tag{3.17}$$

according to Schensted (1961) and DiPrima & Habetler (1969); where the subscripts m and l take the same identities as before. The last function in (3.17) is known as the generalized eigenfunction at the degeneracy, and it is straight forward to show that it satisfies the following boundary conditions:

$$\frac{\partial \Phi_l}{\partial c} = D\left(\frac{\partial \Phi_l}{\partial c} \right) = 0 \quad \text{at} \quad y = \pm 1 \,.$$

When $\hat{v}_0$ is represented by each of the functions given by (3.17), expression (3.15) can be reduced, with the help of the bi-orthogonality relationships (B4-B8) listed in appendix B, to give the results of table 1. It becomes obvious from table 1 that the algebraic (t/R) term in (3.15) survives only when $\hat{v}_0$ is represented by the generalized eigenfunction ($\partial \Phi_l / \partial c$). Also, table 1 reveals that the y-dependence of the normal velocity is maintained as that of the eigenfunction with time in all cases except the last. In that case, the y-dependence of the normal velocity, described by the generalized eigenfunction initially, would cease to resemble that of any eigenfunction as the time grows.

$\hat{v}_0$	$\hat{v}\,(y,t)$
$\Phi_m \;(m = 1, \infty \,;\, m \neq l)$	$\Phi_m \; exp\left(-i\alpha R c_m \, \frac{t}{R} \right)$
Φ_l	$\Phi_l \; exp\left(-i\alpha R c_l \, \frac{t}{R} \right)$
$\frac{\partial \Phi_l}{\partial c}$	$\left[-i\alpha R \; \Phi_l \, \frac{t}{R} + \frac{\partial \Phi_l}{\partial c} \right] exp\left(-i\alpha R c_l \, \frac{t}{R} \right)$

Table 1. Various choices for the y-dependence of initial perturbation velocity normal to the walls and its subsequent temporal development, at a k-αR combination of a degeneracy.

Recall that DiPrima & Habetler (1969) has shown that any function, which vanishes at $y=\pm 1$ and has continuous first derivative, which also vanishes at $y=\pm 1$, can be expanded in terms of the functions given in (3.17). Since $\hat{v}_0$ satisfies these conditions, it can be expanded in terms of the functions in (3.17). Consequently, it is adequate to follow the response due to exciting the basic flow by the generalized eigenfunction $(\partial\Phi_l/\partial c)$ to learn all about the algebraic temporal development of the perturbation field that is caused solely by the presence of a degeneracy. Results for the two-dimensional perturbation flow are presented in §4, and those for the three-dimensional perturbation flow are in §5.

4. Development of two-dimensional perturbation flow

It follows from the preceding section that the amplitudes of the normal and the streamwise components of the two-dimensional perturbation velocity, resulting from the excitation by the generalized eigenfunction, can be expressed as follows:

$$|\hat{v}| = \left|\left(-i\,\Phi_l\,\alpha R\,\frac{t}{R} + \frac{\partial\Phi_l}{\partial c}\right)\right| exp\left(Im(c_l)\,\alpha R\,\frac{t}{R}\right)$$

$$= \sqrt{|\Phi_l|^2\left(\alpha R\frac{t}{R}\right)^2 + 2Im\left\{\Phi_l\left(\frac{\partial\Phi_l}{\partial c}\right)^*\right\}\left(\alpha R\frac{t}{R}\right) + \left|\frac{\partial\Phi_l}{\partial c}\right|^2}\; exp\left(Im(c_l)\,\alpha R\,\frac{t}{R}\right). \tag{4.1}$$

$$|\hat{u}| = \frac{1}{k}\left|\frac{\partial\hat{v}}{\partial y}\right| = \left(\frac{1}{k}\right)\left|\left(-i\,(D\Phi_l)\,\alpha R\frac{t}{R} + \frac{\partial(D\Phi_l)}{\partial c}\right)\right| exp\left(Im(c_l)\,\alpha R\frac{t}{R}\right)$$

$$= \frac{1}{k}\sqrt{|D\Phi_l|^2\left(\alpha R\frac{t}{R}\right)^2 + 2Im\left\{D\Phi_l\left(\frac{\partial(D\Phi_l)}{\partial c}\right)^*\right\}\left(\alpha R\frac{t}{R}\right) + \left|\frac{\partial(D\Phi_l)}{\partial c}\right|^2}\; exp\left(Im(c_l)\alpha R\frac{t}{R}\right). \tag{4.2}$$

Here, *Im* denotes the imaginary part and * denotes the complex conjugates.

In this section, we numerically evaluate the quantitative developments of these amplitudes at certain degeneracies in plane Poiseuille flow. Six degeneracies are listed in table 2 together with their characteristics, which appeared first in Shanthini (1989) and have been refined here by a numerical method outlined in appendix C. In this table, the degeneracies have been grouped into symmetric- and antisymmetric- ones depending on the symmetry of the corresponding eigenfunctions about the centreline of the channel. Of the six degeneracies listed, only the responses of four degeneracies, s1, a1, s3 and a2, are presented here (in that order). The responses of the remaining two degeneracies, s2 and s4, are of the same order as, or less than, those of s3 and a2, which are small in magnitudes, and hence are not presented here. It can be seen in table 2 that the four degeneracies, s1, a1, s3 and a2, have the lowest R_{min} values.

Name	k	αR	c	R_{min}	$\lvert\partial E/\partial c\rvert$
			Symmetric degeneracies, where $E=E_{13}$		
s1	2.5390771	216.6076539	0.72628355-0.16449306i	85.3	0.545×10^{-3}
s2	0.8858195	363.7715555	0.64059541-0.35217672i	410.6	0.270×10^{-4}
s3	1.8911785	527.6455712	0.63566921-0.39023739i	279.0	0.195×10^{-6}
s4	0.5063509	904.2621852	0.66915436-0.31822018i	1785.8	0.958×10^{-4}
			Antisymmetric degeneracies, where $E=E_{24}$		
a1	2.2573726	230.2893044	0.71901575-0.22960311i	102.0	0.133×10^{-4}
a2	2.8047273	620.7022150	0.64452222-0.40971061i	221.3	0.204×10^{-5}

Table 2. Characteristics of six degeneracies of plane Poiseuille flow that are obtained by the method outlined in appendix C.

Evaluating (4.1) and (4.2) demands that the eigenfunctions, the generalized eigenfunctions and their y-derivatives be known at each degeneracy, which is accomplished as follows. Eigenfunction Φ, expressed by (3.12a) or (3.13a), is calculated from $\{\phi_\upsilon\}_{\upsilon=1}^{4}$, which in turn are evaluated by solving the OS equation using a fourth order Runge-Kutta scheme. The generalized eigenfunction $(\partial\Phi_l/\partial c)$ is calculated from the formula obtained by differentiating (3.12a) or (3.13a) with respect to c. (Note that A in expression (3.12a) or (3.13a) is differentiable with respect to c.) This step calls for c-derivatives of $\{\phi_\upsilon\}_{\upsilon=1}^{4}$, which are evaluated by solving the c-derivative of the OS equation,

$$\left\{\left(D^2-k^2\right)^2 - i\alpha R\,(U-c)\left(D^2-k^2\right) + i\alpha R\left(D^2 U\right)\right\}\frac{\partial\phi_v}{\partial c} = -i\alpha R\left(D^2-k^2\right)\phi_v\,,$$

using a fourth order Runge-Kutta scheme. The y-derivatives of the eigenfunctions and the generalized eigenfunctions are obtained as complementaries in the Runge-Kutta schemes. To check the numerical accuracy of Φ and its y-derivatives, the value of c was re-evaluated using the formula

$$c = \frac{\int_0^1 \left\{|D^2\Phi|^2 + 2k^2|D\Phi|^2 + k^4|\Phi|^2 - i\alpha R\,(U\,\Phi^* D^2\Phi - Uk^2|\Phi|^2 + 2|\Phi|^2)\right\}\,dy}{i\alpha R\,\int_0^1 \left\{|D\Phi|^2 + k^2|\Phi|^2\right\}\,dy}\,.$$

This formula is obtained by multiplying the OS equation by Φ^* and then integrating over the interval (-1,1); see e.g. p. 161 of Drazin & Reid (1981). Values of c obtained by this method agreed up to the seventh decimal place of the values given in table 2. Numerical accuracy of $(\partial\Phi_l/\partial c)$ and its y-derivatives were also checked by re-evaluating the values of c using a formula similar to the above, but obtained from the c-derivative of the OS equation, and excellent agreement was observed.

The calculated functions are then normalized such that

$$\frac{1}{2}\left\{\int_0^1 \left|\frac{\partial\Phi_l}{\partial c}\right|^2 dy + \int_0^1 \frac{1}{k^2}\left|\frac{\partial(D\Phi_l)}{\partial c}\right|^2 dy\right\} = 1\,. \tag{4.3}$$

This normalization is equivalent to exciting the basic flow by an initial perturbation having unit 'average energy', and gives one way of comparing the results for different degeneracies. (The energy will be discussed further in §6.)

Shown in figure 1(a-d) are the amplitudes and the phase angles of the *normalized* eigenfunctions and of the *normalized* generalized eigenfunctions of the four degeneracies. It is seen that the amplitudes of the generalized eigenfunctions are larger than those of the eigenfunctions in all cases. In each case, though the amplitude-distribution of the eigenfunction is somewhat similar to that of the generalized eigenfunction, the phase angles are quite different.

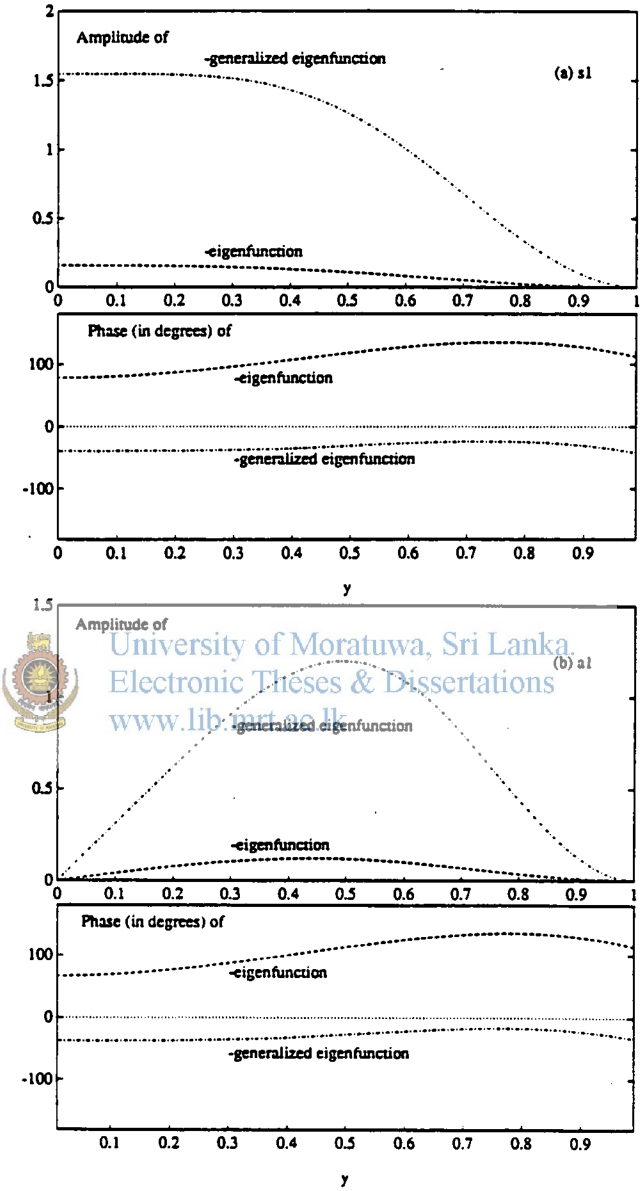

Figure 1. Amplitudes and phase angles of normalized eigenfunctions and generalized eigenfunctions of degeneracies (a) s1, (b) a1, (c) s3 and (d) a2, listed in table 1. The phase angles span from -180 to +180 degrees.

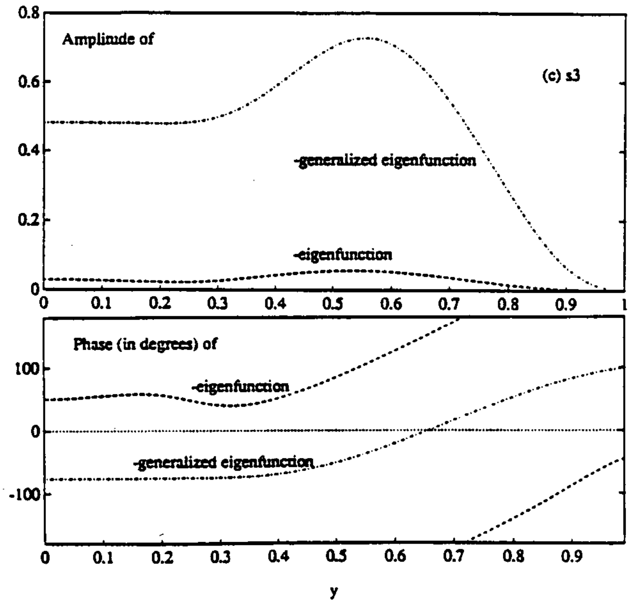

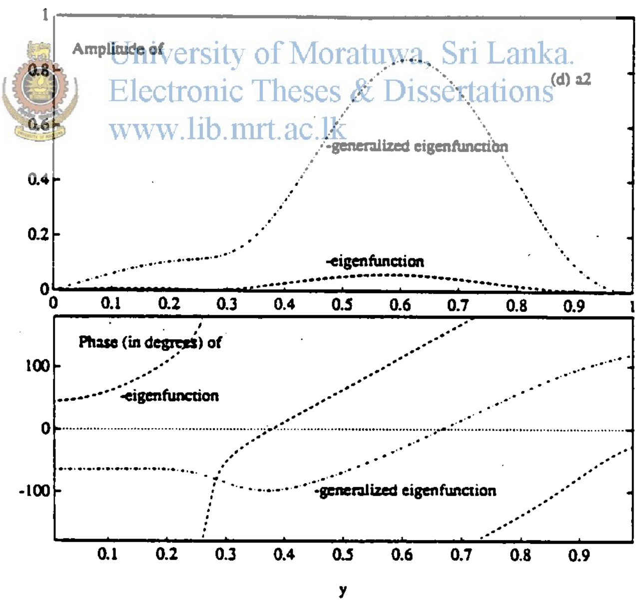

Figure 1. Continued.

The amplitude of the generalized eigenfunction is in fact the initial amplitude of the normal velocity, and hence the initial amplitude of the streamwise velocity is

$$\frac{1}{k}\left|\frac{\partial(D\Phi_l)}{\partial c}\right|.$$

Shown in figure 2 are the numerical values of these initial amplitudes for the four degeneracies. Comparing the initial amplitudes of the normal and the streamwise velocities reveals that the latter attains larger magnitudes than the former in all cases, except in the case of s1. This observation agrees well with the calculations, which show that the initial energy input has been distributed between the two velocity components of each degeneracy, s1, a1, s3 and a2, such that the first integral of (4.3) takes about 67.5%, 30.2%, 12.7% and 9.8% of the initial energy, respectively.

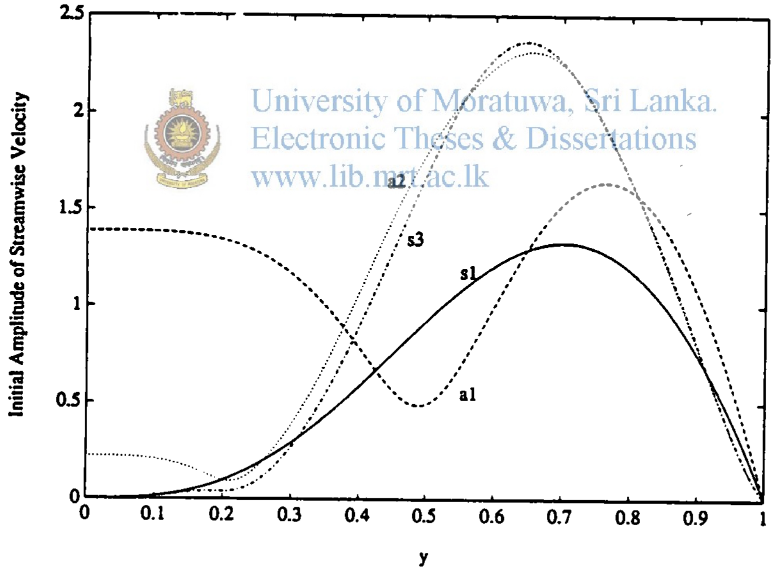

Figure 2. Initial amplitude of the streamwise velocity of the two-dimensional perturbation flow for s1, a1, s3 and a2.

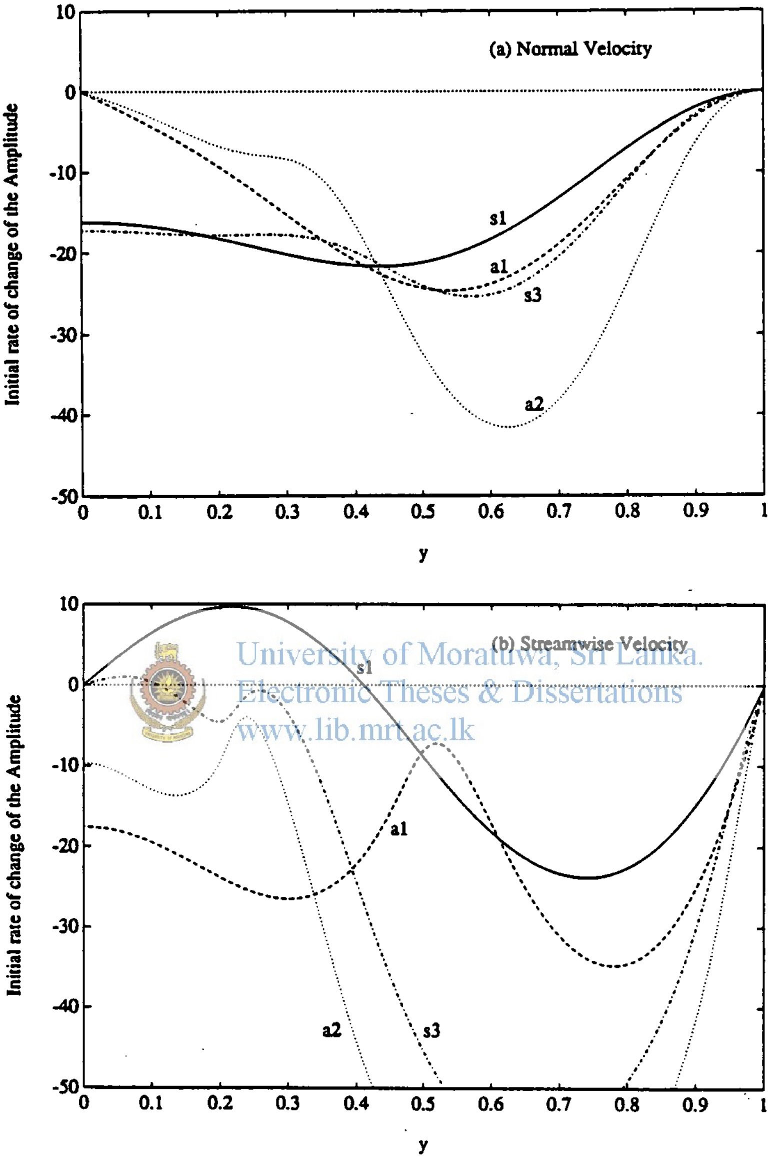

Figure 3. Initial rate of changes of the amplitudes (in degrees) of (a) the normal and (b) the streamwise perturbation velocities for s1, a1, s3 and a2.

Next, the initial rate of change of the amplitude is considered. Based on (4.1) and (4.2), analytical expressions for this quantity becomes:

$$\left(\frac{\partial}{\partial t}|\hat{v}|\right)_{t=0} = \frac{\alpha R}{R}\left|\frac{\partial \Phi_l}{\partial c}\right|\left[\frac{Im\left\{\Phi_l\left(\frac{\partial \Phi_l}{\partial c}\right)^*\right\}}{\left|\frac{\partial \Phi_l}{\partial c}\right|^2} + Im(c_l)\right] \tag{4.4}$$

and

$$\left(\frac{\partial}{\partial t}|\hat{u}|\right)_{t=0} = \left(\frac{\partial}{\partial t}\left\{\frac{1}{k}\left|\frac{\partial \hat{v}}{\partial y}\right|\right\}\right)_{t=0}$$

$$= \frac{\alpha R}{kR}\left|\frac{\partial (D\Phi_l)}{\partial c}\right|\left[\frac{Im\left\{D\Phi_l\left(\frac{\partial (D\Phi_l)}{\partial c}\right)^*\right\}}{\left|\frac{\partial (D\Phi_l)}{\partial c}\right|^2} + Im(c_l)\right]. \tag{4.5}$$

Note that in the case of a two-dimensional perturbation field, a degeneracy exists only when

$$\alpha = k \quad \text{and} \quad R = R_{\min} = \frac{\alpha R}{k},$$

of the corresponding degeneracy. Consequently, the $(\alpha R/R)$-term in (4.4) becomes equal to k, and the $(\alpha R/kR)$-term in (4.5) becomes unity. Numerical values of these rates (in degrees) as a function of y are shown in figure 3(a-b). According to figure 3(a), all four degeneracies have negatives values for the initial rate of change of the normal velocity amplitude. This implies that the normal velocity amplitude of *none* of the four degeneracies grow initially. As with the amplitude of the streamwise velocity (figure 3b), the antisymmetric degeneracies show negative results, but the symmetric degeneracies take positive values at some y-positions close to the centreline of the channel. Of the two symmetric degeneracies, the initial growth indicated by s1 is remarkable and is elaborated in figure 4.

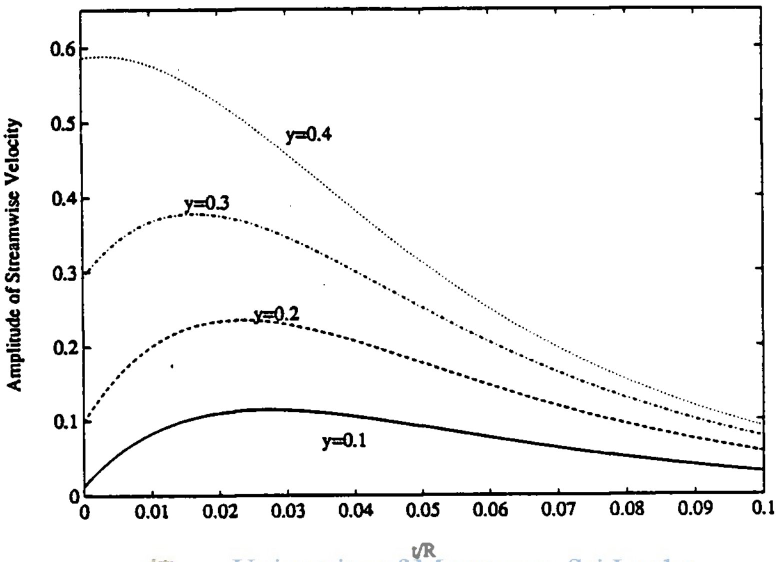

Figure 4. Temporal development of the streamwise velocity amplitude of the two-dimensional flow for s1, shown at y=0.1, 0.2, 0.3 and 0.4.

This figure shows the temporal development of the streamwise velocity amplitude, expressed by (4.2), as a function of (t/R) at four y-positions. It is seen in this figure that the the maximum amplitudes attained at y=0.1, 0.2 and 0.3 are smaller than the initial amplitude at y=0.4. This implies that the temporal growth observed *might* not be large enough to have nonlinear consequences. However, it is to be born in mind that the temporal growth observed - however small - is caused *solely* by the algebraic temporal term due to the presence of degeneracy.

5. Development of three-dimensional perturbation flow

Information about the normal velocity amplitude of the three-dimensional perturbation field remains the same as that described in the preceding section, except for the fact that initial rate of change, plotted in figure 3(a), should be multiplied by $(R_{\min}/R)$ before it is converted into degrees. In the three-dimensional case, the Reynolds number spans the range $R_{\min} < R < \infty$, and since αR and k are constants for each degeneracy, it follows that the streamwise and the spanwise wavenumbers span the ranges $k > \alpha > 0$ and $0 < \beta < k$, respectively. Information about the second component of (2.6), which is no longer the entire streamwise velocity, but a part of it, also remains the same as that described in the preceding section, provided minor changes are made in figure 3(b) to accomodate the correct Reynolds number. Information about the third component of (2.6) is obtained in this section.

The (linear) equation describing the normal vorticity is as follows:

$$\left(\frac{\partial}{\partial t}+U\frac{\partial}{\partial x}\right)\omega-\frac{1}{R}\nabla^2\omega=-\frac{dU}{dy}\frac{\partial v}{\partial z}\ . \tag{5.1a}$$

$$\omega = 0 \quad \text{at} \quad y=\pm 1\,. \tag{5.1b}$$

Using description (2.2) together with (2.4), the above equation can be rewritten as follows:

$$\left(\frac{\partial}{\partial t}+i\alpha U\right)\hat{\omega}-\frac{1}{R}\left(\frac{\partial^2}{\partial y^2}-k^2\right)\hat{\omega} = -i\beta\frac{dU}{dy}\hat{v}\ . \tag{5.2a}$$

$$\hat{\omega} = 0 \quad \text{at} \quad y=\pm 1\,. \tag{5.2b}$$

A formal solution to (5.2) can be obtained using a method similar to that used for solving (3.2). Given in appendix D is the complete solution valid for any initial perturbation subjected to conditions (2.7a-b). In the case of our interest, $\hat{v}_0$ is represented by a generalized eigenfunction and thus solution to (5.2) takes the following simple form:

$$\frac{\hat{\omega}(y,t)}{i\beta R}=\left[-i\,\Xi_l\,\alpha R\frac{t}{R}+\frac{\partial \Xi_l}{\partial c}\right]exp\left(-ic_l\,\alpha R\frac{t}{R}\right)+\sum_{n=1}^{\infty}\Psi_n\,exp\left(-ic_n\,\alpha R\frac{t}{R}\right). \tag{5.3}$$

Here, c_l represents a degeneracy and c_n represent normal vorticity eigenmodes, all of which are always damped (Davey & Reid 1977). The normal vorticity modes of plane Poiseuille flow can be proven to be discrete and infinite in number using arguments which are similar that used by Lin (1961) for the case of the OS modes. It is assumed here that the vorticity modes are simple and that they do not resonate with the OS modes at the k-αR combinations considered. The subscripts on Ξ, $\partial\Xi/\partial c$ and Ψ indicate the values at the respective eigenmodes. Descriptions of Ξ and Ψ, given in appendix D, show that the numerical evalution of these functions could be quite involved. Therefore, we choose to solve for $\hat{\omega}(y,t)$ by solving (5.2) directly using a suitable numerical method. Before the application of numerical method, it is convenient to rewrite (5.2) introducing the following new variables:

$$T = \frac{t}{R} \qquad \text{and} \qquad \hat{\Omega}(y,T) = \frac{\hat{\omega}(y,t)}{i\beta R}. \qquad (5.4a-b)$$

In terms of these variables, after substituting for $\hat{v}(y,t)$ from table 1, equation (5.2a) becomes as follows:

$$\left(\frac{\partial}{\partial T} + i\alpha R U\right)\hat{\Omega} - \left(\frac{\partial^2}{\partial y^2} - k^2\right)\hat{\Omega} = -\frac{dU}{dy}\left[-i\alpha R\ \Phi_l T + \frac{\partial \Phi_l}{\partial c}\right] exp(-i\alpha R c_l T). \quad (5.5a)$$

Note that by introducing (5.4), the explicit Reynolds number dependence of (5.2a) has been removed. According to (5.2b), boundary conditions are available at the walls at $y=\pm 1$. But a close look at (5.5a) suggests that at a symmetric degeneracy, owing to the symmetry of the eigenfunctions and the generalized eigenfunctions and that of the mean flow, $\hat{\Omega}$ is antisymmetric about $y=0$. Similarly, at an antisymmetric degeneracy, $\hat{\Omega}$ is symmetric about $y=0$. Thus, numerical evaluation could be confined to half the channel $(0 \le y \le 1)$ by writing the boundary conditions as follows:

$$\hat{\Omega}(y=0,T) = 0 \qquad \text{and} \qquad \hat{\Omega}(y=1,T) = 0 \qquad (5.5b)$$

for a symmetric degeneracy (i.e. for the anti-symmetric vorticity). For the opposite symmetry,

$$\frac{\partial\hat{\Omega}}{\partial y}(y=0,T) = 0 \qquad \text{and} \qquad \hat{\Omega}(y=1,T) = 0. \qquad (5.5c)$$

As for the initial condition, it follows from (2.7b) that

$$\hat{\Omega}(y, T=0) = 0. \qquad (5.5d)$$

The system described by (5.5) was solved using a second-order accurate Crank-Nicholson method, with (1/200) as y-steps and 0.0005 as T-steps, and the results are illustrated in the figure 5(a-b).

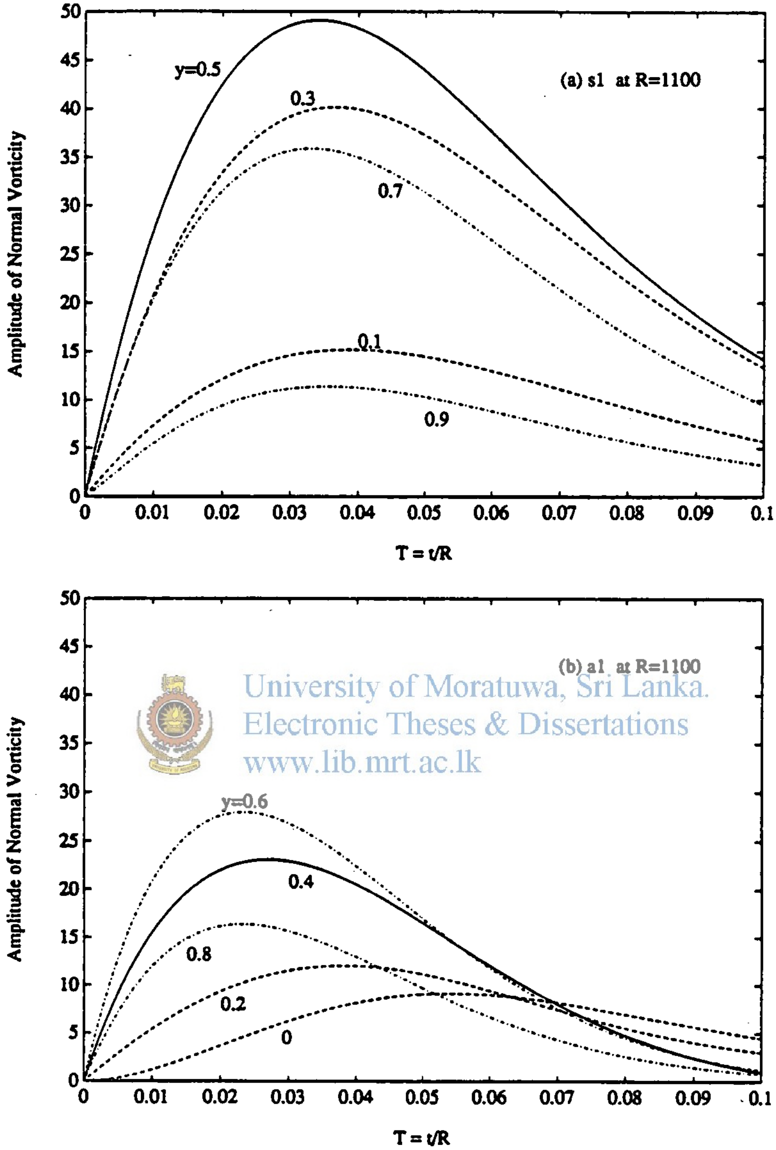

Figure 5. Temporal development of the amplitude of normal perturbation vorticity for (a) s1 and (b) a1, when the flow is excited by the *generalized eigenfunctions*, at R =1100.

Figure 5(a-b) displays the temporal development of the normal vorticity amplitudes, $|\hat{\omega}|$, for two of the four degeneracies at five chosen y-positions. These amplitudes are Reynolds number dependent, and the results shown in figure 5 correspond to R of 1100. (This R is chosen since plane Poiseuille flow is known to be absolutely stable for external excitations at R lower than1100; see e.g. Alavyoon, Henningson & Alfredsson 1986.) Numerical values of the amplitudes at other R-values can be evaluated easily using (5.4b). The first symmetric degeneracy s1 (figure 5a) and the first antisymmetric degeneracy a1 (figure 5b) attain considerably large amplitudes and are in the active phase for about T=0.1. Calculations showed that, at all y-positions, the amplitudes for s3 and for a2 are smaller than 6, which is much smaller than those for s1 and a1. Also, s3 and a2 decay more or less completely before T reaches 0.05.

The numerical results reported changed very little when the y-steps were decreased below (1/200). But, as the T-steps were reduced to one tenth of the value used, the maximum amplitudes, for instance, increased by about 13%. However, this difference is considered insignificant for the scope of this study, and hence T-steps were maintained as 0.0005.

The development of the normal vorticity amplitudes, unlike those of the components discussed in §4, is governed by an infinite number of vorticity eigenmodes in addition to the degeneracy itself. The damping rates of some of these modes, in some cases, are much lower than that of the corresponding degeneracy, as shown in table 3. The vorticity modes are listed in the table in descending order of their $Im(c)$-values, with the degeneracy placed at the appropriate location. Of the infinite number of vorticity modes, only those with $Im(c)$-values higher than -0.5 are shown in the table, since the rest of the vorticity modes may have very little influence upon the response. According to the table, the damping rate of the degeneracy s1 is lower than that of the any associated vorticity modes, and it gives the largest amplitude response. In the case of s3, for instance, there is a vorticity mode with much lower damping rate than that of s1, but the response of s3 is insignificant when compared to that of s1.

From these observations, one surmises that the response of the normal vorticity is largely governed by the damping rate of the degeneracy which forces the normal vorticity. It may also be observed in table 3 that the phase speeds of the vorticity modes span a wide range.

The initial growth and the eventual decay of the normal vorticity amplitudes, displayed by figure 5, are in fact expected since the initial amplitude is zero by choice and the eigenmodes involved are damped. Hence, from figure 5 alone, it is not clear what the degeneracy in particular contributes to the normal vorticity amplitude. In order to gain some insight into this, we also choose to excite the basic flow by the ***eigenfunction*** of the degeneracy. According to table 1 and appendix D, the solution given by (5.3) is now replaced by

$$\frac{\hat{\omega}(y,t)}{i\beta R} = \Xi_l \; exp\left(-ic_l \, \alpha R \frac{t}{R}\right) + \sum_{n=1}^{\infty} \Psi_n \; exp\left(-ic_n \, \alpha R \frac{t}{R}\right). \qquad (5.6)$$

Note that both the algebraic temporal term and the c-derivative of the function, characterizing the presence of a degeneracy, are absent in (5.6). But the damping rates of the eigenmodes involved, and hence the functions Ξ_l and Ψ_n, are identically the same as those in (5.3). Numerical solutions of this case, also evaluated using the Crank-Nicholson method, are presented in figure 6(a-b).

Mode	*c*	Mode	*c*
s1	0.72628355-0.16449306i	1	0.953403-0.068711i
1	0.856288-0.173664i	a1	0.71901575-0.22960311i
2	0.512289-0.289576i	2	0.499679-0.277061i
3	0.696686-0.395815i	3	0.771661-0.255219i
Mode	***c***	**Mode**	***c***
1	0.907652-0.099127i	1	0.971618-0.041057i
2	0.383909-0.210030i	2	0.364347-0.206640i
3	0.784474-0.222818i	3	0.858099-0.154577i
4	0.649705-0.310032i	4	0.745393-0.269879i
s3	0.63566921-0.39023739i	5	0.617956-0.315241i
5	0.673113-0.429848i	a2	0.64452222-0.40971061i
		6	0.674583-0.451717i

Table 3 The least damped normal vorticity eigenmodes, numbered in the order of decreasing magnitudes of the $Im(c)$-values in plane Poiseuille flow at the k-αR combinations of the degeneracies s1, a1, s3 and a2.

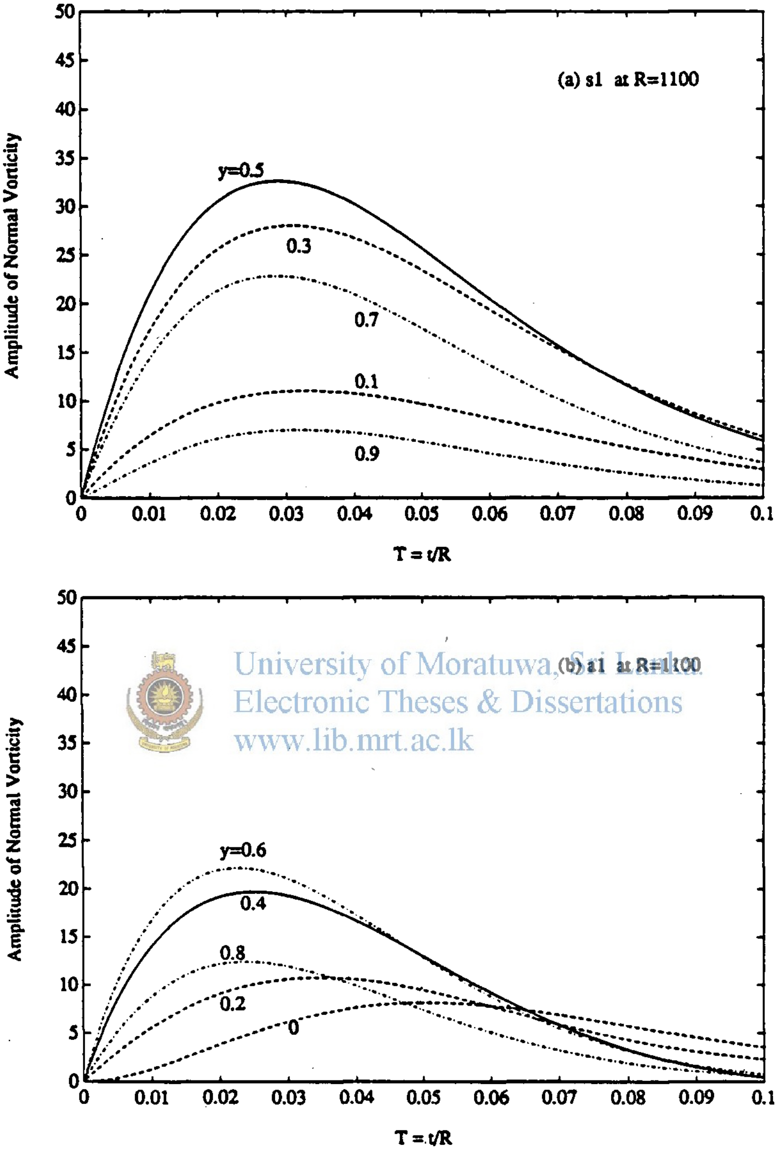

Figure 6. Temporal development of the amplitude of normal perturbation vorticity for (a) s1 and (b) a1, when the flow is excited by the *eigenfunctions*, at R=1100.

The amplitudes in this case are normalized such that

$$\frac{1}{2}\left\{\int_0^1 |\Phi_l|^2\, dy \;+\; \int_0^1 \frac{1}{k^2}|D\Phi_l|^2\, dy\right\} = 1\,,$$

which again corresponds to exciting the basic flow by an initial perturbation field having unit average energy. Temporal histories displayed by both the figures 5 and 6 are qualitatively similar to each other. But, the maximum amplitudes of the former are notably larger than those of the latter; thereby confirming the importance of the contribution due to the algebraic temporal term and the c-derivative of the function that characterizing the presence of a degeneracy.

In concluding this section, we present the temporal development of the amplitude of the streamwise perturbation velocity for the three-dimensional case, which can be compared with its two-dimensional counterpart presented in figure 4. Having known the two-dimensional streamwise velocity and the normal vorticity, equation (2.5a) could be used to evaluate the amplitudes of the streamwise perturbation velocity. The result is shown in figure 7 for the case of degeneracy s1, when it is excited by the generalized eigenfunction, at R=1100. Comparing figures 4 and 7, it becomes obvious that the temporal growth associated with this amplitude is much more significant in the three-dimensional flow than in the two-dimensional flow.

The numerical values of the amplitudes of the streamwise velocity in the three-dimensional flow would increase further with increasing Reynolds number, according to

$$|\hat{u}| = \frac{1}{k^2}\left|\left(\frac{\alpha R}{R}\,\frac{\partial \hat{v}}{\partial y} - i\,\beta^2 R\,\hat{\Omega}\right)\right|\,. \qquad (5.7)$$

The amplitude of the spanwise velocity, on the other hand, would remin almost insensitive for changing Reynolds number since

$$|\hat{w}| = \frac{\beta}{k^2}\left|\left(\frac{\partial \hat{v}}{\partial y} + i\,\alpha R\,\hat{\Omega}\right)\right|\,. \qquad (5.8)$$

(Equations (5.7) and (5.8) have been deduced from (2.5), using the relation (5.4b), in order to bring about the explicit Reynolds number dependence.)

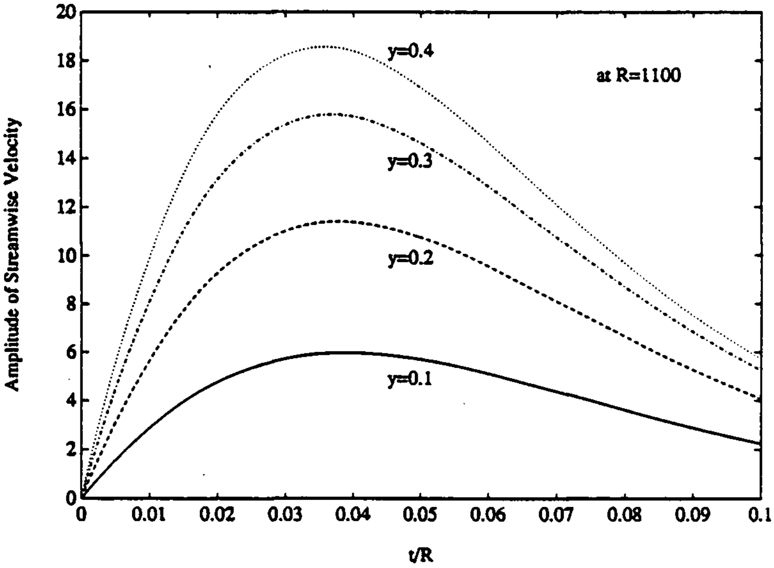

Figure 7. Temporal development of the streamwise velocity amplitude of the three-dimensional perturbation flow for s1 at R=1100. The flow is excited by the ***generalized eigenfunctions***, and the results are shown at y=0.1, 0.2, 0.3 and 0.4.

6. Kinetic energy of the perturbation flow

In the foregoing analyses, comparison among degeneracies was made possible by normalizing the functions involved in such a way that the average energy of the initial perturbation field is unity. In this section, we formally introduce the energy of the perturbation field and investigate into its temporal development in the presence of degeneracies. Energy, as opposed to the amplitudes studied in §§4 and 5, is a global representation of the perturbation field since it involes integration of local quantities over the entire space.

The dimensionless kinetic energy of the perturbation flow, which will be referred to as the perturbation energy, can be defined as

$$K(t) = \frac{1}{2} \int_x \int_y \int_z \left(u^2 + v^2 + w^2\right) dz\, dy\, dx \ . \tag{6.1}$$

The integration is taken from wall to wall in the y-direction, and is taken over exactly one wavelength in each of the direction along which the flow entends to infinity; see e.g p. 425 of Drazin & Reid (1981). Expression (6.1) can then be simplified using (2.2) and (2.5) as follows (cf. Gustavsson 1986):

$$K(t) = \frac{1}{4} \frac{4\pi^2}{\alpha\beta} \int_{-1}^{+1} \left(|\hat{v}|^2 + \frac{1}{k^2} \left| \frac{\partial \hat{v}}{\partial y} \right|^2 + \frac{1}{k^2} |\hat{\omega}|^2 \right) dy \ . \tag{6.2}$$

One major drawback of using (6.2) to calculate the perturbation energy is that K(t) becomes very large when either α or β becomes very small, owing to the fact that K(t) is taken over one wavelength in x- as well as in z- directions. In order to avoid this problem and to provide means for comparing the perturbation energies at different sets of (α, β) values, we introduce the concept of *average* perturbation energy as follows:

$$\langle K(t) \rangle \equiv \frac{K(t)}{(4\pi^2/\alpha\beta)}$$

$$= \frac{1}{2} \int_0^{+1} \left(|\hat{v}|^2 + \frac{1}{k^2} \left| \frac{\partial \hat{v}}{\partial y} \right|^2 \right) dy + \frac{(\beta R)^2}{2k^2} \int_0^{+1} |\hat{\Omega}|^2 \, dy \ . \tag{6.3}$$

(Average perturbation energy can also be referred to as the 'spatial power' in analogous with 'power of time-signals'.) In writing (6.3), we have exploited the symmetry of the functions about y=0, and have used the variable defined by (5.4b) in order to bring about the explicit R-dependence of energy. When the Reynolds number is R_{min}, the average energy is represented by only the first integral term of (6.3). Hence, this term represents the kinetic energy of the two-dimensional perturbation field, and takes the value unity at t=0 in accordance with the normalization used. As R is increased from R_{min}, this term, which remains the same, together with the second integral term of (6.3) yields the total average perturbation energy.

Shown in figure 8(a-d) are the temporal developments of the average perturbation energies for the four degeneracies at R=R_{min}, 1100 and 2200, when the flow is excited by generalized eigenfunctions. (R of 2200 is chosen since at about this R, plane Poiseuille flow totally breaks down according to Alavyoon et al., 1986.) The average perturbation energies at R_{min} start from unity and decay monotonically with time in all cases. This implies that the initial temporal growth of the streamwise velocities of the

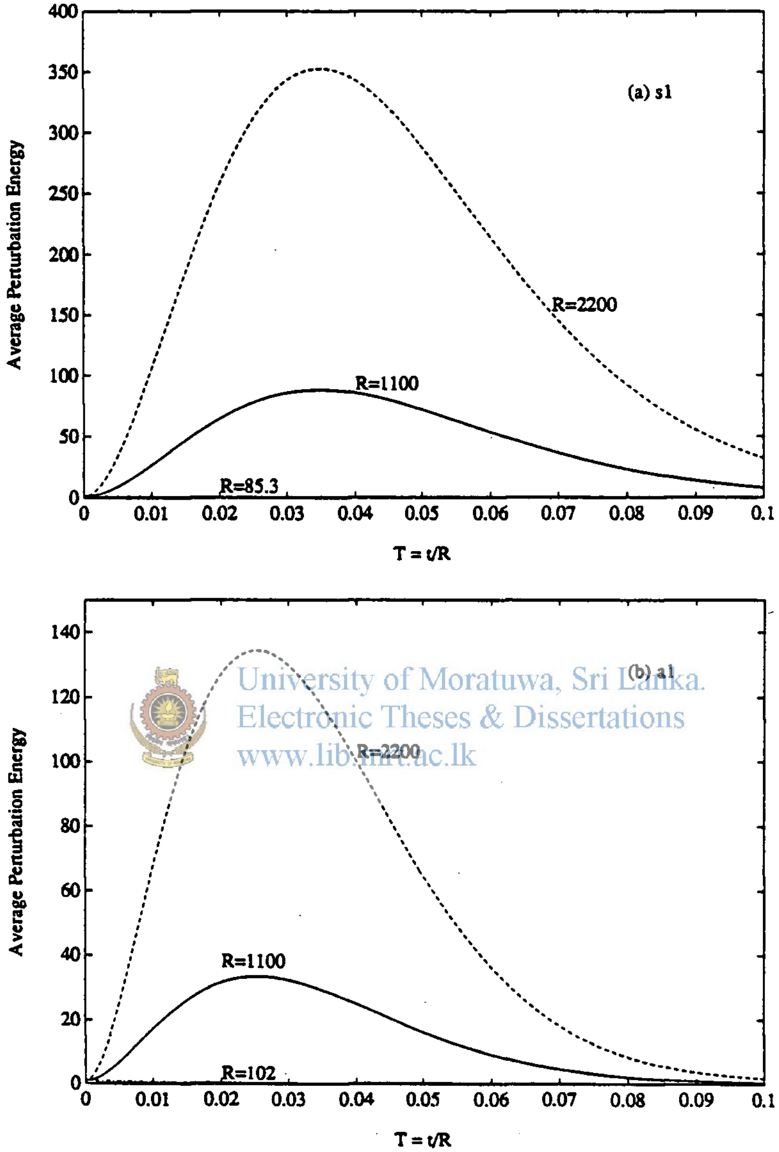

Figure 8. Temporal development of the average perturbation energy for (a) s1, (b) a1, (c) s3 and (d) a2, at $R=R_{min}$, 1100 and 2200, when the flow is excited by the *generalized eigenfunctions*.

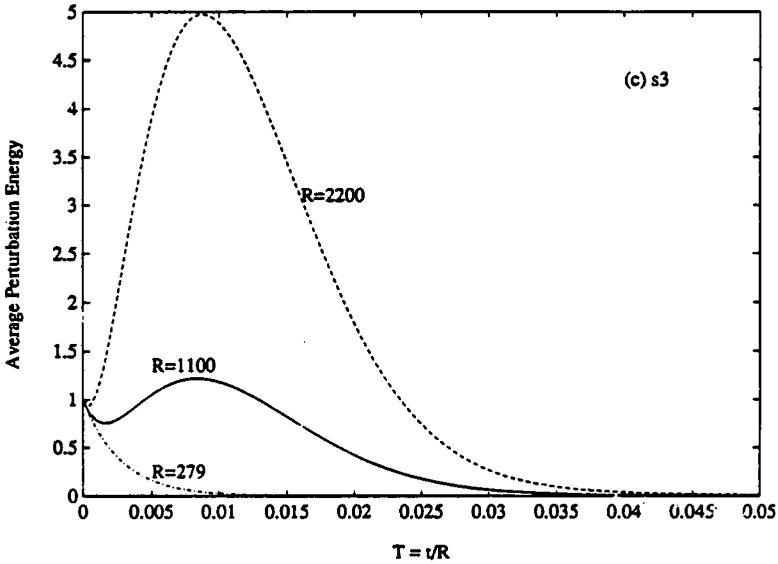

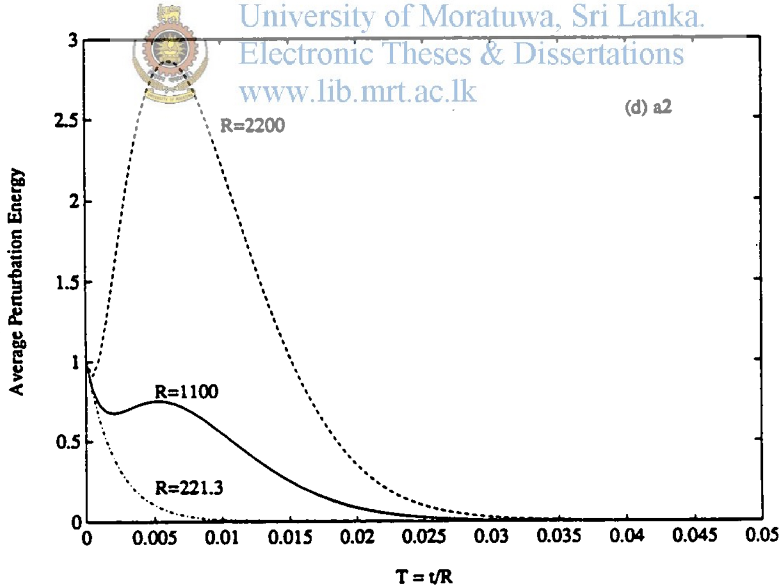

Figure 8. Continued.

two-dimensional flow, observed in figure 3(b), is not strong enough to induce initial growth of the average perturbation energies. At R=1100, the average perturbation energies for s1 (figure 8a) and for a1 (figure 8b) grow so large that they are more or less described by the contribution of the vorticity alone. In cases of s3 (figure 8c) and a2 (figure 8d), owing to the small amplitudes of their normal vorticities, the energies at R=1100 are heavily influened by the decaying first integral term of (6.3) initially. In all four cases, the energies at R=2200 are dominated by the vorticity contribution, and hence 'initial' growth of energy is observed. One final observation worth mentioning is that the T corresponding to the maximum energy is essentially independent of the R in each case of degeneracies.

Figure 9(a-b) shows the temporal development of the average perturbation energy for s1 and for a1, when the flow is excited by the eigenfunction. Comparing this figure with figure 8(a-b) shows that, in the absence of the response which is particular to the degeneracy, the peak values attained by the average energies are almost halved, despite the fact that the initial energies are unity in both cases.

In concluding this section, we note that the initial growth of average perturbation energy is *solely* a consequence of the normal vorticity that is induced by the normal velocity, though the presence of degeneracy, through the generalized eigenfunction, enhances the growth quantitatively. (For more about the induced vorticity, see the recent work by Gustavsson, 1990). Here, we only mention that the induced vorticity contributes towards the perturbation energy by two contradictory means as can be inferred from the following equation, which represents the rate of change of the average perturbation energy with time:

$$\frac{d\langle \mathrm{K}\rangle}{dt} = -\frac{\alpha R}{k^2 R}\int_0^1 \left(-\frac{dU}{dy}\right) |\hat{v}|^2 \frac{\partial \Theta_{\hat{v}}}{\partial y} dy$$

$$-\frac{1}{R}\int_0^1 \left(k^2|\hat{v}|^2 + 2\left|\frac{\partial \hat{v}}{\partial y}\right|^2 + \frac{1}{k^2}\left|\frac{\partial^2 \hat{v}}{\partial y^2}\right|^2\right) dy$$

$$+\frac{\beta^2 R}{k^2}\int_0^1 \left(-\frac{dU}{dy}\right) |\hat{v}|\,|\hat{\Omega}| \cos(\Theta_{\hat{v}} - \Theta_{\hat{\Omega}})\, dy$$

$$-\beta^2 R\int_0^1 \left(|\hat{\Omega}|^2 + \frac{1}{k^2}\left|\frac{\partial \hat{\Omega}}{\partial y}\right|^2\right) dy\ , \qquad (6.4)$$

where $\Theta_{\hat{v}}$ and $\Theta_{\hat{\Omega}}$ denote the phase angles of $\hat{v}$ and $\hat{\Omega}$, respectively.

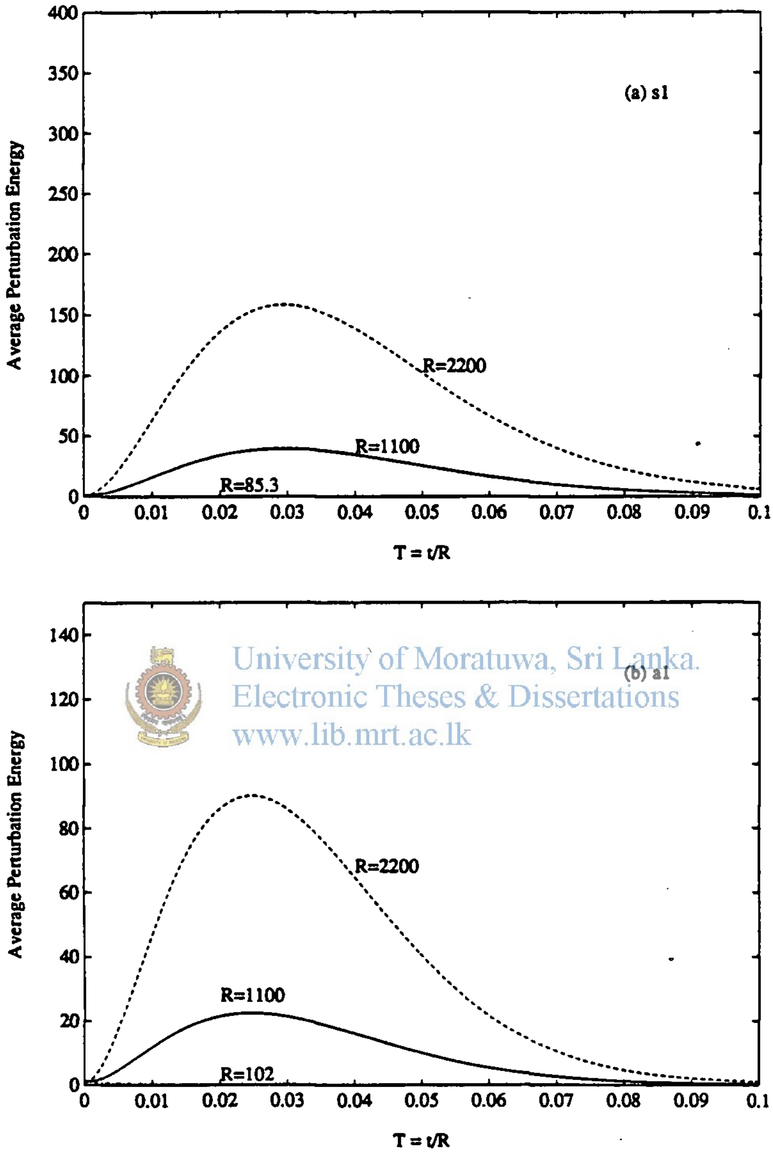

Figure 9. Temporal development of the average perturbation energy for (a) s1 and (b) a1, at $R=R_{min}$, 1100 and 2200, when the flow is excited by the *eigenfunctions*.

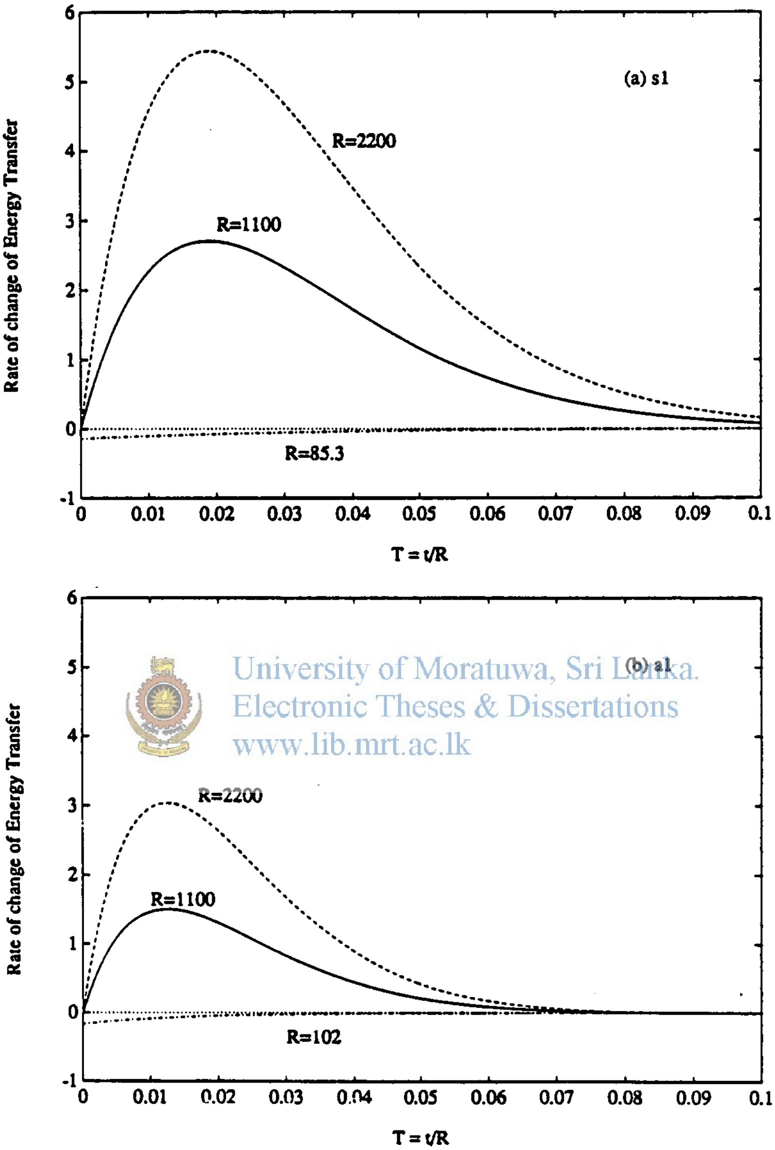

Figure 10. Histories of the rate of change of average kinetic energy transfer from the basic flow to the perturbation flow for (a) s1 and (b) a1, at $R=R_{min}$, 1100 and 2200, when the flow is excited by the *generalized eigenfunctions*.

Equation (6.4) is basically the *Reynolds-Orr Energy Equation* (p. 425 of Drazin & Reid 1981), and is expanded here to elucidate the role of the induced normal vorticity for the flow system considered. The second and the fourth integral terms of (6.4) represent viscous dissipation of the perturbation energy, and are always negative. The signs of the first and the third integral terms of (6.4), which represent the energy *transfer* from the basic flow to the perturbation flow, depend on the phase angles of the normal velocity and the normal vorticity of the perturbation. Of these two terms, it is the one representing the normal vorticity (the third term) which contributes the most to the energy growth of the degeneracies s1 and a1, as revealed by figure 10(a-b). The dashed-dotted curves of figure 10(a-b) represent the rate of energy *transfer* at $R_{\min}$ (i.e. for the two-dimensional case) and it takes negative values in both cases of degeneracies. The solid and the dashed curves of these figures represent the total rate of energy *transfer* at R=1100 and at R=2200, respectively. These curves display clearly the vital role played by the induced normal vorticity in the initial growth of perturbation energy. If the Reynolds number is increased further, then more energy will be extracted from the basic flow, according to (6.4), because of the presence of normal vorticity. None the less, (6.4) also reveals that the energy loss due to viscous dissipation would also increase with increasing Reynolds number.

7. Discussion

Of the degeneracies of plane Poiseuille flow investigated, none shows temporal growth of the amplitude of the normal perturbation velocity. This result is seemingly in contradiction with that of Shanthini (1989), where the first symmetric and the first antisymmetric degeneracies showed initial growth of this amplitude. This difference is due to the different initial perturbations used in these two works. The growths observed in Shanthini (1989) were caused by individual components of the Chebyshev polynomials, which by themselves, as cautioned, do not satisfy the required boundary conditions at the walls. In the present paper, generalized eigenfunction is used as the initial perturbation, which not only satisfies the required boundary conditions but also brings out all that a degeneracy can offer, as described in §3.2. Therefore, as for the temporal growth of the normal velocity amplitude due to degeneracies, the results of this study should be considered final.

As far as the two-dimensional streamwise perturbation velocity is concerned, notable initial growth of its amplitude is exhibited in the vicinity of the centreline of the channel by the first symmetric degeneracy s1. This growth, though small in magnitude, is remarkable since it is caused *purely* by the algebraic temporal term resulting from the presence of the degeneracy. The magnitudes associated with this growth are, however, not strong enough to force the average perturbation energy to grow, at least initially, in the linear regime. Whether or not this growth has nonlinear consequences, via secondary disturbances, remains to be seen.

If, on the other hand, the initial perturbation field is such that the normal component of it *has* spanwise variations, then there will be induction of normal perturbation vorticity. The amplitudes of which grow initially, attain significant peak values - at certain y-positions - and then decay owing to the fact that the eigenmodes involved are temporally damped. The amplitude of the induced vorticity is unique in the sense that it increases with increasing Reynolds number. These features have strong influences upon the temporal development of the streamwise perturbation velocity and, hence, upon the average perturbation energy. Significant growth of the average perturbation energy is observed at Reynolds numbers such as the transitional one of about 1100 and above. It is interesting to note that at R=2200, which is the Reynolds number at which isolated regions of turbulence were reported to appear spontaneously in plane Poiseuille flow (Alavyoon et al. 1986), the average perturbation energies of all four degeneracies investigated grow almost monotonically until they reach their peak values. The peak values of the normal vorticity amplitudes and of the average perturbation energies, for the degeneracy s1 and also for the degeneracy a1, in the transitional Reynolds number range seem large enough to evoke nonlinearity *at the primary level.* The large amplitudes attained by the normal vorticity would alter the basic parabolic flow by extracting its kinetic energy to the perturbation flow. The distortion of the basic flow might lead to nonlinear consequences.

It should be reminded that the contributions of induced vorticity described above are not confined to degeneracies alone; even a simple OS eigenmode, as demonstrated in this paper (and also in Gustavsson 1990), can lead to significant initial growth of the amplitude of the induced vorticity, and hence that of the perturbation energy. It is, however, found in the ongoing analyses that the magnitudes of the induced vorticities and of the perturbation energies are considerably larger when the flow is excited to bring out the response which is particular to the degeneracy, than when it is not, *at the k-αR values of a degeneracy.*

I duly acknowledge the significance of the discussions that L. Håkan Gustavsson, my thesis adviser, and I had in improving the quality of the content of this paper. Also, I am greatly indebted to Hernán Tinoco for the generosity he showed in promtly sharing his knowledge. This work has in part been supported by the National Swedish Board for Technical Development through its program for basic research (STUF).

Appendix A: About $\{\phi_\upsilon\}_{\upsilon=1}^{4}$ and $\{\phi_\upsilon^\dagger\}_{\upsilon=1}^{4}$

Linearly independent solutions to the OS operator, $\{\phi_\upsilon\}_{\upsilon=1}^{4}$, are normalized such that

$$\begin{bmatrix} \phi_1 & \phi_2 & \phi_3 & \phi_4 \\ D\phi_1 & D\phi_2 & D\phi_3 & D\phi_4 \\ D^2\phi_1 & D^2\phi_2 & D^2\phi_3 & D^2\phi_4 \\ D^3\phi_1 & D^3\phi_2 & D^3\phi_3 & D^3\phi_4 \end{bmatrix}_{y=0} = \begin{bmatrix} 1 & 0 & 0 & 0 \\ 0 & 1 & 0 & 0 \\ 0 & 0 & 1 & 0 \\ 0 & 0 & 0 & 1 \end{bmatrix}. \qquad (A1)$$

Linearly independent solutions to the adjoint of the OS operator, $\{\phi_\upsilon^\dagger\}_{\upsilon=1}^{4}$, are normalized such that

$$\begin{bmatrix} \phi_1^\dagger & \phi_2^\dagger & \phi_3^\dagger & \phi_4^\dagger \\ D\phi_1^\dagger & D\phi_2^\dagger & D\phi_3^\dagger & D\phi_4^\dagger \\ D^2\phi_1^\dagger & D^2\phi_2^\dagger & D^2\phi_3^\dagger & D^2\phi_4^\dagger \\ D^3\phi_1^\dagger & D^3\phi_2^\dagger & D^3\phi_3^\dagger & D^3\phi_4^\dagger \end{bmatrix}_{y=0} = \begin{bmatrix} 0 & 0 & 0 & 1 \\ 0 & 0 & -1 & 0 \\ 0 & 1 & 0 & \Lambda \\ -1 & 0 & -\Lambda & 0 \end{bmatrix}, \qquad (A2)$$

where

$$\Lambda = 2k^2 + i\alpha R(1-c).$$

The numerical values of (A2) have been deduced from those of (A1) using the relationship that $\{\phi_\upsilon^\dagger\}_{\upsilon=1}^{4}$ are the respective cofactors of $\{D^3\phi_\upsilon\}_{\upsilon=1}^{4}$ in the matrix on the left-hand side of (A1).

Appendix B: Some important relationships

Following the conventional methods, we pre-multiply the OS equation by a solution to the adjoint equation, integrate the resulting expression over the interval (-1,1) using the method of integration by parts, and then use the OS adjoint equation to obtain the following expression:

$$i\alpha R\ (c_p - c_q)\int_{-1}^{+1} \phi^{\dagger}_{vq}\left(D^2-k^2\right)\phi_{vp}\ dy$$

$$= -\left[\phi^{\dagger}_{vq}D^3\phi_{vp} - D\phi^{\dagger}_{vq}D^2\phi_{vp} + D^2\phi^{\dagger}_{vq}D\phi_{vp} - D^3\phi^{\dagger}_{vq}\phi_{vp}\right]_{-1}^{+1},$$

$$+(2k^2 - i\alpha R c_q)\left[\phi^{\dagger}_{vq}D\phi_{vp} - D\phi^{\dagger}_{vq}\phi_{vp}\right]_{-1}^{+1},$$

$$+i\alpha R\left[U\left(\phi^{\dagger}_{vq}D\phi_{vp} - D\phi^{\dagger}_{vq}\phi_{vp}\right) - DU\ \phi^{\dagger}_{q}\phi_{vp}\right]_{-1}^{+1}.$$

Note that the functions involved in the above expression are *only* the linearly independent solutions to the OS- and its adjoint- equations. Thus, no boundary conditions are available for these functions either at $y= +1$ or at $y= -1$. The second subscripts on these functions denotes that they correspond to the eigenvalues c_p or c_q. By differentiating the above expression with respect to c_p and/or c_q, utilizing the conditions of E (E_{13} or E_{24}) at simple or double zeros, and using the boundary conditions on Φ and on $\Phi^{\dagger}$ we can show that the followings are true.

- At a simple zero of E=0,

$$\left.\frac{\partial E}{\partial c}\right|_{at\ c_p} = i\alpha R\int_0^1 \Phi^{\dagger}_p\left(D^2-k^2\right)\Phi_p\ dy = i\alpha R\left(\Phi^{\dagger}_p\ ,\ \Phi_p\right). \qquad (B1)$$

- At a double zero of E=0, where $(\partial E/\partial c)$=0,

$$\left.\frac{\partial^2 E}{\partial c^2}\right|_{at\ c_p} = (2!)i\alpha R\int_0^1 \Phi^{\dagger}_p\left(D^2-k^2\right)\frac{\partial \Phi_p}{\partial c}\ dy = (2!)i\alpha R\left(\Phi^{\dagger}_p\ ,\ \frac{\partial \Phi_p}{\partial c}\right) \qquad (B2)$$

and

$$\left.\frac{\partial^3 E}{\partial c^3}\right|_{at\ c_p} = (3!)i\alpha R\int_0^1 \frac{\partial \Phi^{\dagger}_p}{\partial c}\left(D^2-k^2\right)\frac{\partial \Phi_p}{\partial c}\ dy = (3!)i\alpha R\left(\frac{\partial \Phi^{\dagger}_p}{\partial c}\ ,\ \frac{\partial \Phi_p}{\partial c}\right), \qquad (B3)$$

where the OS eigenfunction Φ and its adjoint function $\Phi^{\dagger}$ are expressed by (3.12a-c) when $E = E_{13,}$ and by (3.13a-c) when $E = E_{24}$. The subscript p denotes the functional values at the eigenvalue c_p. In writing (B1-B3), we have used the inner-product notation defined by (3.16).

It follows from the above that the well known bi-orthogonality relationships among the eigenfunctions and their adjoint functions in plane Poiseuille flow (see e.g p. 158

of Drazin & Reid 1981) have to be modified as follows to accomodate the presence of degeneracy (cf. Schensted 1961):

- If all the zeros of E=0 are simple, then

$$\left(\Phi_l^\dagger,\Phi_m\right) = \left(\Phi_l,\Phi_m^\dagger\right) = 0 \quad \text{when} \quad c_m \neq c_l\,, \tag{B4}$$

but

$$\left(\Phi_l^\dagger,\Phi_l\right) = \left(\Phi_l,\Phi_l^\dagger\right) \neq 0\,. \tag{B5}$$

- If c_l is a degeneracy among other simple zeros, denoted by c_m, then (B4) still holds, but (B5) is replaced by the followings:

$$\left(\Phi_l^\dagger,\Phi_l\right) = \left(\Phi_l,\Phi_l^\dagger\right) = 0\,. \tag{B6}$$

$$\left(\frac{\partial\Phi_l^\dagger}{\partial c},\Phi_l\right) = \left(\frac{\partial\Phi_l}{\partial c},\Phi_l^\dagger\right) \neq 0\,. \tag{B7}$$

Futhermore,

$$\left(\frac{\partial\Phi_l^\dagger}{\partial c},\Phi_m\right) = \left(\frac{\partial\Phi_l}{\partial c},\Phi_m^\dagger\right) = 0\,. \tag{B8}$$

Appendix C: An efficient method for locating double zeros of an OS eigenvalue problem

The method described here is applicable in locating a *complex* double zero of a *complex* analytic function, which occurs only at a certain combination of two other *real* parameters. For the case studied in this paper, the complex zero is represented by c and the real variables are by k and αR. The method utilizes the fact the analytic function, denoted by E, and its c-derivative, $\partial E/\partial c$, *vanish* at the double zero, i.e. at the degeneracy.

Denoting the coordinates of the degeneracy by c_0, k_0 and $(\alpha R)_0$, the procedure is started by choosing a k and an αR which lie close to k_0 and $(\alpha R)_0$, respectively. This step requires that we somehow know the k - and αR- ranges within which a degeneracy is to be expected. One way of confining the degeneracies is discussed in detail in Shanthini (1989), and we followed that methodology. At this chosen k-αR pair, due to its proximity to the degeneracy, $E(c)$ can be fitted by a 'parabola'. (This parabola describes a four dimensional space since both the variable c and the function $E(c)$ are complex.) Zeros of this parabola, which are solutions to $E(c)=0$, are simple and are approaching each other to produce a double zero, as the chosen k-αR pair approaches k_0-$(\alpha R)_0$. Possibly, one could use the above as a criterion to iterate on k and αR, but, we use an alternate method.

Let us evaluate the extreme value of E, at which $\partial E/\partial c$ vanishes which is in fact one of the two conditions to be fulfilled at the degeneracy. The extreme value, denoted by E_{ext}, changes only when k and/or αR is changed, and it approaches zero as the chosen k-αR pair approaches k_0-$(\alpha R)_0$. The c-value at which $E_{ext}=0$ is of course c_0. The condition that E_{ext} should vanish at the degeneracy will now be used to locate a new k-αR pair which is more close to k_0-$(\alpha R)_0$ than the old k-αR pair, through the following scheme.

Let us assume that, in the neighbourhood of the degeneracy, the real part of E_{ext} can be described by a linear function of k and αR, and the imaginary part of E_{ext} by another. These linear functions are real functions since both k and αR are real variables. The constants of these real functions are then determined using least square fit to the data, which are obtained by evaluating E_{ext} at several (say eight) different k and αR values. These values are chosen to be on a circle centered at the k and αR values with which these calculations are started, and the radius of this circle is chosen according to the desired accuracy. Having determined the constants, it is straight forward to calculate the k and αR values at which both the real and the imaginary parts of E_{ext} vanish. At the new k and αR values, E_{ext} is calculated again. If this E_{ext} is not close to 'zero' then the procedure is repeated, now with the new k and αR values. These calculations are repeated until E_{ext} becomes comparable with the chosen numerical zero.

With the numerical zero of E_{ext} as $O(10^{-9})$ or less, the coordinates of six degeneracies in plane Poiseuille flow were re-evaluated, and the results are listed in table 1. The last column of table 1 shows the absolute values of $(\partial E/\partial c)$ at the respective degeneracies; compare these values with those of Shanthini (1989).

Appendix D: Complete solution to normal (perturbation) vorticity

Formal solution to (5.2) can be obtained using the method of Laplace transform together with variation of parameters (cf. Hultgren & Gustavsson 1981). The solution, subjected to the condition of zero initial normal vorticity, is as follows:

$$\hat{\omega}(y,t) = \hat{\omega}(y,t)|_{OS} + \hat{\omega}(y,t)|_{VV}\,, \qquad (D1a)$$

where

$$\hat{\omega}(y,t)|_{OS} = \sum_{\substack{m=1\\ m\neq l}}^{\infty} i\beta R\,\frac{(\Phi_m^{\dagger}, \hat{v}_0)}{(\Phi_m^{\dagger}, \Phi_m)}\,\Xi_m\, exp\left(-i\alpha R c_m \frac{t}{R}\right)$$

$$+\frac{i\beta R}{\left(\Phi_l^{\dagger}, \frac{\partial \Phi_l}{\partial c}\right)}\left[\left(\Phi_l^{\dagger}, \hat{v}_0\right)\left(-i\alpha R\, \Xi_l \frac{t}{R} + \frac{\partial \Xi_l}{\partial c}\right)\right.$$

$$\left. +\left(\frac{\partial \Phi_l^{\dagger}}{\partial c} - \frac{\left(\frac{\partial \Phi_l^{\dagger}}{\partial c}, \frac{\partial \Phi_l}{\partial c}\right)}{\left(\Phi_l^{\dagger}, \frac{\partial \Phi_l}{\partial c}\right)}\Phi_l^{\dagger}\,, \hat{v}_0\right)\Xi_l\right] exp\left(-i\alpha R c_l \frac{t}{R}\right) \qquad (D1b)$$

and

$$\hat{\omega}(y,t)|_{VV} = \sum_{n=1}^{\infty} i\beta R\, \Psi_n\, exp\left(-i\alpha R c_n \frac{t}{R}\right)\,. \qquad (D1c)$$

Here, the subcripts m, l and n denote the OS simple eigenmodes, the degeneracy and the normal vorticity (VV) eigenmodes, respectively. The symbols Ξ and Ψ represent the followings.

When $\hat{v}_0$ is symmetric,

$$\Xi = -\psi_1 \int_0^y \psi_2 \Phi DU\, d\eta - \psi_2 \int_y^1 \psi_1 \Phi DU\, d\eta + \psi_2 \left(\frac{\psi_1}{\psi_2}\right)_{y=1} \int_0^1 \psi_2 \Phi DU\, d\eta$$

and

$$\Psi = \psi_2\, \frac{(\psi_1 D\psi_2)_{y=1}}{\int_0^1 (\psi_2)^2 d\eta} \int_0^1 \psi_2 \left(F_r + \frac{F}{E}\right) DU\;\, d\eta\,,$$

where

$$F_r = -\phi_1 \int_y^1 \phi_1^\dagger \Delta \, d\eta - \phi_3 \int_y^1 \phi_3^\dagger \Delta \, d\eta + \phi_2 \int_0^y \phi_2^\dagger \Delta \, d\eta + \phi_4 \int_0^y \phi_4^\dagger \Delta \, d\eta,$$

and F is given by (3.7a) and E given by (3.7b).

When $\hat{v}_0$ is antisymmetric

$$\Xi = \psi_2 \int_0^y \psi_1 \Phi DU \, d\eta + \psi_1 \int_y^1 \psi_2 \Phi DU \, d\eta - \psi_1 \left(\frac{\psi_2}{\psi_1}\right)_{y=1} \int_0^1 \psi_1 \Phi DU \, d\eta$$

and

$$\Psi = -\psi_1 \frac{(\psi_2 D\psi_1)_{y=1}}{\int_0^1 (\psi_1)^2 d\eta} \int_0^1 \psi_1 \left(F_r + \frac{F}{E}\right) DU \, d\eta,$$

where

$$F_r = -\phi_2 \int_y^1 \phi_2^\dagger \Delta \, d\eta - \phi_4 \int_y^1 \phi_4^\dagger \Delta \, d\eta + \phi_1 \int_0^y \phi_1^\dagger \Delta \, d\eta + \phi_3 \int_0^y \phi_3^\dagger \Delta \, d\eta,$$

and F is given by (3.8a) and E given by (3.8b).

In either case, the functions $\{\psi_\upsilon\}_{\upsilon=1}^2$ are the linearly independent solutions to the normal vorticity operator,

$$(D^2 - k^2) - i\alpha R(U - c),$$

and are normalized according to

$$\begin{bmatrix} \psi_1 & \psi_2 \\ D\psi_1 & D\psi_2 \end{bmatrix}_{y=0} = \begin{bmatrix} 1 & 0 \\ 0 & 1 \end{bmatrix}.$$

For different choice of $\hat{v}_0$ from (3.17), we can simplify (D1b) using the same arguments as those used to obtain the results of table 1. But simplifying (D1c) further doesn't seem feasible, at least, at this moment.

REFERENCES

ALAVYOON, F., HENNINGSON, D. S. & ALFREDSSON, P. H. 1986 Turbulent spots in plane Poiseuille flow - flow visualization. *Phys. Fluids* 29, 1328-1331.

DAVEY, A. & REID, W. H. 1977 On the stability of stratified viscous plane Couette flow: Part1. Constant buoyancy frequency. *J. Fluid Mech.* 80, 509-525.

DI PRIMA, R. C. & HABETLER, G. J. 1969 A completeness theorem for non-selfadjoint eigenvalue problems in hydrodynamic stability. *Arch. Rat. Mech. Anal.* **34**, 218-227.

DRAZIN, P. G. & REID, W. H. 1981 *Hydrodynamic stability*. Cambridge University Press.

GROSCH, C. E. & SALWAN, H. 1968 The stability of steady and time-dependent plane Poiseuille flow. *J. Fluid Mech.* **34**, 177-205.

GUSTAVSSON, L. H. 1981 Resonant growth of three-dimensional disturbances in plane Poiseuille flow. *J. Fluid Mech.* **112**, 253-264.

GUSTAVSSON, L. H. 1986 Excitation of direct resonances in plane Poiseuille flow. *Stud. Appl. Maths* **75**, 227-248.

GUSTAVSSON, L. H. 1990 Energy growth of three-dimensional disturbances in plane Poiseuille flow. submitted to *J. Fluid Mech.*

LIN, C. C. 1961 Some mathematical problems in the theory of the stability of parallel flows. *J. Fluid Mech.* **10**, 430-438.

SCHENSTED, I. V. 1961 Contributions to the theory of hydrodynamic stability. PhD thesis, University of Michigan.

SHANTHINI, R. 1989 Degeneracies of the temporal Orr-Sommerfeld eigenmodes in plane Poiseuille flow. *J. Fluid Mech.* **201**, 13-34.

Paper IV

Accepted for publication in *Studies in Applied Mathematics*

On the nonlinear development of small three-dimensional perturbations in plane Poiseuille flow - a single mode approach

Rajaratnam Shanthini
Division of Fluid Mechanics, Luleå University of Technology, S-951 87, Luleå, Sweden.

Nonlinear aspects of developing three-dimensional perturbations in plane Poiseuille flow have been elucidated at the primary, instead of the conventional secondary, level. Three-dimensional perturbation velocities generate normal vorticity by stretching and tilting the basic-flow vorticity. The amplitude of the induced normal vorticity and, hence, that of the streamwise perturbation velocity can grow temporally to significant peak values, before the exponential decay predicted by the linear theory sets in. These growths, according to the linear theory, do not influence the amplitudes of the normal perturbation velocity that are monotonically decaying with time. It is shown in this study that the normal velocity continues to be oblivious to the development of induced normal vorticity, even in the nonlinear regime, if the perturbation velocities are described by waves travelling in a single oblique direction. Also, the Reynolds number dependence of the amplitude of the normal vorticity is discussed.

1 Introduction

Laminar-to-turbulent transition is a strongly three-dimensional phenomenon in plane Poiseuille flow and in many other wall-bounded shear flows. At the early stages of transition, however, according to the well-known transformation of Squire [1], small two-dimensional perturbations, that are independent of spanwise direction, are considered more destabilising than the corresponding three-dimensional ones. None the less, for plane Poiseuille flow, the theoretically predicted transitional Reynolds numbers - based on two-dimensional analyses - are much larger than the lowest experimentally observed transitional Reynolds number (≈ 1000). The theoretical prediction is about six times larger in case of very small perturbations [2] and about three times larger in case of finite-amplitude perturbations [3].

Meksyn [4], on the other hand, argued that sufficiently large wavy three-dimensional perturbations, introduced to the flow at some initial instant, could deform the basic parallel flow differently from the corresponding two-dimensional ones. He investigated into the consequences of such deformation and concluded that three-dimensional perturbations were indeed more destabilising than the two-dimensional ones. This difference can be explained by the fact that, in modifying the basic flow, three-dimensionality contributes an additional Reynolds stress term owing to the presence of *vorticity* perturbations normal to the walls.

Normal vorticity is in fact solely a consequence of three-dimensionality of the perturbations. The spanwise variations in the velocity perturbations normal to the walls induce normal vorticity. In other words, it is primarily the tilting of the basic-flow vorticity by the perturbation velocities which generates normal vorticity. It has been shown recently by Gustavsson [5] and by Shanthini [6] that, at about the transitional Reynolds number, even though all the linear eigenmodes are damped, the amplitudes of induced normal vorticity can grow initially to significant peak values. For a single wave component (or Fourier mode), these peak values and also the nondimensionless time corresponding to the peak values increase with increasing Reynolds number. It is also shown by use of Reynolds-Orr Energy equation that the presence of induced normal vorticity also causes considerable amount of kinetic energy to be transferred from the basic Poiseuille flow to the perturbation flow [6].

In this paper, we investigate into some of the nonlinear consequences of the Reynolds number dependent temporal growth of the normal vorticity. Of particular interest is the question whether or not the temporal development of the induced normal vorticity influences the development of normal velocity, at least in the nonlinear regime. The analysis is limited to a nonlinear solution of a single Fourier mode. Of special interest is the wavenumber combination of a temporal degeneracy, upon which the linear formulation is centred (§3). Nevertheless, the analysis should be equally applicable to other wavenumber combinations as well.

2 Governing equations

Three-dimensional (3-D) velocity perturbations (u, v, w), imposed on a parallel flow $(U(y), 0, 0)$, satisfy the nonlinear equations

$$\left\{\left(\frac{\partial}{\partial t}+U\frac{\partial}{\partial x}\right)\nabla^2-\frac{d^2U}{dy^2}\frac{\partial}{\partial x}-\frac{1}{R}\nabla^4\right\}v$$

$$=-\left(\frac{\partial^2}{\partial x^2}+\frac{\partial^2}{\partial z^2}\right)\mathcal{M}v+\frac{\partial^2}{\partial x\partial y}\mathcal{M}u+\frac{\partial^2}{\partial z\partial y}\mathcal{M}w \qquad (2.1)$$

and

$$\left\{\frac{\partial}{\partial t}+U\frac{\partial}{\partial x}-\frac{1}{R}\nabla^2\right\}\eta=-\frac{dU}{dy}\frac{\partial v}{\partial z}-\frac{\partial}{\partial z}\mathcal{M}u+\frac{\partial}{\partial x}\mathcal{M}w. \tag{2.2}$$

Here, η is the perturbation *vorticity* normal to the walls, defined as

$$\eta=\frac{\partial u}{\partial z}-\frac{\partial w}{\partial x}. \tag{2.3}$$

And, the condition of continuity leads to

$$\frac{\partial u}{\partial x}+\frac{\partial w}{\partial z}=-\frac{\partial v}{\partial y}. \tag{2.4}$$

The operator $\mathcal{M}$ used in (2.1) and (2.2) is defined as

$$\mathcal{M}=u\frac{\partial}{\partial x}+v\frac{\partial}{\partial y}+w\frac{\partial}{\partial z}.$$

The equations have been rendered dimensionless using the centreline velocity and the channel half-height as the respective velocity- and length- scales. The Reynolds number R is defined in terms of these scales. The streamwise, normal and spanwise directions are x, y and z, respectively, t is the time and ∇^2 is the three-dimensional Laplacian. The basic plane Poiseuille flow is given by $U=1-y^2$. Equations (2.1) and (2.2) have been derived from the Navier-Stokes equations and the details are available elsewhere [7]. Boundary conditions for the perturbations on the rigid walls (at $y=\pm1$) are linear and homogeneous and are stated when required.

3 Linear development of 3-D perturbations

When the 3-D perturbations are assumed to have small amplitudes, the governing equations are linearized by dropping the terms which consist of the operator $\mathcal{M}$ from (2.1) and (2.2). The resulting system of linear equations is known to allow a solution that is proportional to $\exp[i(\alpha x+\beta z-\alpha ct)]$. Here, α and β are real wavenumbers along the streamwise and spanwise directions, respectively, and c ($=c_r+ic_i$) is the complex phase velocity. For any chosen set of (α,β,R), there exists infinitely many complex phase velocities for plane Poiseuille flow. It has been shown recently in [8] that, when R is larger than a nominal value (85.3 for plane Poiseuille flow), there exists particular combinations of α and β at which temporal degeneracies exist.

A solution to the linearized form of (2.1), at a parameter combination of a degeneracy, can be written as (cf [6])

$$v = \left\{ \sum_{n=1}^{\infty} A_n \Phi_n e^{-i\alpha c_n t} + \tilde{A}_l \left(-i\alpha t \Phi_l + \frac{\partial \Phi_l}{\partial c} \right) e^{-i\alpha c_l t} \right\} e^{i(\alpha x + \beta z)} + \text{c.c.}, \quad (3.1)$$

where A_n are complex constants and c.c. denotes complex conjugate. The complex phase-velocities c_n and the complex functions Φ_n are the respective eigenvalues and the corresponding eigenfunctions of the Orr-Sommerfeld (OS) eigenvalue-problem. The subscript l denotes a degeneracy and the bracketed term represents the response due to a degeneracy. Here $\tilde{A}_l$ is a complex constant and the complex function $(\partial\Phi_l/\partial c)$ is the generalized eigenfunction at the degeneracy. It has been shown in [6] that, despite the algebraic temporal term in (3.1), the normal velocity amplitude decays monotonically in accordance with the negative values of c_i.

Nevertheless, the spanwise variations in the normal velocity acting upon the basic-flow vorticity induce normal vorticity according to the linearized form of (2.2). The induced vorticity is given by

$$\eta = i\beta R \left\{ \sum_{m=1}^{\infty} B_m \Psi_m e^{-i\alpha C_m t} + \left(-i\alpha t \Xi_l + \frac{\partial \Xi_l}{\partial c} \right) e^{-i\alpha c_l t} \right\} e^{i(\alpha x + \beta z)} + \text{c.c.}, \quad (3.2)$$

where B_m are complex constants. The complex phase velocities C_m and the complex functions Ψ_m are the respective eigenvalues and the corresponding eigenfunctions of the normal vorticity (NV) eigenvalue-problem. And, Ξ_l is the solution to the inhomogeneous problem

$$\left\{ (\mathcal{D}^2 - k^2) - i\alpha R(U - c_l) \right\} \Xi_l = \frac{dU}{dy} \Phi_l,$$

where k $(=\sqrt{\alpha^2 + \beta^2})$ is the resultant wavenumber and c_l is the complex phase velocity corresponding to the degeneracy. For the purpose of illustration, v of (3.1) is represented only by the response of the degeneracy, and the constant $\tilde{A}_l$ is set to unity without loss of generality. The full solution (3.2) was obtained in recognition that it is needed to satisfy any initial condition on η (see [6] and also [5]).

First, we present the development of normal vorticity induced by the least damped symmetric degeneracy. (This degeneracy results from the coalescence between the first and the second least damped OS modes, that are symmetric about $y = 0$, and occurs at $k \approx 2.539$ and $\alpha R \approx 216.61$ [8]). Computations revealed that, at R=1100, the amplitudes of the induced normal vorticity of the single wave component grew initially, reached *significant* peak values and then decayed; *even though the forcing OS mode and the corresponding NV eigenmodes were all decaying* [6]. The least damped antisymmetric degeneracy also showed similar responses. (This degeneracy results from the coalescence between the first and the second least damped antisymmetric OS modes and occurs at $k \approx 2.257$ and $\alpha R \approx 230.29$ [8]). The growth of induced vorticity caused the kinetic energy of the perturbation flow to grow initially. The perturbation energy at $R = 1100$ grew up to about 90 times its initial value in case of the symmetric degeneracy and to about 35 times its initial value in case of the antisymmetric degeneracy. When R is doubled, the maximum of the symmetric degeneracy went up to about 350 and that of the antisymmetric one to about 135. The (t/R)-values corresponding to these maxima remained at about 0.035 in the former and at about 0.025 in the latter.

Gustavsson [5] has, on the other hand, computed the normal vorticity which was induced only by the least damped OS eigenmode, at several combinations of k and αR. The amplitudes of the induced normal vorticity - of a single Fourier mode - also exhibited significant initial growth, but the (t/R)-values at which the maxima occurred were larger than 0.035. He also observed that the peak values became larger as α became smaller; that is, for scales increasingly elongated in the streamwise direction. For almost all combinations of k and αR, the (t/R)-values corresponding to the peak values remain more or less the same, which is about 0.084 for antisymmetric vorticity (induced by the symmetric least damped OS mode) and about 0.057 for vorticity of opposite symmetry.

These calculations imply that, at about the transitional Reynolds number, the amplitudes of the normal vorticity and, hence, the perturbation energy could be in the growing phase for about 30 to 80 units of the dimensionless time, *though all the associated eigenmodes are damped.* Also, the maxima reached are significantly large. Using the expressions (3.1) for v and (3.2) for η in (2.3) and (2.4), the remaining two perturbation velocities can be evaluated. It is shown in [6] that the amplitudes of u, like η, show significant initial growth. As for the amplitudes of w, it is influenced very little by the initial growth of η. The normal velocity v, on the other hand, is totally independent of η, and hence, continues to decay monotonically according to the linear theory.

It becomes obvious from these results that, even if all the eigenmodes are temporally damped at about the transitional R, owing to three-dimensionality, the order of magnitudes of the velocity perturbations u, v and w do not remain comparable at all times. Subsequently, we realize that, three-dimensionality makes the assumption of linear theory invalid. And, hence, the development of three-dimensional perturbations should be followed by the full nonlinear equations. Before moving onto such investigations, another aspect of the induced normal vorticity will be considered.

4 Reynolds number dependence of 3-D perturbations

It was observed both in [5] and in [6] that the maxima of the normal vorticity amplitudes, *corresponding to a single Fourier mode*, would increase if R was increased, but the corresponding (t/R)-values would remain unchanged.

This Reynolds number dependent growth can be explained by the almost linear R-dependence of the amplitude of the normal vorticity, revealed by (3.2), at fixed k and αR values when β is close to k. However, the amplitude of the normal velocity, expressed by (3.1), has no such R-dependence once k and αR are fixed. It follows from these observations that the temporal growth of streamwise velocity amplitude of a single Fourier component also would depend upon the Reynolds number, but the spanwise velocity would be almost insensitive to changing Reynolds number (see [6] for details).

In order to separate the Reynolds number dependence of the amplitudes of the perturbations from the spatial extentions of the perturbations with increasing Reynolds number, we introduce the space-scale

$$\mathcal{X} = \frac{x}{R} \tag{4.1a}$$

and also the time-scale

$$\mathcal{T} = \frac{t}{R}. \tag{4.1b}$$

Even after introducing these new scales in (3.1) and (3.2), the Reynolds number dependence of the amplitudes of normal vorticity and, hence, of the streamwise velocity remain. Thus, it is clear that the amplitudes and, hence, the maxima of the normal vorticity and the streamwise velocity increase with increasing Reynolds number, for perturbations expressed in terms of a single wave component, at fixed values of k and αR. However, in cases where the perturbation quantities in the real space are recovered by Fourier addition (rather integration) of individual wave components, it is not clear how the real quantities depend upon the Reynolds number. More work have to be carried out on this aspect of the growth process, and for the time being, we restrict ourselves to the case of a single wave component (or Fourier mode).

To complete the preceding renormalizations, the dependent variables are renormalized as follows:

$$(\mathcal{U},\ \mathcal{V},\ \mathcal{W},\ \mathcal{N}) = \left(\frac{u}{R},\ v,\ w,\ \frac{\eta}{R}\right). \tag{4.1c}$$

Let us take (1/R) as the small parameter and expand the perturbations as follows:

$$\begin{Bmatrix} \mathcal{U} \\ \mathcal{V} \\ \mathcal{W} \\ \mathcal{N} \end{Bmatrix} = \frac{1}{R}\begin{Bmatrix} \mathcal{U}^{(1)} \\ \mathcal{V}^{(1)} \\ \mathcal{W}^{(1)} \\ \mathcal{N}^{(1)} \end{Bmatrix} + \frac{1}{R^2}\begin{Bmatrix} \mathcal{U}^{(2)} \\ \mathcal{V}^{(2)} \\ \mathcal{W}^{(2)} \\ \mathcal{N}^{(2)} \end{Bmatrix} + \mathcal{O}(\frac{1}{R^3}). \tag{4.2}$$

Substituting (4.1) and (4.2) into equations (2.1)-(2.4) and collecting the lowest-order terms, we get the following equations:

$$\left\{\left(\frac{\partial}{\partial \mathcal{T}} + U\frac{\partial}{\partial \mathcal{X}}\right)\left(\frac{\partial^2}{\partial y^2} + \frac{\partial^2}{\partial z^2}\right) - \frac{d^2U}{dy^2}\frac{\partial}{\partial \mathcal{X}} - \left(\frac{\partial^2}{\partial y^2} + \frac{\partial^2}{\partial z^2}\right)^2\right\}\mathcal{V}^{(1)}$$

$$= -\frac{\partial^2}{\partial z^2}\mathcal{M}^{(1)}\mathcal{V}^{(1)} + \frac{\partial^2}{\partial \mathcal{X}\partial y}\mathcal{M}^{(1)}\mathcal{U}^{(1)} + \frac{\partial^2}{\partial z\partial y}\mathcal{M}^{(1)}\mathcal{W}^{(1)}. \tag{4.3}$$

$$\left\{\frac{\partial}{\partial \mathcal{T}} + U\frac{\partial}{\partial \mathcal{X}} - \left(\frac{\partial^2}{\partial y^2} + \frac{\partial^2}{\partial z^2}\right)\right\}\mathcal{N}^{(1)} = -\frac{dU}{dy}\frac{\partial \mathcal{V}^{(1)}}{\partial z} - \frac{\partial}{\partial z}\mathcal{M}^{(1)}\mathcal{U}^{(1)}. \tag{4.4}$$

$$\frac{\partial \mathcal{U}^{(1)}}{\partial z} = \mathcal{N}^{(1)}. \tag{4.5}$$

$$\frac{\partial \mathcal{U}^{(1)}}{\partial \mathcal{X}} + \frac{\partial \mathcal{W}^{(1)}}{\partial z} = -\frac{\partial \mathcal{V}^{(1)}}{\partial y}. \tag{4.6}$$

The operator $\mathcal{M}^{(1)}$ used in (4.3) and (4.4) is defined as

$$\mathcal{M}^{(1)} = \mathcal{U}^{(1)}\frac{\partial}{\partial \mathcal{X}} + \mathcal{V}^{(1)}\frac{\partial}{\partial y} + \mathcal{W}^{(1)}\frac{\partial}{\partial z}.$$

Observe that, though the three-dimensional perturbations are still considered small in magnitudes, the perturbations of the lowest order are governed no longer by linearized equations. Owing to the Reynolds number dependence of some of the perturbation quantities, the development of the three-dimensional perturbations are to be followed by equations (4.3)-(4.6). At close look, we recognise that these four equations closely resemble the original equations (2.1)-(2.4) governing the perturbation flow. Therefore, we return to those equations to study more about the behaviour of three-dimensional perturbations, no matter whether they are big or small.

5 Nonlinear development of 3-D perturbations

Owing to the nonlinearity of (2.1) and (2.2), the solution procedure becomes rather involved. These equations, together with (2.3) and (2.4), can certainly be solved from the outset by numerical simulations - where the development of some initial perturbations could be followed by direct computations. We, however, are more interested in the general features of solutions than solutions which are particular to some initial perturbations.

Let us first investigate into the nonlinear properties of a solution in the form of an oblique wave travelling in one single direction. Unlike in the linear case, nonlinearity evokes higher harmonics of this fundamental wave and also distorts the basic flow. Hence, we assume the following form for the solution:

$$\left\{\begin{array}{c} u \\ v \\ w \\ \eta \end{array}\right\} = \left\{\begin{array}{c} \hat{u}_0(y,t) \\ \hat{v}_0(y,t) \\ \hat{w}_0(y,t) \\ \hat{\eta}_0(y,t) \end{array}\right\} + \sum_{m=1}^{\infty} \left\{\begin{array}{c} \hat{u}_m(y,t) \\ \hat{v}_m(y,t) \\ \hat{w}_m(y,t) \\ \hat{\eta}_m(y,t) \end{array}\right\} e^{im(\alpha x+\beta z)}$$

$$+ \sum_{m=1}^{\infty} \left\{\begin{array}{c} \hat{u}^*_m(y,t) \\ \hat{v}^*_m(y,t) \\ \hat{w}^*_m(y,t) \\ \hat{\eta}^*_m(y,t) \end{array}\right\} e^{-im(\alpha x+\beta z)}, \qquad (5.1)$$

where $*$ denotes complex conjugation. A little thought suggests that

$$\hat{v}_0 \equiv \hat{\eta}_0 \equiv 0.$$

Substitution of (5.1) in (2.1)-(2.4) yields, after some algebra, the equations governing $\hat{u}_m$, $\hat{v}_m$, $\hat{w}_m$ and $\hat{\eta}_m$. These equations are discussed below.

The normal velocity component $\hat{v}_m$ (for $m \geq 1$) is described by the equation

$$\left[\left\{\frac{\partial}{\partial t} + im\left(\alpha U + \alpha\hat{u}_0 + \beta\hat{w}_0\right)\right\}\left(\frac{\partial^2}{\partial y^2} - m^2k^2\right)\right.$$

$$\left. -im\frac{\partial^2}{\partial y^2}\left(\alpha U + \alpha\hat{u}_0 + \beta\hat{w}_0\right) - \frac{1}{R}\left(\frac{\partial^2}{\partial y^2} - m^2k^2\right)^2\right]\hat{v}_m$$

$$= \sum_{q=1}^{m-1}\left\{m^2k^2\left(-\frac{q}{m-q}\frac{\partial\hat{v}_{m-q}}{\partial y}\hat{v}_q + \hat{v}_{m-q}\frac{\partial\hat{v}_q}{\partial y}\right)\right.$$

$$\left. + \frac{m}{m-q}\frac{\partial}{\partial y}\left(\frac{\partial\hat{v}_{m-q}}{\partial y}\frac{\partial\hat{v}_q}{\partial y}\right) - \frac{m}{q}\frac{\partial}{\partial y}\left(\hat{v}_{m-q}\frac{\partial^2\hat{v}_q}{\partial y^2}\right)\right\}$$

$$+\sum_{q=1}^{\infty}\left\{m^2k^2(m+2q)\left(\frac{1}{m+q}\frac{\partial\hat{v}_{m+q}}{\partial y}\hat{v}_q^* + \frac{1}{q}\hat{v}_{m+q}\frac{\partial\hat{v}_q^*}{\partial y}\right)\right.$$

$$+\frac{m}{m+q}\left(\frac{\partial\hat{v}_{m+q}}{\partial y}\frac{\partial^2\hat{v}_q^*}{\partial y^2} - \frac{\partial^3\hat{v}_{m+q}}{\partial y^3}\hat{v}_q^*\right)$$

$$\left. +\frac{m}{q}\left(\hat{v}_{m+q}\frac{\partial^3\hat{v}_q^*}{\partial y^3} - \frac{\partial^2\hat{v}_{m+q}}{\partial y^2}\frac{\partial\hat{v}_q^*}{\partial y}\right)\right\} \tag{5.2a}$$

with the boundary conditions

$$\hat{v}_m = \frac{\partial\hat{v}_m}{\partial y} = 0 \quad \text{at} \quad y = \pm 1. \tag{5.2b}$$

Note that the first summation term of (5.2a) has its upper limit as $(m-1)$ and , hence, is applicable only for $m \geq 2$. The operator on the left-hand side of (5.2a) is in fact the same as that of the linear case except for the basic flow modifications. The nonlinear interaction terms of (5.2a) are exclusively determined by the normal perturbation velocity components themselves. Other perturbation velocities enter the equation *only* in the form of basic flow modifications.

The normal vorticity component $\hat{\eta}_m$ (for $m \geq 1$) is described by the equation

$$\left[\frac{\partial}{\partial t} + im(\alpha U + \alpha\hat{u}_0 + \beta\hat{w}_0) - \frac{1}{R}\left(\frac{\partial^2}{\partial y^2} - m^2k^2\right)\right]\hat{\eta}_m$$

$$= -im\left\{\beta\frac{dU}{dy} + \frac{\partial}{\partial y}(\beta\hat{u}_0 - \alpha\hat{w}_0)\right\}\hat{v}_m$$

$$+\sum_{q=1}^{m-1}\left\{\frac{m}{m-q}\frac{\partial\hat{v}_{m-q}}{\partial y}\hat{\eta}_q - \frac{m}{q}\hat{v}_{m-q}\frac{\partial\hat{\eta}_q}{\partial y}\right\}$$

$$+\sum_{q=1}^{\infty}\left\{\frac{m}{m+q}\left(\frac{\partial\hat{v}_{m+q}}{\partial y}\hat{\eta}_q^* - \frac{\partial\hat{\eta}_{m+q}}{\partial y}\hat{v}_q^*\right)\right.$$

$$\left. +\frac{m}{q}\left(\hat{v}_{m+q}\frac{\partial\hat{\eta}_q^*}{\partial y} - \hat{\eta}_{m+q}\frac{\partial\hat{v}_q^*}{\partial y}\right)\right\} \tag{5.3a}$$

with the boundary conditions

$$\hat{\eta}_m = 0 \quad \text{at} \quad y = \pm 1. \tag{5.3b}$$

The first summation term of (5.3a) is applicable only for $m \geq 2$. Both the basic-flow velocity and the basic-flow vorticity are modified. The nonlinear interaction terms (5.3a) are determined by the products of normal perturbation velocity and vorticity components.

The streamwise velocity $\hat{u}_m$ and the spanwise velocity $\hat{w}_m$ are described by

$$\hat{u}_m = \frac{i}{mk^2}\left(\alpha\frac{\partial \hat{v}_m}{\partial y} - \beta\hat{\eta}_m\right) \tag{5.4}$$

and

$$\hat{w}_m = \frac{i}{mk^2}\left(\beta\frac{\partial \hat{v}_m}{\partial y} + \alpha\hat{\eta}_m\right), \tag{5.5}$$

respectively, for the case of $m \geq 1$. Equations (5.2)-(5.5) are to be supplemented also by their complex conjugates.

To obtain the complete system of equations, however, two more equations are needed (along with their complex conjugates) to describe the basic flow modifications in the streamwise and in the spanwise directions. These equations can be derived from the equations governing the perturbation *vorticities* in these directions. The streamwise perturbation vorticity is described by

$$\left\{\frac{\partial}{\partial t} + U\frac{\partial}{\partial x} - \frac{1}{R}\nabla^2\right\}\left(\frac{\partial w}{\partial y} - \frac{\partial v}{\partial z}\right) = -\frac{dU}{dy}\frac{\partial w}{\partial x} - \frac{\partial}{\partial y}\mathcal{M}w + \frac{\partial}{\partial z}\mathcal{M}v \tag{5.6}$$

and the spanwise perturbation vorticity is described by

$$\left\{\frac{\partial}{\partial t} + U\frac{\partial}{\partial x} - \frac{1}{R}\nabla^2\right\}\left(\frac{\partial v}{\partial x} - \frac{\partial u}{\partial y}\right) = -\frac{dU}{dy}\frac{\partial w}{\partial z} + \frac{d^2U}{dy^2}v - \frac{\partial}{\partial x}\mathcal{M}v + \frac{\partial}{\partial y}\mathcal{M}u. \tag{5.7}$$

Substituting (5.1) in (5.6)-(5.7) and extracting only the amplitude terms from the resulting equations yield the following equations governing the basic-flow modifications in the streamwise and in the spanwise directions:

$$\left(\frac{\partial}{\partial t} - \frac{1}{R}\frac{\partial^2}{\partial y^2}\right)\frac{\partial \hat{u}_0}{\partial y} = -\frac{2}{k^2}\Im\left(\frac{\partial^2}{\partial y^2}\sum_{q=1}^{\infty}\left\{\frac{\alpha}{q}\hat{v}_q\frac{\partial \hat{v}_q^*}{\partial y} - \frac{\beta}{q}\hat{v}_q\hat{\eta}_q^*\right\}\right).$$

$$\left(\frac{\partial}{\partial t} - \frac{1}{R}\frac{\partial^2}{\partial y^2}\right)\frac{\partial \hat{w}_0}{\partial y} = -\frac{2}{k^2}\Im\left(\frac{\partial^2}{\partial y^2}\sum_{q=1}^{\infty}\left\{\frac{\beta}{q}\hat{v}_q\frac{\partial \hat{v}_q^*}{\partial y} + \frac{\alpha}{q}\hat{v}_q\hat{\eta}_q^*\right\}\right).$$

Here $\Im$ denotes the imaginary part. These equations can be integrated with respect to y once to obtain

$$\left(\frac{\partial}{\partial t} - \frac{1}{R}\frac{\partial^2}{\partial y^2}\right)\hat{u}_0 = -\frac{2}{k^2}\Im\left(\frac{\partial}{\partial y}\sum_{q=1}^{\infty}\left\{\frac{\alpha}{q}\hat{v}_q\frac{\partial \hat{v}_q^*}{\partial y} - \frac{\beta}{q}\hat{v}_q\hat{\eta}_q^*\right\}\right) \tag{5.8}$$

and

$$\left(\frac{\partial}{\partial t}-\frac{1}{R}\frac{\partial^2}{\partial y^2}\right)\hat{w}_0=-\frac{2}{k^2}\Im\left(\frac{\partial}{\partial y}\sum_{q=1}^{\infty}\left\{\frac{\beta}{q}\hat{v}_q\frac{\partial\hat{v}_q^*}{\partial y}+\frac{\alpha}{q}\hat{v}_q\hat{\eta}_q^*\right\}\right), \tag{5.9}$$

where the constants of integrations have been set to zero. This step is justified if we assume that the perturbations do not alter the pressure gradient determining the basic flow. (The same srgument has been applied to the two-dimensional case, see [9] for instance.) These equations are to be supplemented with the boundary conditions

$$\hat{u}_0=\hat{w}_0=0 \quad \text{at} \quad y=\pm 1. \tag{5.10}$$

It becomes clear from (5.8)-(5.10) that the basic flow modifications in the streamwise and in the spanwise directions are caused by the nonlinear interactions among the normal velocity components themselves as well as *by the interaction between the normal velocity and vorticity components.*

Therefore, it appears that the development of the normal vorticity perturbations may enter the equation governing the normal velocity perturbations through the basic-flow modifications. In order to confirm this speculation, we carry out the following analysis. Observe that the basic-flow modification terms enter the normal velocity equation (5.2) only in the form of $(\alpha\hat{u}_0+\beta\hat{w}_0)$ and its second derivative with respect to y. We can obtain an equation governing this cumulative term by properly adding (5.8) and (5.9) and the result becomes:

$$\left(\frac{\partial}{\partial t}-\frac{1}{R}\frac{\partial^2}{\partial y^2}\right)(\alpha\hat{u}_0+\beta\hat{w}_0)=-2\Im\left(\frac{\partial}{\partial y}\sum_{q=1}^{\infty}\left\{\frac{1}{q}\hat{v}_q\frac{\partial\hat{v}_q^*}{\partial y}\right\}\right). \tag{5.11}$$

The interesting feature of (5.11) is the *absence* of normal vorticity perturbations from it. Therefore, it becomes clear that the normal vorticity perturbations *do not* enter the equations for normal velocity perturbations even through the terms representing the basic flow modifications.

From these observations we conclude that, when the perturbations are described by waves travelling in one single direction, the development of the normal perturbation velocity components are determined only by the interactions among themselves. The development of the induced normal vorticity has then no influence upon the normal perturbation velocity.

6 Discussion

In the linear case, the amplitude of the normal perturbation vorticity and, thus, that of the streamwise perturbation velocity grow temporally to significant peak values. But, these growths do not influence the amplitudes of the normal perturbation velocity that are monotonically decaying with time.

These growths, however, are to be followed by nonlinear equations at about the transitional Reynolds number. The nonlinear analyses show that if the perturbations are described by waves travelling in one *single* oblique direction, then the nonlinear interactions can be grouped into two catogories. One is due to the interactions among the normal velocity components themselves, which has its equivalence also if the perturbation flow were two-dimensional. The other is due to the nonlinear interaction between the normal velocity components and the normal vorticity components, which would not exist if the perturbation flow were two-dimensional. Both of these interactive terms contribute towards modifying the basic flow in the streamwise as well as in the spanwise directions.

In the nonlinear equations governing the normal velocity perturbations, however, it is only the first kind of interactions that appears. This implies that the normal velocity would be oblivious to the development of the induced normal vorticity, even in the nonlinear regime, when the perturbations are taken to be waves travelling in a single oblique direction.

In concluding, we recall that the analyses of Gustavsson [5] revealed that the temporal development of the amplitudes of normal vorticity is most significant for structures elongated in the streamwise direction; that is for the case $\alpha = 0$. The nonlinear analyses presented in §5 can be extended to include this extreme case by simply setting α to zero in the expressions concerned. The result is that, as in the case of non-zero α, the normal velocity perturbations are insensitive to the temporal development of the normal vorticity.

None the less, in the case of non-zero streamwise wavenumber, describing the perturbations as waves travelling in two oblique directions might change this monotonous behaviour of the normal velocity. The wave considered here travels in (α, β)-direction. For every wave which travels in this direction, there exists another wave which travels in $(\alpha, -\beta)$-direction. When the fundamental is described by both of these waves, nonlinearity leads to a solution which is of more complex form than that described by (5.1). Preliminary investigations have indicated that, in such a description, the normal velocity would become sensitive to the development of the induced vorticity. The details of the interaction are a matter of prime concern and are left for future studies.

Acknowledgements

I thank L. Håkan Gustavsson, my thesis adviser, for his enthusiastic contributions towards the contents of this paper. This work has in part been supported by the national Swedish Board for Technical Development through its program for basic research (STUF).

References

1. H. B. SQUIRE, On the stability for three-dimensional disturbances of viscous fluid flow between parallel walls, *Proc. Roy. Soc. London* A 142:621-628 (1933).

2. S. A. ORSZAG, Accurate solution of the Orr-Sommerfeld stability equation. *J. Fluid Mech.* 50:689-703 (1971).

3. T. HERBERT, Periodic secondary motions in a plane channel. In *Proc. Int. conf. Numer. Methods Fluid Dyn.* (ed. A. I. van de Vooren and P. J. Zandbergen), pp. 235, Springer-Verlag (1976).

4. D. MEKSYN, Stability of laminar flow between parallel planes for two- and three-dimensional finite disturbances, *Zeitschrift für Physik* 178:159-172 (1964).

5. L. H. GUSTVSSON, Energy growth of three-dimensional disturbances in plane Poiseuille flow, submitted to *J. Fluid Mech.* (1990).

6. R. SHANTHINI, Influence of temporal degeneracies upon the development of perturbation field - in plane Poiseuille flow, submitted to *J. Fluid Mech.* (1990).

7. D. J. BENNEY and L. H. GUSTVSSON, A new mechanism for linear and non-linear hydrodynamic instability, *Stud. Appl. Math.* 64:185-209 (1981).

8. R. SHANTHINI, Degeneracies of the temporal Orr-Sommerfeld eigenmodes in plane Poiseuille flow, *J. Fluid Mech.* 201:13-34 (1989).

9. C. L. PEKERIS and B. SHKOLLER, The neutral curves for periodic perturbations of finite amplitude of plane Poiseuille flow, *J. Fluid Mech.* 39:629-639 (1969).

"... The meeting was at five-thirty in the afternoon, but at five-thirty when I turned the university corner I was held up by a couple of squirrels (one was the mother and the other a callow youth, ten days old, probably on his second day's outing). One might legitimately ask how an adult could ever allow his plans to be diverted by a couple of squirrels, but I still think if there ever was an occasion for an adult to waive all other engagements it was this..."

- R. K. NARAYAN (*At the Portal*)